Structural and Functional Insights into Telomerase Recruitment

by

Eric Matthew Smith

A dissertation submitted in partial fulfillment
of the requirements for the degree of
Doctor of Philosophy
(Chemical Biology)
in the University of Michigan
2018

Doctoral Committee:

Assistant Professor Jayakrishnan Nandakumar, Chair
Associate Professor Patrick O'Brien
Associate Professor Lyle Simmons
Associate Professor Raymond Trievel

Eric Matthew Smith

ericms@umich.edu

ORCID iD: 0000-0002-5385-4558

For my mom, dad, and brother.

Acknowledgements

First and foremost, I would like to thank my parents and grandparents for their continuous encouragement throughout my life. Mom and Dad there is no way I would be here today without your unwavering positive attitude and your example of good work ethic. I would also like to thank my brother, I am lucky to have such a supportive best friend.

As I started graduate school I was fortunate to meet with JK to discuss a potential rotation. Immediately in that meeting his enthusiasm for telomere biology was infectious, and after the first week of my rotation I knew I wanted to work in his lab. Thank you JK for being an enthusiastic, supportive, and dedicated mentor. I am grateful for your patience and kindness. To current and former members of the Nandakumar lab, Valerie, Sheri, Devon, Oana, Alam, Shilpa, Ritvija, Jackie, Kamlesh and Jonathan, thank you for your friendship. I want to thank Valerie for spending so much time training me when I started in the lab, for her continual advice, and friendship. I also want to thank my committee members Pat O'Brien, Lyle Simmons, Ray Trievel, and Carol Fierke for their support, feedback, and suggestions over the last four years.

I wouldn't have made it through many things, including graduate school if it weren't for my friends. To Sheri I will always appreciate you, and I will miss our daily Comet coffee runs. Thank you Brian Stoll for the many good times we have had over the past 20 years. Thank you Rob Kononowech, Ed O'Brien, Bill Chopik, Ryan Bremner, James Soliman, Nick Niewolak, Bobby Tenuta, Shyama Nandakumar, and

Tyler Beyett for being there to listen and make me laugh. Thank you to all my friends who I play soccer and hockey with on the Biohazards, Mott Fosters' Kids, and Gates. Particularly Michael Scott, for his friendship and his initial invitation to come play hockey in Ann Arbor.

I would like to thank the Career Training in the Biology of Aging Training Grant (T32AG000114) for not only providing me funding, but a platform to learn and grow as a scientist. Additionally, I would also like to thank the Program in Chemical Biology for allowing me a place to grow and learn as a scientist. Finally I would like to thank the University of Michigan for helping shape me into the person I am today. I was lucky enough to attend Michigan as an undergraduate and a graduate student, and the eleven years I have spent in Ann Arbor have been some of the most rewarding of my life.

Table of Contents

List of Tables

List of Figures

Abstract

Telomeres are nucleoprotein complexes that cap the ends of linear chromosomes and preserve genomic integrity. They help overcome two biological problems posed by linear chromosomes. The first problem, called the end protection problem, is solved by the shelterin complex. Shelterin is the six-protein complex that forms the major protein constituent of telomeres, coating telomeric DNA to protect chromosome ends from being misrecognized by the DNA damage response and repair machineries. The shelterin component TPP1 also helps solve the second problem associated with linear chromosomes called the end replication problem, which arises because replicative polymerases cannot fully synthesize DNA at chromosome ends. TPP1 recruits the ribonucleoprotein (RNP) enzyme telomerase to telomeres, where it compensates for telomere attrition by addition of telomeric repeats, thereby enabling continued cell division in stem and germ line cells. The lack of telomerase in most somatic cells limits their unregulated division. However telomerase is upregulated in ~90% of cancers, qualifying it as an attractive target for anti-cancer drug design.

Mutations in telomere and telomerase associated genes can lead to a variety of telomeropathies, the most prominent of which is an inherited bone marrow failure syndrome called dyskeratosis congenita (DC). As a consequence of these mutations, patients with DC have extremely short telomeres. Our lab was involved in characterizing DC in a patient who was heterozygous for an in frame deletion of lysine 170 (K170) in the shelterin protein TPP1. Although K170 is found near a region of residues in TPP1

responsible for recruiting telomerase, referred to as the TEL patch, this residue was not identified in previous screens. Here, using a combination of biochemistry and cell biology, we demonstrate that this mutation causes a defect in the ability of TPP1 to recruit telomerase or stimulate its repeat addition processivity, and affects its ability to maintain telomere length *in vivo*. Using X-ray crystallography, I illustrate that TPP1 K170Δ alters the TEL patch, spatially displacing two critical glutamates. Finally, we use CRISPR-Cas9 gene editing to show that introducing this mutation in a heterozygous context is sufficient to cause telomere shortening in human cells, thereby providing important insights into the genetics of DC.

While the surface on TPP1 that is responsible for telomerase recruitment has been well characterized, it is not as clear which regions of the protein subunit of telomerase (TERT) are important for this interaction. The TEN domain and the IFD of TERT have been implicated in TPP1 binding, although only one specific interaction between the TEN domain and the TEL patch has been identified. Here, I use an alanine scanning mutagenesis screen in conjunction with an in-cell recruitment assay to identify one region each in the TEN domain and IFD that contain residues necessary for telomerase recruitment to the telomere. These mutations showed wild-type telomerase RNP assembly but hindered TPP1-stimulated telomerase activity *in vitro* and adversely affected the extension of telomeres by telomerase in cultured cells. In summary, my studies have helped pinpoint the TERT side the TPP1-telomerase interface that is critical for both cancer cell proliferation and normal stem cell function.

Chapter 1

Introduction[1]

1.1 Introduction

Eukaryotic chromosomes are linear and end in nucleoprotein complexes called telomeres. Telomeric DNA is composed of a repetitive sequence (GGTTAG/CCAATC in humans) that is largely double-stranded (ds; 10-15 kb in humans), but ends in a short single-stranded (ss; 50-500 nt in humans) G-rich 3' overhang [1]. Linear chromosomes present two major biological hurdles at chromosome ends: the end replication and end protection problems. The end protection problem occurs when the natural ends of linear chromosomes are misrecognized by the DNA damage response and repair machinery as double strand breaks requiring repair [1]. The six-protein complex shelterin, consisting of proteins POT1, TPP1, TIN2, TRF1, TRF2, and Rap1, solves the end protection problem by coating telomeric DNA (Figure 1.1) [1-12]. While TRF1 and TRF2 recognize ds telomeric DNA, POT1 binds the ss overhang with high specificity and affinity [5,13]. By coating telomeric DNA, the shelterin complex sequesters it away from the ATM and ATR mediated DNA damage response pathways [1,14]. Although linear chromosomes must be protected from the DNA damage response machinery, they must

[1] A modified version of this chapter comes from a review titled "The structural biology of chromosome end maintenance" that is in submission to Cellular and Molecular Life Sciences written by Devon Pendlebury, Jayakrishnan Nandakumar and myself. I wrote all sections that appear here with input and comments from Jayakrishnan Nandakumar.

also allow recruitment of telomerase to those ends to solve the second problem associated with linear chromosomes called the end replication problem.

Telomerase, a ribonucleoprotein enzyme is able to solve the end replication problem by adding telomeric repeats to the extreme ends of linear chromosomes helping to maintain telomere length over time. The action of telomerase is essential for the continued division of stem and germ line cells. Telomerase conducts this function with the help of a core protein component called Telomerase Reverse Transcriptase (TERT), which amongst many features contains a catalytic reverse transcriptase domain for DNA synthesis [15-17]. Telomerase also contains an RNA subunit called Telomerase RNA component (TERC or TR) which harbors the template for the synthesis of telomeric repeats at the extreme 3' end of the chromosome [18,19]. Telomerase counteracts DNA attrition that would normally be observed due to the end replication problem by synthesizing several telomeric repeats at chromosome ends (Figure 1.1) [20].

Telomerase is expressed in both germ line and stem cells to facilitate their continued cell division [21]. It is therefore not surprising that mutations in telomere- and telomerase-associated genes result in inherited stem cell-dysfunction diseases collectively known as "telomeropathies", the most notable of which is dyskeratosis congenita or DC [22,14,23]. Normally nondividing cells lacking telomerase enter a non-proliferative state called senescence once their telomere length falls below a certain threshold [24]. This is an anti-tumorigenic mechanism to prevent uncontrolled cell division. However if a rare cell escapes senescence and aberrantly resumes telomerase expression to re-establish telomere length maintenance, it could attain "replicative

immortality", a hallmark of cancer [25,26]. In fact an overwhelming majority of cancers (~90%) show telomerase expression [27,28], and thus this enzyme is a promising target for anti-cancer drug discovery.

1.2 Double stranded end protection

Telomeric DNA is both double stranded and single stranded and must be protected from being misrecognized as a DNA lesion by DNA damage response and repair machinery. Two shelterin components, TRF1 and TRF2 bind the double stranded region of telomeric DNA, protecting it from erroneous DNA damage responses (Figure 1.1) [3,29]. Both proteins have a C-terminal myb domain that binds in a sequence specific manner to the major groove of ds telomeric DNA (Figure 1.2) [30-33]. TRF2 is able to use this feature to block the ATM mediated DNA damage response (Figure 1.1) [5,1,34-36]. TRF2 also facilitates the formation of T-loops, specialized telomeric DNA conformations in which the 3' end of the telomere invades the double stranded region of telomeric DNA, potentially providing an additional mechanism to protect chromosome ends [37-39]. Both TRF2 and TRF1 also contain a TRF homology domain (TRFH) which simultaneously facilitates the homodimerization of TRF1 and TRF2, while also preventing their heterodimerization [40]. Beyond dimerization the TRFH domain allows both TRF1 and TRF2 to recruit specific accessory proteins to the telomere. TRF1 interacts with proteins that contain an F-X-L-X-P motif (where X can be any amino acid), the most notable of which is the shelterin protein TIN2. TRF2 has a preference for binding proteins containing a Y-X-L-X-P motif, examples of which include the nuclease Apollo/SNM1B and the DNA damage response protein NBS1 [41]. Outside of the TRFH domain, TRF2 also interacts with shelterin component Rap1, which functions in

repressing homology directed repair (HDR) [42,43]. While the ability to directly protect ds telomeric DNA is vital; TRF1 and TRF2 have a second major role at the telomere, which is the recruitment of the rest of shelterin (RAP1, TIN2, TPP1, and POT1) for faithful end protection and end replication (Figure 1.1). The importance of these proteins is highlighted by the fact that knocking out either TRF1 or TRF2 causes embryonic lethality in mice [44,45].

1.3 Single stranded end protection

The very end of any eukaryotic chromosome is single-stranded and thus a potential substrate for illicit homology-driven recombination or repair. Thus a major challenge in end protection involves preventing this DNA from participating in such processes. The G-rich 3' ss overhang of telomeric DNA is also involved in end replication as it provides the site for telomerase to bind and extend chromosomes. Both of these functions are either directly dictated by (in case of end protection) or facilitated by (in case of end replication) proteins that bind the ss overhang.

1.3.1 Ciliates provide the first insights

The first major structural insights into G-rich 3' ss DNA-binding proteins came from the structure of the *Sterkiella nova* (*S. nova*; formerly *Oxytricha nova*) proteins TEBP-α and TEBP-β, which bind as a heterodimer to ss DNA at chromosome ends (*left*; Figure 1.3A) [46,47]. The TEBP-α protein is composed of three oligosaccharide/oligonucleotide binding (OB) domains. The two N-terminal OB domains collectively form a DNA-binding domain (DBD) that binds specifically to the 3' ss overhang of the telomeric DNA. [47,48]. The protein-DNA interface is formed between residues on both TEBP-α and β, and the bases and deoxyribose groups of the DNA.

Thus, this interface is rich in hydrogen bonding, hydrophobic, and pi-stacking interactions. In fact almost every base in the protein-DNA co-crystal structure stacks with an aromatic amino acid or another base. Following the track that the DNA takes through the structure reveals that the 3' end interacts not only with TEBP-α, but also several residues in TEBP-β (*left*; Figure 1.3A). The terminal 3' nucleotide G11 folds back to stack with nucleotide T7 burying the extreme end of the chromosome within the protein-DNA complex (*left;* Figure 1.3A). Because of these extensive interactions, the TEBP-α and TEBP-β heterodimer is able to protect the ss tail of the telomere from potential interactions with DNA damage response proteins. Although this structure provides a compelling solution to the end protection problem, it is likely that the TEBP-α-β-DNA complex undergoes a conformational change to allow telomerase to access to extend the chromosome ends.

1.3.2 Protection of ss DNA at chromosome ends by human POT1-TPP1

Human telomeres are longer than that of *S. nova* and are composed of more proteins, but they still must overcome the same biological hurdles. The protein that protects the ss overhang at human chromosome ends is called POT1 (Figure 1.1, 1.3), a homolog of which also exists in *Schizosaccharomyces pombe* (*S. pombe*) [7]. Not surprisingly, both *S. pombe* and human POT1 have a similar overall structure to that of *S. nova* TEBP-α [49,13]. The DNA binding domain (DBD) of human POT1 uses two N-terminal OB domains (OB1 and OB2) to bind to the ss overhang of telomeric DNA (*right*; Figure 1.3A). A crystal structure of this complex details how the OB1 of POT1 is able to interact with the first six bases of the 10 nt telomeric sequence (1-TTAGGG-6) (*left*; Figure 1.3B) in a fashion similar to that of the homologous *S. pombe* POT1pN protein

fragment (not shown). Both structures detail stacking interactions between aromatic residues in POT1 and the bases of the telomeric DNA. In addition to these stacking interactions, OB1 makes several hydrogen bonds with the telomeric DNA. OB2 of human POT1 makes less extensive hydrogen bonds with telomeric DNA, but the four 3' bases in the crystal structure (7-TTAG-10) all stack with aromatic residues present on OB2 (*right*; Figure 1.3B). Interestingly, OB2 of *S. pombe* Pot1 exhibits lower sequence specificity compared to the adjacent OB1 domain and binds optimally to a 9-mer DNA sequence [50]. Although the overall structure of human POT1's DBD is very similar to that of TEBP-α's DBD, the track of the DNA through the two OB domains in these structures is strikingly different (Figure 1.3C). In POT1 the DNA is kinked as it passes from OB1 to OB2. This occurs because the two OB domains in the POT1 structure are oriented differently relative to one another than they are in the *S. nova* structure (Figure 1.3A). Additionally the 3' end of the DNA does not curve back towards POT1 as it does in the *S. nova* structure (Figure 1.3C). These differences may be attributed to the fact that the *S. nova* structure contains the full TEBP-α-β complex bound to DNA while the POT1-DNA structure lacks both TPP1 (mammalian TEBP-β homolog) and the TPP1-binding domain of POT1. Alternatively, these structural differences may suggest distinct species-specific solutions for end protection (see discussion of human POT1-TPP1-DNA SAXS data below).

The high affinity and specificity of POT1 for ss telomeric DNA provides an elegant mechanism for protection against an ATR kinase mediated response and subsequent homologous recombination (HR) at chromosome ends [49,51]. An essential initial step for HR is binding of the participating ss DNA with Replication protein A

(RPA), a heterotrimer composed largely of OB domains [52]. By binding ss telomeric DNA with high affinity and sequence specificity, POT1 blocks access of RPA to prevent ATR activation at chromosome ends (Figure 1.1) [53]. Indeed, mutations in the DNA-binding domain of POT1 are associated with chromosome end aberrations including fusions in several chronic lymphocytic leukemias (CLL) and familial melanomas (FM), highlighting the importance of this protein in maintaining genome integrity [54,55].

1.3.3 POT1-TPP1 interface

The first structural insights into how the POT1-TPP1 heterodimer forms to protect chromosome ends and to facilitate end replication came from analysis of the TEBP-α-β complex. TEBP-α has a third C-terminal OB domain that makes extensive interactions with a C-terminal region of TEBP-β that is partly helical but mostly extended in conformation (Figure 1.3A). However the C-terminus of POT1 does not share much sequence similarity with TEBP-α making it unclear if TPP1 and POT1 would interact in a similar manner. Two similar structures of the C-terminus of POT1 in complex with the POT1 binding domain (PBD) of TPP1 were solved using X-ray crystallography [56,57]. These structures revealed that the C-terminus of POT1, like TEBP-α, forms an OB domain that is able to make extensive interactions with TPP1 (Figure 1.4A). Unexpectedly, the authors also identified an additional TPP1-binding element within POT1: a Holliday junction resolvase like domain (HJRD) inserted within POT1's third OB domain (OB3). In both structures the two α-helices and a 3_{10} helix of TPP1's PBD lie in grooves formed by the OB3 and the HJRD domains of POT1. Somatic mutations associated with several CLL and FL malignancies are mapped to the TPP1-binding region of POT1 [56,57]. This is not surprising, because the inability to bind TPP1 will

prevent recruitment of POT1 to telomeres, thereby unleashing chromosome end deprotection [53,58,59].

Although there is no high-resolution structure for the human POT1-TPP1-DNA complex, small-angle X-ray scattering (SAXS) analysis of the TPP1-N-POT1-DNA complex has revealed an elongated V shaped envelope. In the model generated with these data, TPP1 OB is proposed to be distal to both the DBD of POT1 and the telomeric DNA [56]. This is in stark contrast to the overall heart-shaped structure of TEBP-α-β-DNA that brings both subunits in close proximity and allows them to interact simultaneously with ss DNA. A high-resolution human POT1-TPP1-DNA structure will be instrumental to address the apparent differences in how ss DNA ends are protected in *S. nova* versus human.

1.3.4 Hierarchical assembly of shelterin at telomeres

POT1 is required for telomere maintenance, yet it cannot arrive at the chromosome end without being recruited by its binding partner TPP1 [58]. Before recruiting POT1, TPP1 must itself localize to telomeres with the help of the shelterin protein TIN2 [60,61]. TIN2 plays a central role at telomeres as it is able to bind TRF1, TRF2, and TPP1. TIN2 recruitment to telomeres requires binding to TRF1 [62]. Although binding to TRF2 is not mandatory for TIN2 recruitment to telomeres, it is important for stabilizing TRF2 protein for proper repression of ATM mediated damage response [63]. Due to the hierarchical nature of shelterin assembly, defects in TIN2 recruitment or expression negatively impact TRF2, POT1, and TPP1 function. Indeed depletion of TIN2 results in the activation of both ATM and ATR DNA damage response pathways [62].

1.4 Chromosome end replication

The second problem associated with linear chromosomes is called the end replication problem. Maintenance of eukaryotic genomes is complicated due to the inability of replicative DNA polymerases to synthesize nucleotides at the extreme 3' ends of linear chromosomes. Telomerase catalyzes the addition of telomeric repeats (TTAGGG sequence in mammals) to the ends of linear chromosomes (Figure 1.1A) [18,19,15,17]. In humans, telomerase adds ~50 nucleotides of telomeric DNA during every round of replication, which helps compensate for the attrition of DNA that occurs due to the end replication problem. This function is necessary to facilitate the continued division of stem and germ line cells and mutations in telomere and telomerase associated genes can lead to a variety of diseases called telomeropathies.

1.4.1 The role of TPP1 in telomerase recruitment

One major question that still eludes the field is how telomerase accesses a chromosome end that is so efficiently protected by POT1-TPP1. POT1-TPP1 plays a dual role at telomeres by stimulating telomerase activity and processivity while also protecting telomeric DNA [64]. POT1 tethers TPP1 close to the 3' end, where TPP1 is able to directly recruit telomerase to the telomere using its N-terminal OB domain [60,64,65]. The crystal structure of the TPP1 OB domain illustrates a five-stranded β-barrel that resembles the OB domain found in TEBP-β (*Left;* Figure 1.4B) [64]. Several independent studies led to the discovery of the TEL patch (TPP1 glutamate (E) and leucine (L)-rich patch) in TPP1 OB as a critical surface element for binding telomerase [66-68]. Three critical glutamate residues in the TEL patch (E168, E169, and E171) lie in a long flexible loop that protrudes from the β-barrel and ends in a short α-helix (*right;*

Figure 1.4B). In the asymmetric unit of the TPP1 OB crystal structure, TPP1 forms a non-physiological dimer using its largely hydrophobic N-terminal tail. This region, termed the NOB (N-terminus of the OB domain), is also involved in recruiting telomerase (*right;* Figure 1.4B) [69]. Although much has been uncovered about the surface of TPP1 that recruits telomerase, far less is known about the surface of telomerase that interacts with TPP1. To date, only one direct salt-bridging interaction is firmly mapped between human TPP1 and telomerase [70].

1.4.2 Telomerase RNA

Although the length and sequence of telomerase RNA can vary widely between species, the RNA often contains three structurally conserved domains: the template/pseudoknot, the CR4/5 (STE) domain, and the H/ACA box (Figure 1.5A) [71,72]. The secondary structure conservation of these motifs highlights the essential role they play in telomerase function. The 5' end of TR folds into a template-containing pseudoknot. The template is flanked by a 5' template boundary element (TBE) and a 3' template recognition element (TRE) (Figure 1.5A) [73-77]. The ss TRE helps TERT recognize and position the template in the active site of the enzyme to facilitate repeat addition processivity. The template boundary element (TBE) prevents the addition of nucleotides outside of the defined telomeric repeat. Telomerase is a processive enzyme, extending chromosome ends by adding multiple telomeric repeats per replication cycle. It is still unclear how the template is translocated to the end of the nascent terminal repeat to facilitate continued addition although a few models have been proposed. Single molecule FRET and biochemical experiments suggest an accordion model. In this model the TBE and template recognition element (TRE)

expand and contract to allow movement of the template during the catalytic cycle [78]. Another hypothesis is inspired by the mode of action of translesion DNA polymerase *v*. It suggests that after synthesis of a telomeric repeat, the GT-rich newly synthesized DNA loops out into a non-canonical hairpin, while the template translocates to pair with the AG at the 3' end. Ultimately, an incoming dGTP allows the DNA to realign so another step of synthesis can proceed [79]. Further biophysical and structural studies will be necessary to gain a better understanding of telomerase repeat addition processivity. Outside of the template the pseudoknot is formed by a series of helices and loops for which several structures from ciliates, yeast, and vertebrates exist [80,81].

Following the pseudoknot is the CR4/5 domain (SL4 region in *Tetrahymena*), which is the major TERT-binding domain within telomerase RNA (Figure 1.5A). Crosslinking studies [82] combined with the solved crystal structure of the CR4/5 domain bound to the TRBD (Telomerase RNA binding domain) from the fish *Oryzias latipes* (medaka) [83] have provided atomic details of the interface between the core telomerase RNA and protein subunits that depends both on sequence and conformation of the RNA. The CR4/5 domain forms a three-way junction that takes on an L-shape (Figure 1.6A). Two stems, P6 and P6.1, of the CR4/5 domain directly interact with TERT by forming hydrogen bonds between their RNA backbone and residues on two separate TERT surfaces (Figure 1.6A) [83]. While the structure of the human CR4/5 domain remains unsolved, there is an NMR structure of human stem P6.1 that is structurally similar to that of *Oryzias latipes* (medaka), suggesting the human CR4/5 may interact with TERT in a similar manner [84].

TRBD forms the protein half of the interface between TERT and the CR4/5 of TR. Sequence conservation suggests TERT TRBDs from many organisms contain three motifs (CP, QFP, and T motifs) that are important for binding TR (Figure 1.5B). Vertebrate TRBDs have an additional vertebrate specific RNA binding motif (VSR) found on the N-terminal portion of the TRBD. All four of these motifs have been shown biochemically to take part in TR binding at some capacity [82,83,85]. Atomic details of this interface have been elucidated with the help of TRBD structures from *Tetrahymena*, medaka, and *Tribolium castaneum.* Each of these structures have been solved in complex with a TR fragment, while the structure of the TRBD from *Takifugu rubripes* (Japanese puffer fish) has been solved in apo form [83,85-89]. In all cases the TRBD is mostly helical with some globular portions with the differences in the structures residing mainly in the N-terminal linker region.

At the far 3' end of the mature RNA lies the H/ACA domain. The H/ACA domain ensures TR stability by acting as a scaffold for proteins such as Dyskerin, GAR1, NHP2, and NOP10 (Figure 1.5A) [90-92]. One such element within the H/ACA domain is the CAB box which is responsible for binding the telomerase accessory protein TCAB1 and essential for Cajal body localization of telomerase [93-95]. TCAB1 can help stimulate telomerase activity through an interaction between its WD40 repeat domain and the CAB box of TR. This interaction stabilizes the CR4/5 domain so that it can interact with the TRBD of TERT creating an active form of telomerase [96]. The recent cryo-EM structure of human telomerase has provided the first structural information as to how the H/ACA domain interacts with dyskerin, GAR1, NHP2, NOP10, and TCAB1 (discussed further below) [97].

1.4.3 Telomerase Reverse Transcriptase (TERT)

The second portion of the telomerase holoenzyme is the reverse transcriptase TERT. TERT is largely made up of four conserved domains: the telomerase essential N-terminal domain (TEN), the TERT RNA binding domain (TRBD), the reverse transcriptase domain (RT), and the thumb domain also called C-terminal extension (CTE) (Figure 1.5B) [98]. Along with the cryo-EM structure of human telomerase, many studies have helped elucidate structural aspects of TERT in ciliates, yeast, and insects among other species.

One major focus of structural studies has been the essential TEN domain. Structural studies in *Hansenula polymorpha* and *Tetrahymena thermophila* suggest that although the TEN domain sequence varies widely between species, the core structure is well conserved (Figure 1.6C and D) [99,100]. Although structural data for the human TEN domain is unavailable, functional data confirms it is essential for recruiting telomerase to telomeres. Mutations in the DAT (Dissociates Activities of Telomerase) region of the TEN domain render the enzyme unable to function *in vivo*, yet it retains catalytic activity *in vitro* (Figure 1.5B) [101]. Indeed *in vivo* telomerase function is rescued by linking the mutant telomerase to either POT1 or TRF2, further suggesting a role for the DAT region in telomerase recruitment to telomeres [102]. Three mutants in the DAT region (K78E, G100V, and R132E) of human telomerase have been implicated in reducing TPP1's ability to stimulate processivity [70,103,104]. Charge-swap experiments suggest a direct interaction between residue K78 in the DAT region of the TEN domain and E215 in the TEL patch of TPP1 [70]. Although establishing this direct interaction was paramount towards building an understanding of telomerase

recruitment, much more remains to be learned regarding the remaining residues of the TEN domain and other regions of telomerase that interact with TPP1. TPP1's OB domain, specifically the TEL patch and NOB regions, are essential for telomerase recruitment to telomeres (Figure 1.4B; *right*) [66,68,69]. Together these data strongly suggest a direct interaction between the TPP1 TEL patch or NOB region and the DAT region in the TEN domain of telomerase.

The TEN domain has also been implicated in binding nucleic acids. HSQC NMR experiments involving primer DNA and template RNA, both alone and as hybrids, titrated with *Hansenula polymorpha* TEN domain revealed that the TEN domain was able to interact more specifically with DNA/RNA hybrids [100]. This supports the fact that the TEN domain helps facilitate recognition of the DNA-RNA template hybrid in the active site [105]. Additionally crosslinking data suggest that the TEN domain binds DNA in a fashion that would allow it to act as an anchor site 5' to the template/DNA duplex [106,107]. The interaction between the TEN domain and DNA/RNA could help facilitate telomerase processivity by helping orient the primer/template hybrid for proper catalysis.

The three subsequent domains make up the TERT ring (Figure 1.5B). The first of these is the TRBD which is responsible for interacting with the CR4/5 domain of TR forming the major interface between TERT and TR (discussed above). Structural information about the rest of the TERT catalytic subunit comes largely from crystal structures of the *T. castaneum* catalytic subunit (TcTERT; Figure 1.7A) and the human CTE domain (Figure 1.6B) [87,88,108]. Structures exist for both non-canonical RNA-DNA hairpin-bound and apo TcTERT [87,88]. Both structures suggest that the catalytic core of the telomerase protein subunit is similar to that of retroviral reverse

transcriptases and viral RNA polymerases [87]. The structure is composed of an RT domain and a CTE, which together form a hand–like structure composed of fingers and palm domains in the RT, and a thumb domain represented by the CTE. Together the TRBD, fingers, palm, and thumb form a ring with a positively charged cavity where the RNA-DNA hairpin resides (Figure 1.7A). This TERT ring interacts with the RNA-DNA hairpin in a manner that orients the RNA template in the active site, generating a conformation that allows for the synthesis of additional nucleotides. To facilitate this, the 5’ end of the RNA interacts with the fingers and palm regions while the thumb interacts with the minor groove formed by the RNA-DNA heteroduplex. A rigid loop in the thumb domain forms the primer grip region that directs the 3’ end of the DNA toward the active site of the protein. The thumb domain is also in close contact with the TRBD and has been shown to interact with CR4/5 through an FVYL motif (Figure 1.5A) [109]. The FVYL motif was further shown to be important in both structural and biochemical studies of the human CTE, where dyskeratosis congenita-associated mutations have been found (Figure 1.6B) [108]. The fingers and CTE also contain residues that have been implicated in recruiting telomerase [68]. The CTE contains a second DAT region called C-DAT that when mutated doesn’t affect telomerase activity *in vitro,* but stops telomerase from maintaining telomere length *in vivo* [110]). Unlike the N-DAT it is less clear if the C-DAT plays a direct role in telomerase recruitment as it wasn’t tested if the *in vivo* telomere shortening phenotype is rescued by linking the mutants to POT1 or TRF2 [110]. Finally, TERT is unique among reverse transcriptases in that it has an insertion in fingers domain (IFD), which has residues that have also been implicated in TPP1 binding [111-113]. Specifically, an IFD mutant, hTERT-V791Y, showed defective

telomerase recruitment and was not stimulated by TPP1 (and POT1) overexpression, suggesting that this mutation interferes with TERT-TPP1 binding. Although the *Tc*TERT structures have yielded unprecedented insight into telomerase structure and function, it should be noted that the *T. castaneum* telomerase RNA subunit has not been identified. Moreover the *Tc*TERT protein lacks a TEN domain and contains a relatively inconspicuous IFD domain. Thus it remains possible that mammalian telomerase has acquired new functionalities relative to its flour beetle counterpart or that these orthologs perform some functions using divergent structural mechanisms.

The most comprehensive structural information available for the telomerase holoenzyme and its associated proteins comes from the human and *Tetrahymena thermophila* telomerase EM structures [114-116]. The negative stain EM structures for the human and *Tetrahymena* enzymes gave the first insights into the organization of the full RNP. The three-dimensional structure of human telomerase shows two globular lobes connected by a flexible linker region suggesting telomerase may form a dimer. This dimer was hypothesized to be formed by the H/ACA domain of TR [114,117]. This quaternary structure remains controversial as some reports suggest human telomerase acts as a monomer while others suggest that dimeric telomerase is the functional enzyme [114,118-120]. Atomic models were built from the low-resolution 23 Å human and 25 Å *Tetrahymena* telomerase EM maps [116]. Recently a more detailed depiction evolved from the cryo-EM structures of *Tetrahymena* and human telomerase that were solved to a resolution of 4.8 Å and 10.2 Å respectively [115,121,97]. The human structure shows an overall bilobal shape similar to the original negative stain EM map, however the cryo-EM structure of human telomerase depicts that one of these lobes

contains the catalytic core of TERT and TR; and the other contains the H/ACA domain bound to the biogenesis protein core composed of one TCAB1, two dyskerin, two NOP10, and two GAR1 protein subunits [97]. Nevertheless a gold labeling experiment shows the presence of a small population of telomerase that is dimeric although the biochemical/biological importance of this, if any, remains unknown [97]. The model built from the cryo-EM map further depicts the formation of a TERT ring similar to that of TcTERT (Figure 1.7B). In 2015 an 8.9 Å structure of *Tetrahymena* telomerase was published [115]. This resolution allowed determination of secondary structure elements and the building of a structural model with the help of solved crystal and NMR structures of the protein subunits (or their close homologs) and the corresponding RNA. This structure, which confirmed the monomeric status of *Tetrahymena* telomerase RNP, allowed the first opportunity to place the TEN domain with respect to the catalytic ring structure of TERT. The *Tetrahymena* TEN domain was modeled above the CTE on the front (active) side of the TERT ring. The template-DNA hybrid falls in close proximity to the TEN domain consistent with NMR data that suggest an interaction between the TEN domain of *Hansenula polymorpha* and DNA-RNA hybrids [100]. The authors were able to identify an RPA-like heterotrimeric TEB1-TEB2-TEB3 complex and also a CST-like complex P75-P45-P19 complex. Interestingly, the TEN domain is part of a complex interaction network with the TPP1 homolog p50, RPA homologs TEB1, and TEB2, and the IFD. The recently published 4.8 Å resolution structure of *Tetrahymena* telomerase reveals the structural details of this complex interaction network even further by providing the first structural information about both p50 and the IFD (Figure 1.8). The IFD forms an L shape that begins with two interacting helices that form the short arm of

the L and are connected by the long arm of the L which is made up of a long extended β-sheet region termed as the TRAP (Figure 1.8). The TRAP is able to interact with the TEN domain, RBD, and RT to form a newly discovered third ring that helps trap the pseudoknot of TR onto the TERT ring [121]. The IFD and TEN domain are shown in close proximity and form a surface on TERT that is in close proximity to p50. p50 forms an OB fold like that of TPP1 (Figure 1.8). It is made up of a six stranded β-barrel that places its TEL patch like region in close proximity to the TEN and IFD [121]. This structure provides the first three-dimensional insights into how telomerase may be recruited to the telomere in the human system and supports the previous data that implicates the importance of the TEN and IFD domains of human telomerase in the enzymes recruitment to the telomere through TPP1.

1.5 Dyskeratosis congenita; a telomerase deficiency disease

While expression of telomerase in somatic cells can have adverse consequences, telomerase expression in stem cells is imperative for continued replication over the course of a species lifespan [21]. Therefore it is not surprising that mutations in telomerase or telomerase-associated factors can lead to a variety of telomerase deficiency diseases called telomeropathies. The most notable telomeropathy is called dyskeratosis congenita (DC). DC is an inherited bone marrow failure syndrome that is initially identified by a diagnostic triad of nail dystrophy, oral leukoplakia, and skin hyperpigmentation [23,22]. Its mode of inheritance can be variable as it has been shown to be X-linked recessive, autosomal recessive, or autosomal dominant [122,123]. Patients with DC also have a predisposition to a variety of cancers, aplastic anemia, liver disease, and pulmonary fibrosis [122]. At a molecular level DC is

characterized by having blood leukocyte telomere lengths in the less than first percentile for the patient's age. Patients with DC often suffer from bone marrow failure as a result of a depleted hematopoietic stem cell pool [123,22,14].

Given that the TEL patch is imperative for telomerase recruitment it can be predicted that mutations in the TEL patch would lead to telomeropathies, such as DC. Indeed a mutation in the OB domain of TPP1 was identified in two separate families, adding it to the list of ten other genes (*DKC1*, *TERC*, *TERT*, *RTEL1*, *TINF2*, *CTC1*, *NOP10*, *NHP2*, *WRAP53*, and *PARN*) that are mutated in patients with DC [124,125]. Our lab was involved in identifying a mutation in a patient that had a particularly severe form of DC called Hoyeraal-Hreidarsson (HH) syndrome [124]. HH Patients have even shorter telomeres than most DC patients, making them susceptible to additional complications such as immunodeficiency, developmental delay, and cerebellar hypoplasia [126,123]. The second patient identified by a separate lab suffered from hematopoietic deficiencies and aplastic anemia, but not HH [125]. Using whole exome sequencing, the two independent research groups found that both patients were heterozygous for an in frame deletion of lysine 170 of TPP1. While deletion of lysine 170 was shown to affect telomerase recruitment and telomerase processivity, it was unclear how lysine 170, which is not part of the TEL patch, impacted telomerase action. While telomeropathies like DC can be devastating, the recent gains in our understanding of the holoenzyme may lead to development of individual therapies that could combat the variety of mutations in telomerase associated genes that lead to telomere shortening seen in patients.

1.6 Dissertation outline

Although previous studies by our lab and others have identified individual patients suffering from telomeropathies with an in frame deletion of lysine 170 in TPP1 protein, the mode of action of this mutation was unclear. Chapter 2 contains structural, biochemical, and genetic data that describe in detail how an in frame deletion of lysine 170 in TPP1 affects telomerase action. Biochemical and cell biological assays were performed to show how deletion of lysine 170, but not its substitution to alanine, impaired telomerase localization and function at telomeres. Crystal structures of the OB domain of TPP1 harboring either the lysine deletion or a lysine to alanine substitution showed how the disease mutation altered the orientation of two critical glutamates in the TEL patch. Ultimately, CRISPR-Cas9 technology was used to introduce one copy of TPP1 K170Δ into HEK293T cells and demonstrate progressive telomere length shortening over time – recapitulating the cellular hallmark of DC and other telomeropathies. Chapter 2 is an adaption of a research paper published in *Proceedings of the National Academy of Sciences of the United States of America* in 2016 [127].

While the surfaces on TPP1 that are responsible for recruiting telomerase have been studied extensively, the corresponding surface on telomerase that interacts with TPP1 has remained largely elusive. Biochemical, crystallographic, and EM studies have begun to elucidate many important details about telomerase. These studies provide insight into how its RNA and protein subunits work together to synthesize nucleotides at the extreme ends of chromosomes. Recent cryo-EM structures of both human and *Tetrahymena* telomerase have shed light on the overall organization of this

complex holoenzyme. The most recent 4.9 Å *Tetrahymena* telomerase structure gives the first structural information on how telomerase might be recruited to the telomere, building on the biochemical experiments that identified the TEN domain and IFD of TERT as being critical elements for this process. Still it is not known what surface on telomerase is involved in the interaction with the TEL patch and NOB region of TPP1. Chapter 3 focuses on using an alanine scanning mutagenesis screen to uncover regions in both the TEN domain and IFD that are important for recruitment of telomerase through its interaction with TPP1. Mutations that were found to affect telomerase recruitment were subjected to two additional tests to determine how they affect the ability of POT1-TPP1 to stimulate telomerase processivity and the ability of telomerase to maintain telomere length *in vivo*. Finally, Chapter 4 discusses conclusions and ongoing work along with future directions for the research presented in Chapters 3 and 4.

1.7 Figures

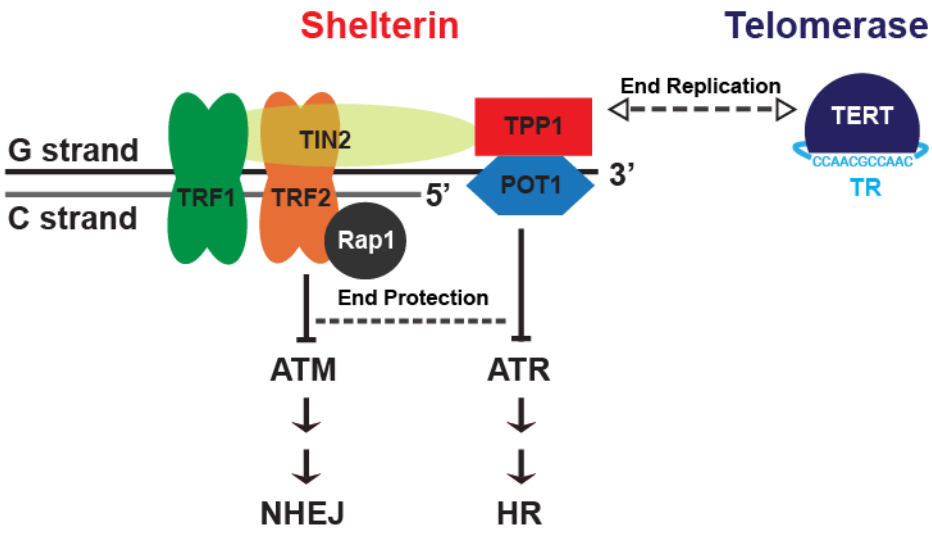

Figure 1.1 The shelterin complex facilitates end protection and end replication. Schematic showing the six proteins of the shelterin complex (TRF1, TRF2, RAP1, TIN2, TPP1, and POT1) protecting chromosome ends from ATM and ATR mediated DNA damage response. The schematic also depicts how the shelterin complex is able to facilitate end replication by recruiting telomerase to the telomere through TPP1.

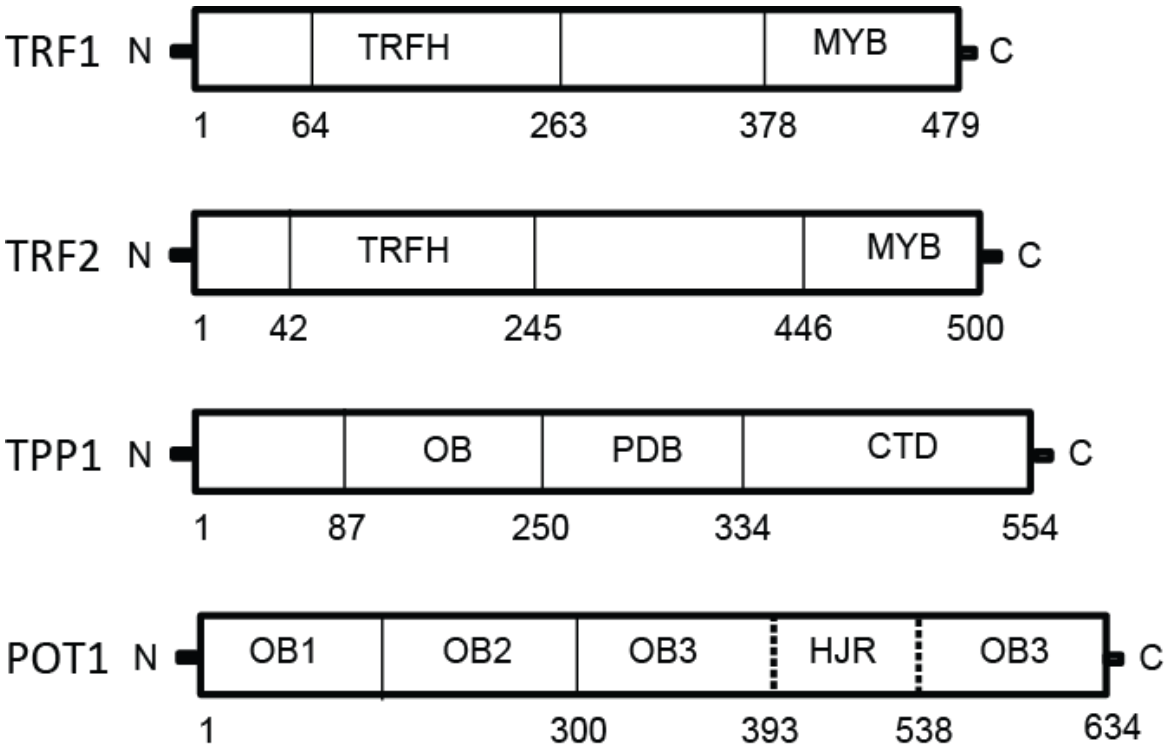

Figure 1.2 Domain diagrams of TRF1, TRF2, TPP1, and POT1.
Domain diagrams of the four shelterin proteins discussed in detail in the text. TRFH: TRF homology domain. OB: oligonucleotide/oligosaccharide-binding domain. PDB: POT1 binding domain. CTD: C-terminal domain. HJR: Holliday junction resolvase like domain.

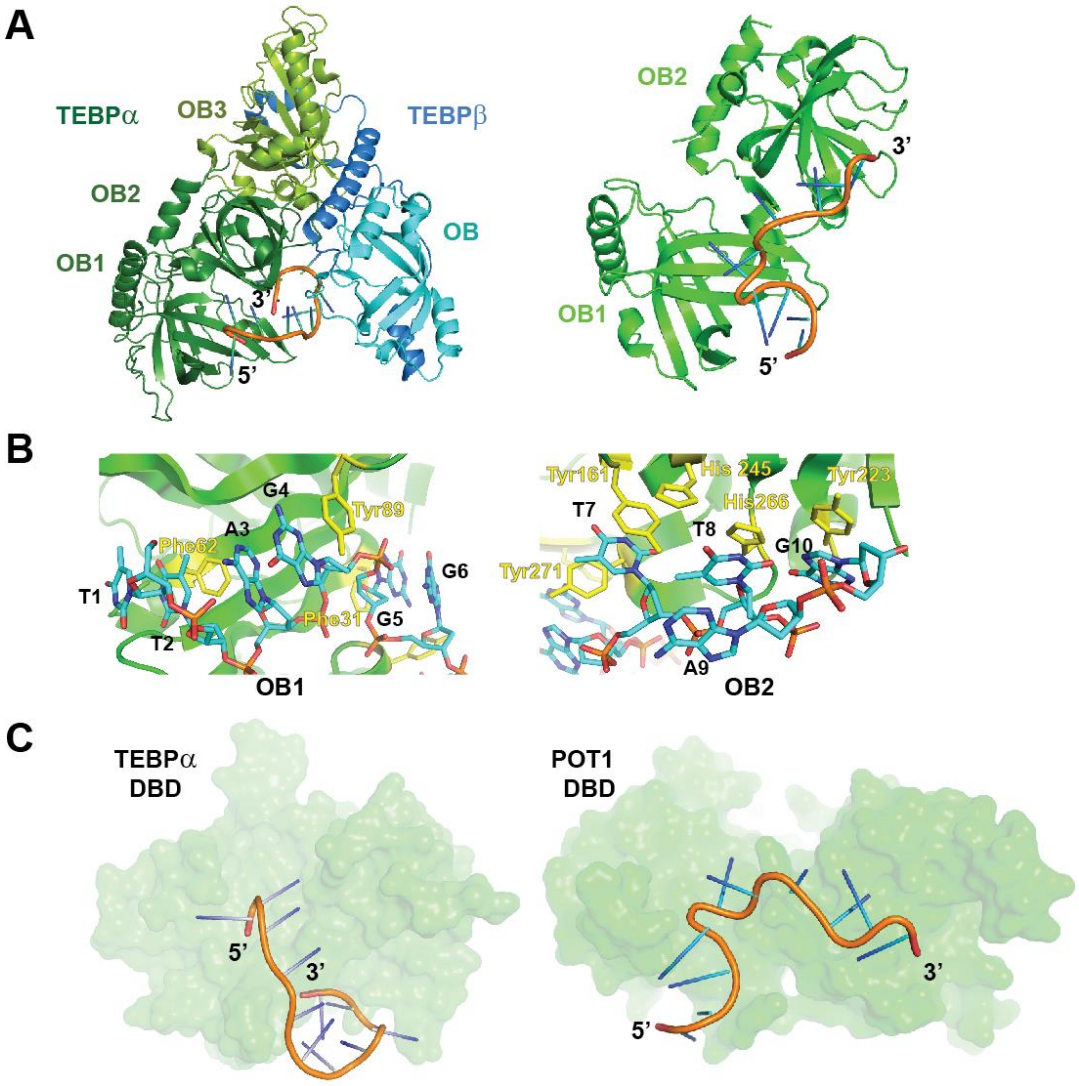

Figure 1.3 Single stranded DNA end protection.
(A) Left: the solved crystal structure of the TEBP-α-β in complex with ss DNA (5'-d(GGGTTTTGGGG)-3') (PDB ID: 2I0Q). The DBD and TEBP-β binding domain of TEBP-α are shown in forest green and split pea green, respectively. The TEBP-α binding domain and OB domain of TEBP-β are shown in blue and cyan, respectively. Right: The human POT1 DNA binding domain (DBD; PDB ID: 1XJV) shown in green in complex with telomeric DNA (5'-d(TTAGGGTTAG)-3'). The DNA is shown in cartoon representation. B) Views showing stacking interactions between the two OB domains of hPOT1 DBD and telomeric DNA. The stacking protein and DNA residues are shown in stick representation. C) Views of TEBP-α DBD in complex with telomeric DNA (left; from the TEBP-α-β-DNA structure) and POT1 DBD in complex with telomeric DNA (right) to highlight the different tracks adopted by the DNA molecules in the two structures. The proteins are shown in surface representation and the DNA is rendered in cartoon representation.

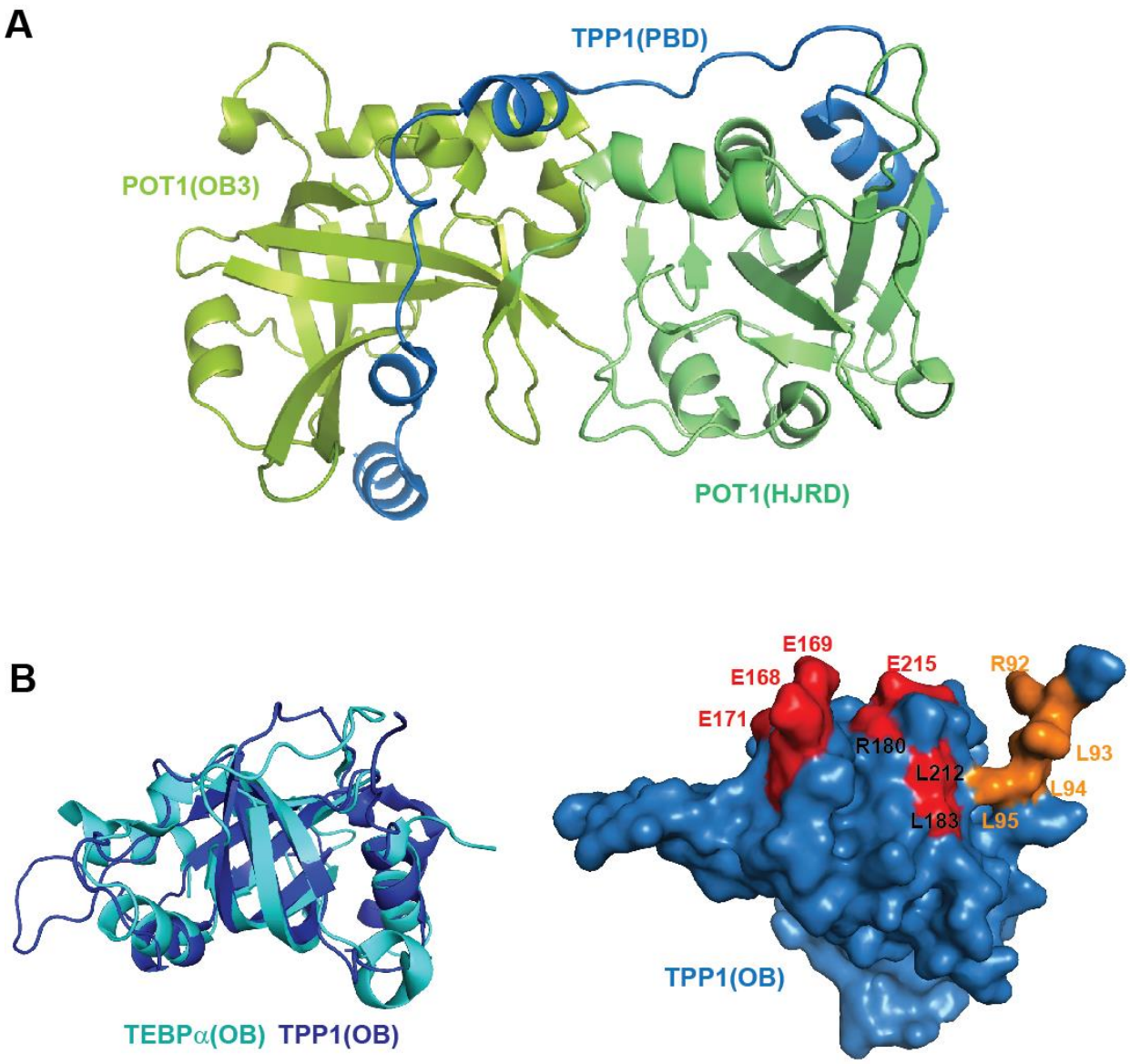

Figure 1.4 Structures of TPP1 domains.
(A) The crystal structure of the C-terminal domains of POT1 (green) in complex with the POT1 binding domain (PBD) of TPP1 (blue) (PDB ID: 5UN7 and 5H65). B) Left: Overlay of the human TPP1 OB domain (dark blue; PDB ID: 2I46) and the OB domain of TEBP-β (cyan; PDB ID: 2I0Q). Right: Surface view of the TPP1 OB domain. TEL patch residues are shown in red and NOB residues are shown in orange.

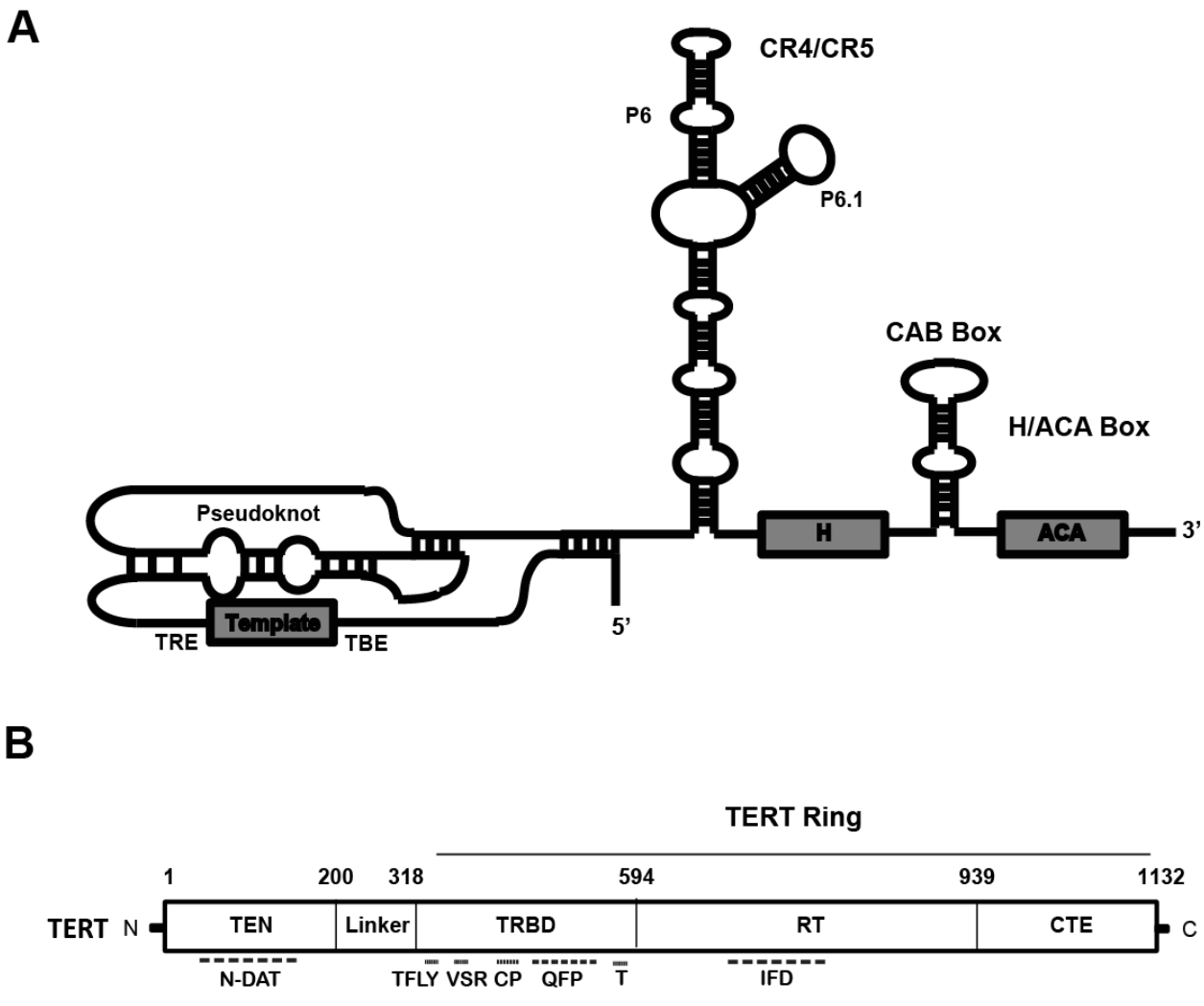

Figure 1.5 Domain layout of Telomerase RNA and Telomerase Reverse Transcriptase.
(A) Cartoon of the secondary structure of human telomerase RNA (TR). TRE: Telomerase Recognition Element. TBE: Telomerase Boundary Element. Secondary structure adapted from figures in Schmidt et al. *Genes and Development* 2015, and Nguyen et al. *Nature* 2018. (B) Domain diagram of human TERT shown with several functional elements; the position of the IFD is highlighted in the reverse transcriptase domain. TEN: telomerase N-terminal domain, TRBD: telomerase RNA binding domain, RT: reverse transcriptase domain, CTE: C-terminal extension, N-DAT: N-terminal dissociates activities of telomerase, VSR: vertebrate-specific recognition motif, IFD: insertion in the fingers domain.

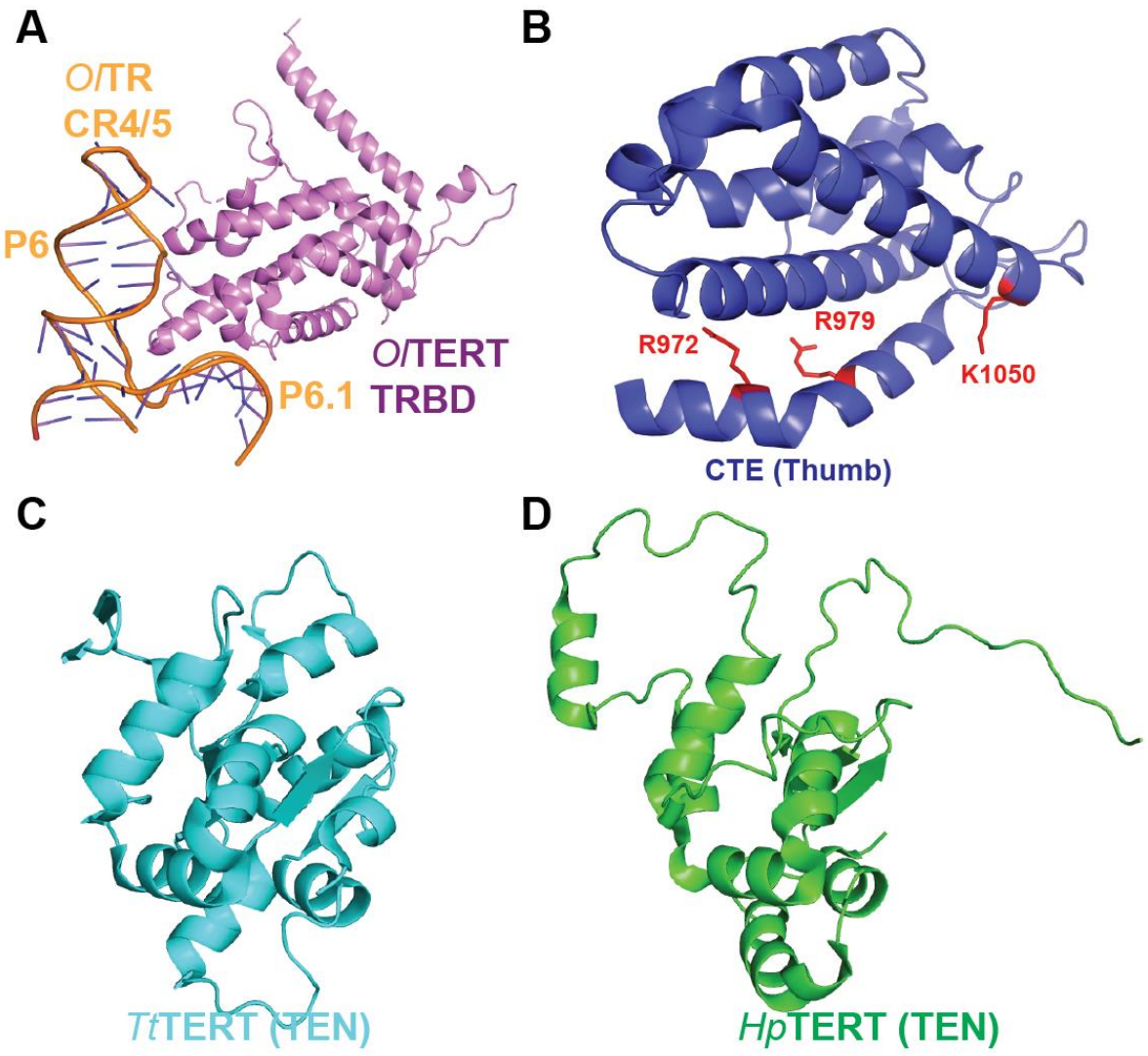

Figure 1.6 Solved structures of telomerase domains.
(A) *Oryzias latipes* TERT RNA binding domain (TRBD) bound to the CR4/5 domain of cognate TR (PDB ID: 4O26). (B) Atomic resolution structure of the CTE (thumb) domain of human TERT (PDB ID: 5UGW). Dyskeratosis congenita (DC) associated mutations are highlighted in red. (C) Crystal structure of Tetrahymena telomerase TEN domain (PDB ID: 2B2A). (D) NMR structure of the *Hansenula polymorpha* TEN domain (PDB ID: 5LGF).

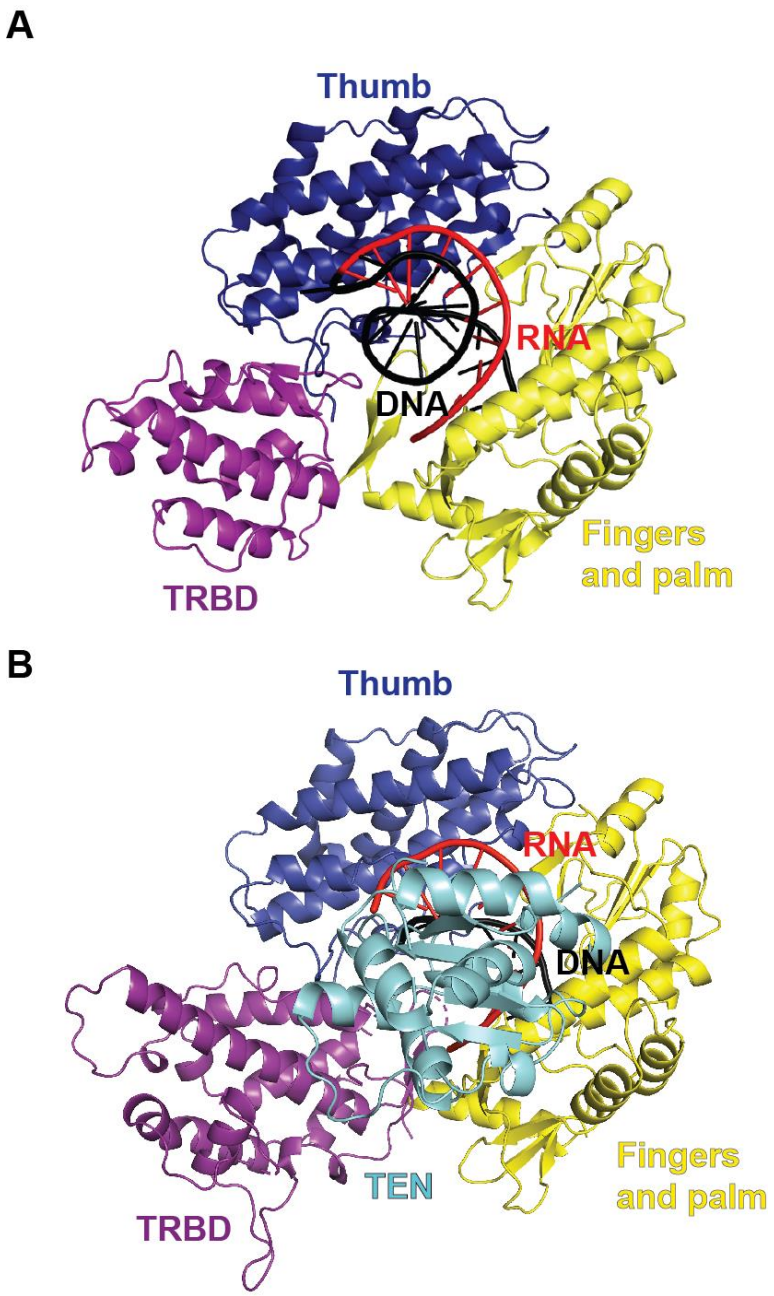

Figure 1.7 Structure of the TERT ring from *Tribolium castaneum* and human telomerase.
(A) The *Tribolium castaneum* TERT ring bound to an RNA-DNA hairpin (PDB ID: 3KYL). Nucleic acid is rendered in cartoon representation with the RNA in red and DNA in black. The TRBD domain is shown in purple, the fingers and palm are shown in yellow, and the thumb is shown in blue. (B) The human TERT ring bound to an RNA-DNA complex (PDB from supplementary information of Nguyen et al. *Nature* 2018). Nucleic acid is rendered in cartoon representation with RNA in red and DNA in black. The TRBD is shown in purple, the RT domain (fingers and palm) are shown in yellow, the CTE (thumb) is shown in dark blue, the TEN domain is shown in cyan.

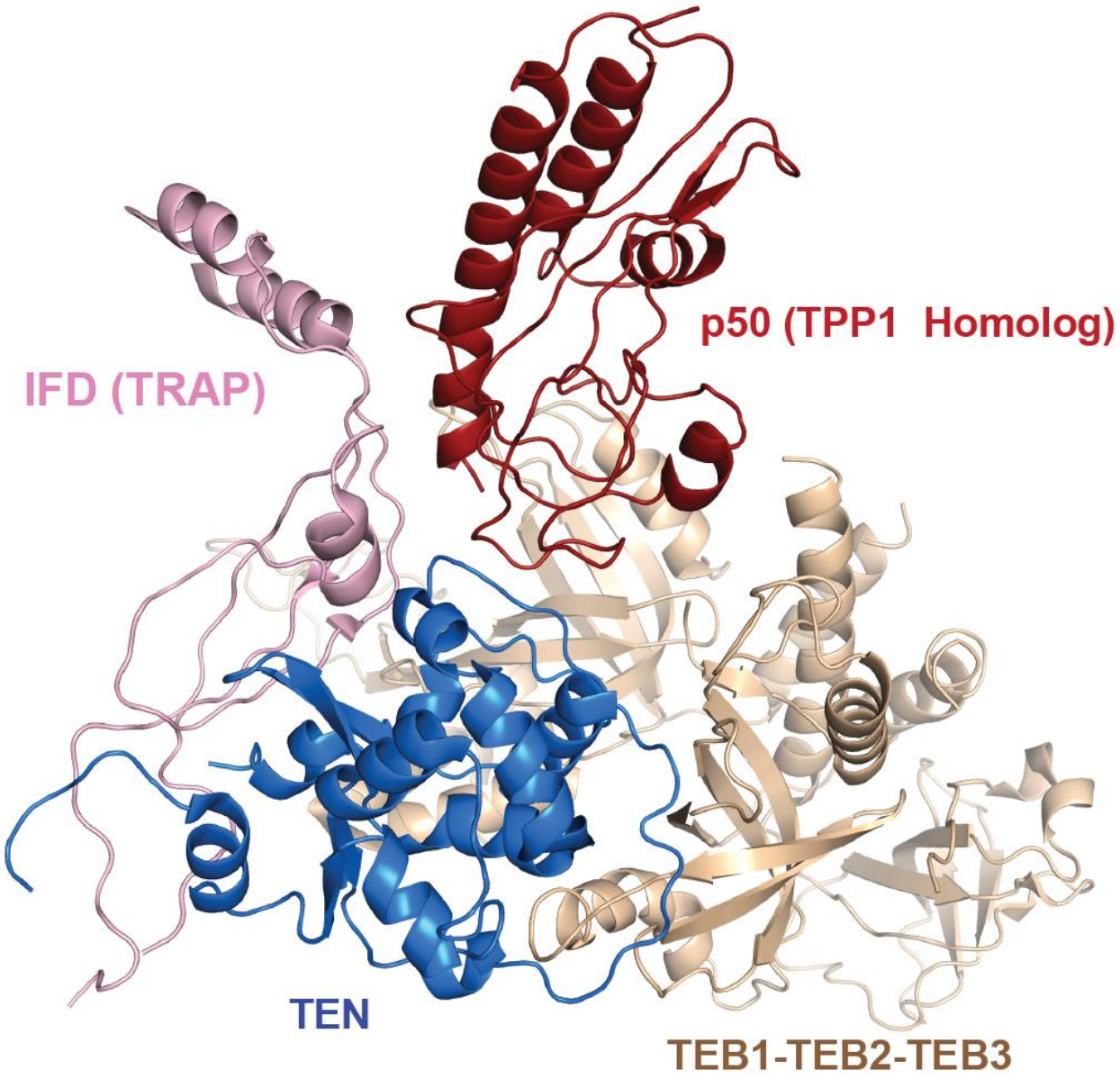

Figure 1.8 Structure of the TEN, IFD, P50, and TEB complex of *Tetrahymena* telomerase.
Close up view of the model of the Tetrahymena telomerase structure built from the 4.8 Å cryo-EM map (PDB ID: 6D6V) that includes p50 (red), the TEB1-TEB2-TEB3 complex (brown), the TEN domain (blue), and the IFD(TRAP) (light pink).

Chapter 2

A mutation in the telomeric protein TPP1 causes dyskeratosis congenita[2]

2.1 Abstract

Telomerase is a unique ribonucleoprotein complex that helps solve the end replication problem by synthesizing telomeric repeats at the ends of linear chromosomes. This action is important to facilitate continued cell division in cell types such as germ line and stem cells. In fact mutations in telomerase and telomere associated genes can lead to a variety of stem cell failure diseases. The most prominent of these diseases is called dyskeratosis congenita (DC). Here we describe the structural and functional consequences that an in frame deletion of amino acid K170 found in the OB domain of TPP1 protein has on telomere biology.

[2] A modified version of this chapter is published in Proceedings of the National Academy of Sciences (DOI: 10.1073/pnas.1605685113)) I expressed and purified the proteins used for the primer extension assays and pull down experiments. I performed pull down experiments and carried out IF-FISH experiments to test for telomerase recruitment. Both Valerie Tesmer and I quantified all IF-FISH images. I purified protein, obtained crystals, and solved the structures of TPP1 constructs. Together Kamlesh Bisht and I performed the telomere ChIP experiments and the first replicate of the telomerase assay in Figure 2.1. I performed the telomerase assay in Figure 2.2. The WT TPP1 and the E169A/E171A stable cell lines were created by Jayakrishnan Nandakumar as previously described [5]. Kamlesh Bisht created the K170Δ and K170A stable cell lines, CRISPR cell lines, performed TRF blots, and performed the mutant mixing telomerase assays. He also performed replicates of the primer extension assay in Figure 2.1.

2.2 Introduction

The discovery of the TEL patch of TPP1 prompted the prediction that this region could be a hotspot for mutations that cause telomerase-deficiency diseases such as DC. Our lab and others recently reported a case of a severe variant of DC, Hoyeraal-Hreidarsson syndrome (HH) [124], in which the proband was heterozygous for a deletion of a single amino acid of the TPP1 protein, namely, lysine 170 (K170) [124]. This study placed TPP1 on a list with ten other genes (DKC1, TERC, TERT, RTEL1, TINF2, CTC1, NOP10, NHP2, WRAP53, and PARN) that are found mutated in DC and other telomere-related disorders [128]. Indeed, a heterozygous TPP1 K170Δ mutation was also reported in another unrelated family, where it was implicated in causing aplastic anemia and other related hematopoietic complications in the proband [125]. In both families, the presence of the K170Δ mutation correlated strongly with short telomeres. Transient overexpression of K170Δ in cultured human cells resulted in a decrease in telomerase recruitment [125,124] and a reduction in the ability of TPP1 to stimulate telomerase processivity (the ability of telomerase to continue DNA synthesis without dissociating from a bound primer) [124]. These results invoke a direct role for the K170Δ mutation in reducing telomerase function in dividing cells. However it is unknown whether the heterozygous K170Δ mutation is sufficient to cause telomere shortening in dividing human cells without additional genetic modifiers.

The placement of K170 directly adjacent to E168, E169, and E171 strongly suggests that this amino acid facilitates the ability of the TEL patch to recognize telomerase. However, inspection of the crystal structure of the OB domain of wild-type (WT) TPP1 revealed that the side-chains of E168, E169, and E171, but not K170, are

exposed to the solvent (Figure 2.1A) [64]. This suggests that E168, E169, and E171 are poised to interact with telomerase, consistent with the deleterious consequences associated with alanine mutations of these residues [66,67,129]. In sharp contrast, the side-chain of K170 is buried in the TPP1-OB structure, making a cation-π interaction with the aromatic ring of W167 (Figure 2.1A). It is therefore unclear how deletion of this residue ultimately translates into reduced telomerase function. Here, we performed a series of biochemical, cytological, genetic, and X-ray crystallographic experiments to show that deletion of K170 (i) disrupts the spatial positioning of critical glutamate residues in the TEL patch; (ii) is sufficient to cause telomere shortening when present in a heterozygous context; and (iii) does not elicit dominant negative effects on the wild-type protein. Together these studies provide valuable insights into the role of TPP1 in telomere length regulation, and help reveal the molecular underpinnings of telomerase deficiency diseases such as DC.

2.3 Results

2.3.1 Deletion of K170, but not its substitution to alanine, reduces telomerase processivity

The deleterious effect of the TPP1 K170Δ mutation on telomerase processivity is not due to a defect in binding to POT1 as K170Δ binds POT1 similar to WT TPP1 protein (Figure 2.2A). To further understand the molecular basis of telomerase deficiency caused by this DC mutation, we engineered a K170A mutation in the TPP1-N vector for expression in *E. coli.* [TPP1-N encodes amino acids 90-334 of human TPP1, a construct of TPP1 that is sufficient for binding POT1 and telomerase, and amenable to *in vitro* studies [64].] TPP1-N constructs of K170A, WT, K170Δ, and E169A/E171A (EE-

AA) proteins were purified as described previously [64,130] (Figure 2.2B). We performed direct primer extension assays to determine how each of the TPP1-N variants contributes to telomerase processivity in the presence of POT1 (Figure 2.1B and C). The WT protein displayed the expected increase in telomerase processivity [64], giving rise to a large fraction of longer DNA products. Both K170Δ and E169A/E171A failed to increase telomerase processivity to WT TPP1-N levels as expected from previous studies (Figure 2.1B and C) [124,66]. Strikingly, mutation of K170 to alanine resulted in only a modest reduction in telomerase processivity (Figure 2.1B and C) that was not statistically significant in experiments performed in triplicate ($P = 0.08$). This result suggests that the positive charge of K170 is not critical for telomerase processivity. In sharp contrast, E169D/E171D (glutamate → aspartate mutations that retain negative charge), but not E169Q/E171Q (glutamate → glutamine mutations that are iso-steric and polar but lack the negative charge), was able to stimulate telomerase processivity (Figure 2.2C). These results are fully consistent with the structure of TPP1-OB WT, which indicates that the glutamates, but not K170, of the TEL patch loop are accessible to telomerase.

2.3.2 Deletion of K170, but not its substitution to alanine, reduces telomerase recruitment to telomeres and telomere lengthening

Given that deletion of K170 reduces telomerase processivity but substitution of K170 to alanine does not, we next asked how K170A impacts telomerase recruitment. To this end, we engineered HeLa cell lines stably expressing either FLAG-TPP1 K170A or FLAG-TPP1 K170Δ protein using the Flp-recombinase based single-site integration strategy [66]. We analyzed two clones each of FLAG-TPP1 K170A and FLAG-TPP1

K170Δ in parallel with FLAG-TPP1 WT and E169A/E171A clones that have been characterized previously (see Figure 2.3C for FLAG immunoblots). We performed immunofluorescence (IF) to detect FLAG TPP1 and fluorescence in situ hybridization (FISH) against TR to detect telomerase localization in HeLa cells transiently overexpressing telomerase [66] The K170A mutation did not negatively impact telomerase recruitment, as telomerase was readily detectable at 90% of the FLAG-TPP1 foci in cells stably expressing K170A (Figure 2.3A and B). In sharp contrast, telomerase recruitment was inefficient in K170Δ and E169A/E171A cells, which exhibited 34% and 7% telomerase recruitment to telomeres, respectively. These studies are in agreement with a previous study showing a severe (10-fold) reduction in recruitment of TERT to TPP1-OB E168R that was tethered to a LacO repeat array, but only a modest (< 2-fold) defect when K170A was used [68].

Because the K170A mutation had only a modest effect on telomerase recruitment and processivity, we anticipated that overexpression of K170A will elongate telomeres akin to observations with overexpression of WT TPP1 [65,66,129]. In contrast, K170Δ overexpression would be expected to result in short telomeres, as observed with E169A/E171A overexpression (15). Indeed, overexpression of K170A resulted in elongation of telomeres (Figure 2.4A). The modest reduction in the slope of telomere lengthening in the two K170A clones compared to the WT clone (Figure 2.4B) is in agreement with similar effects seen in the telomerase processivity and recruitment results presented here and in previous LacO-tethering studies [68]. In sharp contrast, overexpression of K170Δ failed to lengthen telomeres as a function of time in culture (Figure 2.4A and B). The telomere shortening rate and the final telomere length of both

K170Δ clones were very similar to that of the E169A/E171A clone shown here and that of other E169A/E171A clones described previously [66]. This is the first demonstration of a cause-effect relationship between the K170Δ mutation and telomere shortening in human cells, providing the most direct evidence so far for the causative role that this mutation plays in telomere biology disorders.

2.3.3 Deletion of K170 results in a major restructuring of the TEL patch

The results presented thus far, considered with the structure of TPP1-OB WT, support the hypothesis that the side-chain of K170 is not involved in binding telomerase directly. To gain a deeper understanding of how this portion of the TEL patch recognizes telomerase, we crystallized TPP1-OB K170Δ and TPP1-OB K170A under conditions similar to those that yielded TPP1-OB WT crystals [64]. We solved the structure of these mutant proteins to 3.0 Å with molecular replacement using the WT structure as the search model (see Table 2.1 and Methods). The overall three dimensional structures of the two mutants are very similar to that of the WT structure (Figure 2.5A). The r.m.s. deviations of the Cα backbone (total of 282 Cα atoms aligned) for the WT vs. K170Δ, WT vs. K170A, and K170Δ vs. K170A structures were 0.3Å, 0.4 Å, and 0.3 Å, respectively. However, and consistent with the functional data presented here, a unique feature present in the WT and K170A structures was conspicuously absent in the K170Δ structure. This feature is a bulge in the loop containing residues W167, E168, E169, K170, and E171 that we term the TEL patch “knuckle” (see Figure 2.1A). This feature is absent in the K170Δ structure, as can be discerned in the overlay of the overall three-dimensional structures (Figure 2.5A) as well as the 2Fo – Fc electron density for this region (Figure 2.5B). Deletion of the entire K170 residue

displaces two of the critical TEL patch glutamates, E168 and E169, by 3.1 Å and 3.6 Å (at Cα positions), respectively, relative to their positions in the WT structure. In contrast, E168 and E169 residues are almost superimposable between the WT and K170A structures (Figure 2.5B). Although the electron density for side-chain atoms in the TEL patch loop is less well-defined compared to that for the main chain atoms in each of the three structures, it is reasonable to conclude that the large displacements of the Cα positions of E168 and E169 between the WT and K170Δ structures will translate to comparable displacements of the respective side-chain atoms (Figure 2.5C). Together, our results demonstrate that the main chain atoms of K170 facilitate a conformation of the TEL patch that presents the critical, negatively charged E168 and E169 side-chains for a productive electrostatic interaction with telomerase.

2.3.4 A single K170Δ allele is sufficient to cause telomere shrinkage in cultured human cells

The data presented thus far provide strong evidence and a structural rationale for a causal role of the TPP1 K170Δ mutation in telomerase dysfunction. However it is still unclear how this mutation, present in a heterozygous state in two unrelated families [124,125] is sufficient to cause severe telomere shortening. It is possible that other disease modifiers cooperate with K170Δ to cause telomere shortening in these families. However, our overexpression studies demonstrating that the K170Δ mutation reduces telomerase function (Figure 2.1 and Figure 2.2) support the alternative possibility that reducing the dose of a functional TEL patch to half is sufficient to cause telomere shortening via either haploinsufficiency or dominant negative effects of the mutation. Such overexpression studies are not suitable for distinguishing between

haploinsufficiency versus dominant negative effects, because TPP1 overexpression in these cells is 25-fold above endogenous levels [66]. The overexpressed mutant protein will completely replace endogenous WT protein at telomeres [because of competition of binding to TIN2, which recruits TPP1 to telomeres [53], causing the telomeres to resemble the homozygous state. To recapitulate the heterozygous nature of the K170Δ in the absence of overexpression caveats, we introduced the K170Δ mutation in HEK 293T cells using CRISPR-Cas9 technology [131,132]. Figure 2.6A shows the general scheme for cleavage of the ACD gene (which codes for the TPP1 protein) by three guide RNAs (g1, g2 and g3). Using transient transfection of plasmids encoding Cas9 and guide RNAs, we observed efficient cleavage of the gene coding for TPP1 with each of the three guide RNAs, and with a cocktail of the three guides (as inferred from the Surveyor nuclease assay; Figure 2.6 B; Methods). We were unable to detect the cleavage of the top predicted off-targets [133] of guide RNAs 2 or 3 (Figure 2.6C). Based on these results, we proceeded to cleave the TPP1 locus in HEK 293T cells using a combination of guides 2 and 3. Mutagenic single-stranded oligo-deoxyribonucleotide donors (ssODNs) were used as the substrate for homology-directed repair (HDR) of the cleaved locus.

To introduce precise changes in the human ACD gene coding for human TPP1 protein we designed two different ssODNs. The first contained the K170Δ mutation, while the second harbored only silent mutations in the coding region of TPP1 (Figure 2.6A). The latter ssODN upon integration in the genome would yield cells expressing WT TPP1. However these cells would have been subjected to the same conditions (e.g. identical guide RNA mediated cleavage) experienced by K170Δ-edited cells. These

silently-edited WT cells, which we refer to as WT* cells, served as the control against which we compared K170Δ-edited cells. Each ssODN contained additional silent mutations to serve two purposes. The first set of silent mutations destroyed the protospacer/ PAM sequences to prevent cleavage of the gene coding for TPP1 by Cas9 post-repair (Fig. 2.6A). The second set of silent mutations introduced a KpnI restriction site to facilitate the screening of clones (Fig. 2.6A). Evidence for editing was readily observed in both WT* and K170Δ transfection experiments based on the results of the KpnI screening assay (Figure 2.6D; Methods). The fraction of the intensities of the digestion products relative to that of the undigested products indicated the efficiency of intended mutagenesis (i.e. fraction of HEK 293T cells that were edited), which we determined to be ~5%. Next, we proceeded to isolate clones containing the K170Δ (or the WT*) mutation by diluting these transfected cells.

We isolated clones that contained either the WT* mutation or the K170Δ mutation. The presence of the edited allele/s was inferred from KpnI digestion profiles and Sanger DNA sequencing of the TPP1 locus (Figure 2.6E; Table 2.2). Sanger DNA sequencing of the TPP1 locus in all isolated clones was consistent with the presence of three TPP1 alleles in HEK 293T cells. This was also in agreement with chromosome-specific centromere FISH experiments showing that HEK 293T cells are triploid for chromosome 16, which contains the gene coding for TPP1 (Figure 2.7A). Partial but not total digestion by KpnI of PCR amplicons spanning the edited site suggested that the WT* and K170Δ clones were heterozygous for the engineered mutations (Figure 2.6E). DNA sequencing further revealed that in all WT* and K170Δ clones, the third TPP1 allele underwent erroneous repair that resulted in gross insertion/deletion mutations

("indels") in the TPP1 gene (detailed sequence information in Table 2.2). Therefore the WT* clone was bi-allelic for WT TPP1 TEL patch function (Δ/wt*/wt*), representing more closely the status of the TPP1 gene in normal human cells (Table 2.2). The two clones containing K170Δ were also bi-allelic for TPP1, containing one K170Δ allele and one WT allele (Δ/K170Δ/wt), representative of the K170Δ genotype in individuals harboring this mutation (Table 2.2). All of the bi-allelic TPP1 clones showed a reduction in TPP1 protein levels compared to the unedited cell line, as expected from the loss of one allele (Figure 2.7B).

We performed telomere restriction fragment blots to determine the effect of the heterozygous K170Δ mutation on telomere length. The WT* clone maintained telomere length in a stable manner similar to unedited HEK 293T cells (Figure 2.7C). This result suggests that two copies of the TPP1 gene are sufficient for telomere length maintenance in HEK 293T cells; and that our genome editing strategy did not result in any unexpected changes in telomere length. Both clones that were heterozygous for the K170Δ mutation showed telomere shortening as a function of time in culture (Figure 2.7C). This result demonstrates that a single copy of the K170Δ allele is sufficient to decrease telomere length in proliferating human cells.

2.3.5 Presence of K170Δ does not alter the ability of WT TPP1 to facilitate telomerase function

The ability of a single TPP1 K170Δ allele to elicit telomere shortening may be explained either by dominant-negative effects of the mutant protein on the WT protein or simply by a reduced dosage of WT TPP1 protein. The possibility of a dominant-negative mechanism becomes relevant in light of a study invoking TPP1 dimerization through its

OB domain in an Akt1-mediated phosphorylation-dependent manner [114]. Some studies also suggest that the human telomerase holoenzyme functions as a homodimer, although other studies contradict this notion [114,134,97]. To directly test for dominant-negative effects of the TPP1 K170Δ protein, we first performed telomerase-catalyzed primer-extension assays involving two types of mutant-WT TPP1 protein-mixing experiments. In the first type of experiment, all reactions included TPP1-N WT protein at a constant concentration of 200 nM (and POT1 protein at a constant concentration of 500 nM). TPP1-N K170Δ was titrated into these reaction mixtures (before addition of telomerase). As shown in Figure 2.8 A, addition of TPP1-N WT in the absence of K170Δ shows the characteristic stimulation of telomerase processivity (Figure 2.8A, compare lanes 1 and 2) [66,64]. Addition of TPP1-N K170Δ protein in sub- or superstoichiometric amounts to 200 nM TPP1-N WT failed to reduce telomerase processivity (Figure 2.8A, compare lanes 3–5 with lane 2). In the second experiment, we added increasing amounts of WT TPP1 protein to reactions containing K170Δ protein held at a constant concentration of 200 nM. Substoichiometric amounts of WT protein were sufficient to stimulate telomerase processivity in the presence of 200 nM K170Δ protein (Figure 2.8A, compare lanes 14–16 with lane 10). These results suggest that the K170Δ protein does not exert any negative effects over the ability of WT TPP1 protein to stimulate telomerase processivity in vitro.

Next, we performed mutant-WT TPP1 mixing telomerase recruitment experiments in HeLa cells using IF-FISH. In these experiments, we transfected HeLa cells with a myc-tagged TPP1 WT-expressing plasmid (plus an empty vector plasmid), a FLAG-tagged TPP1 K170Δ-expressing plasmid (plus an empty vector plasmid), or a

mixture of plasmids for myc-tagged TPP1 WT and FLAG-tagged TPP1 K170Δ coexpression. Coexpression of TPP1 WT protein at levels comparable to that of TPP1 K170Δ (Figure 2.8B) resulted in the efficient rescue of the telomerase recruitment defect (Figure 2.8C). We conclude from these experiments that TPP1 WT colocalizing with TPP1 K170Δ at telomeres is able to recruit telomerase to these foci.

Next, we performed telomere ChIP experiments [60]. For this, HeLa 1.2.11 cells were transfected with plasmids encoding TERT, TR, and either TPP1 WT, TPP1 K170Δ, or a mixture of plasmids to express both TPP1 constructs. Immunoprecipitations were performed with an anti-TERT antibody and the associated telomeric DNA signal was detected using Southern dot blots (Figure 2.8D). Although an ~20% reduction in the amount of telomerase associated with telomeres was observed for K170Δ relative to WT, there was no evidence of a telomerase recruitment defect when a mixture of the TPP1 constructs was present in the cells.

Finally, we performed a CRISPR-Cas9 knockout experiment to isolate HEK 293T clones containing only one functional copy of the gene coding for TPP1 (Δ/Δ/wt). Comparison of these cells to the K170Δ-edited cells described above (Δ/K170Δ/wt) could reveal any dominant-negative effects of K170Δ. Using the same CRISPR-Cas9 strategy described above, we isolated a HEK 293T clone that contained only one unedited allele of the gene coding for TPP1 (Δ/Δ/wt) (Table 2.2). As expected, the TPP1 protein level in Δ/Δ/wt cells was less than in Δ/wt/wt cells or in unedited cells (wt/wt/wt) (Figure 2.9A). Telomere length measurements as a function of time in culture demonstrated that Δ/Δ/wt cells exhibited robust telomere shrinkage (Figure 2.9B). Telomere shortening in Δ/Δ/wt cells was accelerated compared with that in Δ/K170Δ/wt

cells (Figure 2.9C), clearly ruling out any dominant-negative effect of the K170Δ mutation. The milder telomere shortening phenotype in Δ/K170Δ/wt cells compared with the Δ/Δ/wt cells is consistent with the modest (yet reproducible) ability of TPP1 K170Δ protein to stimulate telomerase processivity relative to the “no TPP1” control (Fig. 2.1B)

Combined, our biochemical and cytological experiments failed to reveal a dominant-negative role of the K170Δ mutation in telomerase action. Therefore, telomere shrinkage in cells of individuals harboring the TPP1 K170Δ mutation is likely caused by reduced dosage of a functional TEL patch.

2.4 Discussion

Here, we solved the structure of a human protein mutant associated with DC. The TPP1–OB K170Δ structure clearly reveals the loss of a structural motif that we term the TEL patch “knuckle.” Loss of this motif rearranges the spatial positioning of glutamates E168 and E169 that are critical for telomerase recruitment and action at telomeres. Our structures provide a straightforward structural rationale for telomerase-deficiency caused by K170Δ, and inspire the search for small molecules that can rescue the telomerase-binding defect of the K170Δ mutation. In addition, our structures also detail the precise contribution of the affected amino acid K170 to telomerase function. Given that K170A does not substantially alter stimulation of telomerase processivity, telomerase recruitment, or the conformation of the TEL patch knuckle, we conclude that K170 side-chain does not bind telomerase directly, but rather facilitates a productive TEL patch conformation for binding telomerase. The modest reduction in telomerase function caused by K170A observed here and in previous studies (17) is not easily explained by our crystal structures. We envision that the cation–π interaction between

the K170 side-chain and W167 (Figure 2.1A) contributes to the dynamics (or lack thereof) of the TEL patch knuckle in a manner that is (modestly) conducive to telomerase binding, but not captured by our (static) crystal structures.

Gene therapy against DC will only be effective or justified if the disease mutation is sufficient to cause the underlying cellular phenotype (telomere shortening). Here, we used CRISPR-Cas9 technology to introduce the K170Δ mutation in HEK 293T cells. Our results clearly demonstrate that presence of a single allele of K170Δ is sufficient to reduce telomere length, ruling out the necessity of other genetic modifiers to elicit this effect. This is especially pertinent to the individual with Hoyeraal–Hreidarsson syndrome in our recent study, who inherited a TPP1 P491T variant (on a separate allele) in addition to the K170Δ mutation [124]. Our studies make the prediction that reversing the K170Δ mutation in the presence (or absence) of P491T will stall telomere shortening. However, our gene-editing studies are limited to one cell line. In this regard, a previous study by Sexton et al. [67] in human embryonic stem cells (hESCs) failed to elicit a telomere length phenotype when a TPP1 mutant lacking residues 166–172 was expressed in a heterozygous context. Regardless of the precise factors influencing the telomere length phenotype in these studies these context-dependent phenotypes highlight the challenges that lie ahead for gene therapies targeted at genetically defined diseases like DC.

The heterozygous nature of the TPP1 disease mutation raises the possibility of potential dominant-negative effects, arising from the ability of TPP1 and telomerase to dimerize, driving telomerase deficiency in the proband. We performed protein-mixing experiments to directly test the effect of K170Δ on TPP1 WT function. Neither the

telomerase processivity nor the telomerase recruitment WT-mutant mixing experiments (IF-FISH and telomere ChIP) revealed any evidence for a dominant-negative effect for K170Δ. Assuming that our mixing experiments recapitulated the functionally relevant oligomeric status (if any) of TPP1 and telomerase in the cells, we conclude that the TEL patch performs its function independent of the oligomeric status of TPP1 or telomerase. Finally, the TPP1 Δ/Δ/wt cells that we engineered showed robust telomere shortening, further ruling out the involvement of any dominant-negative effects of the TPP1 K170Δ mutation in human cells.

In conclusion, the K170Δ mutation in TPP1 provided us a unique opportunity to dissect the structural, biochemical, and genetic underpinnings of a case of DC, yielding valuable insights into disease mechanism and encouraging therapeutic strategies to counter this disease.

2.5 Materials and methods

2.5.1 Plasmid constructs

The following plasmids have been described previously: the pET-Smt3-TPP1-N plasmid [64] for expression and purification of human TPP1-N; the p3X-FLAG-TPP1-BI4 plasmid [130] for expression of human TPP1 (87 aa - 544 aa) in a doxycycline-induced manner in the HeLa-EM2-11ht cell line [135]; the p3X-FLAG-TPP1-CMV plasmid [129] for expression of human TPP1 (87 aa - 544 aa) in HeLa and HEK 293T cells; and the pTERT-cDNA6/myc-His C and phTR-Bluescript II SK(+) plasmids for transiently overexpressing telomerase [66]. The bicistronic expression vector pX330-U6-Chimeric_BB-CBh-hSpCas9 for site-specific genome editing in cultured human cells

was a gift from Feng Zhang (Addgene plasmid # 42230) [133] and obtained upon signing an MTA.

2.5.2 Site-directed mutagenesis of plasmids

Mutations in TPP1-expression plasmids were introduced with fully complementary mutagenic primers (Integrated DNA Technologies) using the QuikChange® Site-Directed Mutagenesis Kit (Agilent Technologies). The TPP1 sequences in the mutant plasmids were sequenced to confirm both the presence of the intended mutation and the absence of unwanted errors introduced during PCR amplification/cloning.

2.5.3 Protein expression and purification

WT and mutant constructs of Smt3-TPP1-N and Smt3-TPP1–OB fusion proteins were obtained upon purification from lysates of isopropyl β-d-thiogalactopyranoside-induced BL21(DE3) cells, as described previously [124]. Nickel-agarose chromatography was used as the first step of purification, followed by treatment with Ulp1 protease (material transfer agreement with Cornell University for pUlp1 vector) to cleave the Smt3 tag. Size-exclusion chromatography (Superdex 75; GE Life Sciences) was performed as the final step of protein purification. The His-Sumostar-hPOT1 baculoviral expression plasmid described previously [124] was used to express full-length POT1 in baculovirus-infected High Five cells (Life Technologies) using vendor recommendations. Sumostar-POT1 fusion protein was purified from insect cell lysates using nickel-agarose chromatography. The tag was cleaved with SUMOstar protease (Life Sensors) and the released POT1 protein was further purified by anion exchange (HiTrap Q HP; GE Life Sciences), and size-exclusion chromatography (Superdex 200; GE Life Sciences). GST-fusions of TPP1-N proteins were expressed from plasmids derived from the pGEX-

6P-2 vector (GE Life Sciences) in Escherichia coli and the GST-fusion proteins were purified from cell lysates using glutathione affinity chromatography following the manufacturer's instructions (glutathione Sepharose 4B beads; GE Life Sciences).

2.5.4 Telomerase activity assays

Soluble cell extracts were prepared from HEK 293T cells that were transfected with TERT- and TR-encoding plasmids, as described previously [124]. The extract was used as the source of telomerase enzyme in direct telomerase primer extension assays based on previously published protocols [124]. Each 20-µL reaction containing 50 mM Tris·Cl (pH 8.0), 1 mM MgCl2, 1 mM spermidine, 30 mM KCl, 5 mM β-mercaptoethanol, 1 µM of primer a5 (TTAGGGTTAGCGTTAGGG), 500 µM dATP, 500 µM dTTP, 2.92 µM unlabeled dGTP, 0.17 µM radiolabeled dGTP (3,000 Ci/mmol), and 3 µL of cell extract was incubated at 30 °C for 30 min. Next, 100 µL of buffer containing 3.6 M ammonium acetate and 20 µg of glycogen was used to quench each reaction, and the DNA products were precipitated with 70% (vol/vol) ethanol. The pellets were resuspended in H_2O (10 µL), mixed with loading buffer containing 95% (vol/vol) formamide (10 µL), heated at 95 °C for 10 min, and resolved on a 10% (wt/vol) acrylamide, 7M urea, 1× TBE sequencing-size gel. Dried gels were imaged on a phosphorimager (Storm; GE), and analyzed using Imagequant TL (GE Life Sciences) software. Processivity calculations were performed as described previously [124].

2.5.5 GST pull down assays

For the GST pulldowns, 150 µL of Glutathione Sepharose 4B beads (GE Life Sciences) were washed three times with 500 µL wash buffer [25 mM Tris (pH 7.0), 150 mM NaCl, and 2 mM BME). After the final wash step, the beads were resuspended in a 1:1 slurry

with wash buffer. To 30 µL of the bead slurry, 20 µg of GST-labeled WT TPP1-N, TPP1-N K170Δ, or TPP1–OB (90–250) proteins were added, and the protein bead mixtures were incubated with rocking for 1.5 h at 4 °C. 20 µg of POT1 (amino acids 299–634) protein was then added to the beads and incubation was continued for a further 1.5 h at 4 °C. Following incubation, the beads were washed three times with wash buffer as described above and boiled for 10 min in SDS-containing protein denaturation buffer. The denatured proteins samples were resolved on a 10% (wt/vol) SDS/PAGE gel and visualized with Coomassie blue stain.

2.5.6 Structure determination of TPP1-OB K170Δ and TPP1-OB K170A

Crystals of TPP1-OB K170Δ and TPP1-OB K170A were obtained by optimizing conditions that were reported to yield TPP1-OB WT crystals [64]. To obtain diffraction quality crystals of TPP1-OB K170Δ, 1 µl of protein was mixed with 1 µl of reservoir solution (3.6 M sodium formate, 100 mM Tris-Cl (pH 8.0) for TPP1-OB K170Δ; 3.7 M sodium formate, 100 mM Tris-Cl (pH 7.0), 2% methanol for TPP1-OB K170A) and incubated at 16 °C in hanging-well format. Crystals were cryoprotected and harvested as reported for WT protein [64]. X-ray diffraction data were obtained at the LS-CAT beam line 21-ID-D of the Advanced Photon Source. Data were processed using either HKL2000[136] (TPP1-OB K170Δ) or MOSFLM[137] (TPP1-OB K170A). To obtain a complete dataset with high redundancy, two separate datasets of TPP1-OB K170A were merged. For this, two individual data sets were processed using MOSFLM [137] followed by merging into a single dataset using BLEND (CCP4i suite) [138]. The data were scaled using SCALA (CCP4i) and intensities were converted to structure factors using CTRUNCATE (CCP4i). Molecular replacement solutions were found with

MOLREP (CCP4i) using the TPP1–OB WT (PDB ID code 2I46) structure as the search model. Residues 166–172 were removed in initial refinement steps to reduce model bias. The 2Fo – Fc density from restrained refinement was used to build in the deleted amino acids in Coot (CCP4i). Model building was performed using the program Coot [139] and the models were iteratively refined using REFMAC (CCP4i). As in the WT structure, density for the TEL patch loop/knuckle residues is only defined in one (subunit A) of the two subunits in the asymmetric unit. The PDB code for TPP1–OB K170Δ is 5I2X and for TPP1-OB K170A is 5I2Y. The two new structures exhibited excellent geometry, and contained no residues in the disallowed regions of the Ramachandran plot (Table 2.1). Figures depicting structures were prepared in Pymol, with the exception of the panel containing electron density, which was prepared using Coot.

2.5.7 Stable cell line generation using HeLa-EM2-11ht cells and p3X-FLAG-TPP1-F3 plasmids

HeLa-EM2-11ht cells were co-transfected in a 6-well format using Lipofectamine 2000 (Life Technologies) with 1 µg each of the p3X-FLAG-TPP1-F3 (WT or mutant) and 1 µg of a Flp recombinase-expressing plasmid that also codes for puromycin resistance. The next morning, cells were selected for 24 h using puromycin (5 µg/ml; Sigma-Aldrich). Subsequently, fresh medium lacking puromycin but including ganciclovir (50 µM; Sigma-Aldrich) was added and negative selection was conducted for 10 days. 12 individual clones were picked from each transfection and expanded. Positive clones were selected based on green fluorescence arising from their IRES-GFP locus downstream of the FLAG-TPP1 cDNA sequence. Two positive clones for each TPP1 mutant were expanded until they grew to confluency in 6 cm or 10 cm culture dishes and induced

with 200 ng/ml doxycycline to study the effect of TPP1 mutations in cells. Stable cell lines expressing TPP1 WT and TPP1 E169A/E171A used in this study were engineered in a similar fashion, and have been described previously [130].

2.5.8 CRISPR-Cas9 mediated TEL patch mutagenesis in HEK 293T cells

The Zhang Laboratory (Broad Institute of MIT and Harvard, McGovern Institute for Brain Research, and Departments of Brain and Cognitive Sciences and Biological Engineering, Massachusetts Institute of Technology, Cambridge, MA) open access CRISPR design tool was used to design guide RNAs against the gene coding for TPP1 (crispr.mit.edu/). An ~200-bp sequence spanning exon two, which encodes the TEL patch of TPP1, was submitted to the CRISPR design tool for guide RNA design. Based on a high CRISPR design tool score and low probability off target cleavage events, a total three guide RNAs were selected for cloning. The selected guide-sequence oligonucleotides were annealed, phosphorylated using T4 polynucleotide kinase enzyme, and cloned into the Bbs1 site of the bicistronic expression vector pSpCas9 (BB # 42230) (30). The sequences of guide RNA used to cleave TPP1 were as follows: (Guide1- GTTCGGCTTCCGCGGGACAG; Guide2- AGAAGGAGTTCGGCTTCCGC, Guide3- GAGAAGGAGTTCGGCTTCCG).

2.5.8.1 ssODN design.

ssODNs with desired mutations were used as a template to introduce TEL patch mutations in the gene coding for TPP1. The ssODNs were designed to contain ~75 bases flanking sequences on each side of the mutation site. To avoid any cleavage after repair has occurred, silent mutations were introduced to destroy the spacer/PAM sequences in the ssODNs. Silent mutations creating a Kpn1 restriction site on the

mutated locus were also introduced to facilitate screening of repaired clones. The sequences of the designed ssODNs are as follows. Note that intronic sequences are shown in lowercase and exon 3 sequences are shown in uppercase. The introduced Kpn1 site (GGTACC) is underlined. In the K170Δ ssODN, the deletion of the K170Δ codon (AAG) is denoted by an asterisk (*). The italicized “AGA” sequence is a silent mutation (replacing the CGC codon for arginine) that destroys the PAM sequence to prevent cleavage by Cas9 post-DNA repair.

WT ssODN:

ggccttgtgttcaggtgggcccggcagtgaggatcctgcttgttgcagGGAGGAGAAGGAGTTCGGCTTCA
GAGGTACCGAGGGCCGGCTGCTGCTGCTGCAGGACTGCGGGGTTCATGTCCAGG
TCGCTGAGGGCGGCG

K170Δ ssODN:

ggccttgtgttcaggtgggcccggcagtgaggatcctgcttgttgcagGGAGGAG*GAGTTCGGCTTCAGA
GGTACCGAGGGCCGGCTGCTGCTGCTGCAGGACTGCGGGGTTCATGTCCAGGTC
GCTGAGGGCGGCG

2.5.8.2 Surveyor nuclease assay to determine cleavage efficiency.

For the Surveyor nuclease assay, 0.3 × 106 HEK 293T cells were transfected in 12-well plates with 1 μg of guide RNA containing plasmids using 2.5 μL Lipofectamine 2000 (Life Technologies). Cells were ∼80% confluent at the time of transfection. After 72 h of transfection, cells were trypsinized and harvested by centrifugation. Genomic DNA from collected cells was prepared using GenElute Mammalian Genomic DNA Purification Kit (#G1N70; Sigma). Next, 150–200 ng of isolated genomic DNA was used for PCR amplification with Surveyor primer pairs using Phusion DNA polymerase in a 50 μL

reaction volume. After PCR, 4 µL of each reaction was loaded on an agarose gel to check the uniformity and efficiency of amplification among different samples. Amplification products were PCR purified using a PCR purification kit (#28106 Qiagen) and subjected to the Surveyor nuclease assay using the manufacturer's protocol (Surveyor Mutation Detection Kit; catalog #706025; Transgenomic). Upon completion of the reaction, the products were visualized using ethidium bromide-stained, 2% (wt/vol) GTG agarose gels.

2.5.8.3 Efficiency of TEL patch mutagenesis using ssODNs.

For efficiency of TEL patch mutagenesis using ssODNs, 0.3 × 106 HEK 293T cells were transfected in 12 well plates with 1 µg of puromycin-resistant guide RNA containing plasmids and 1.2 µL (10 µM) of mutagenic ssODN, using 3.5 µL Lipofectamine 2000 and OptiMEM medium. Twenty min later, the mixture was added drop-wise to cells that were incubated in antibiotic-free medium. After 5 h the media was changed to antibiotic-containing media. One day later, 1 µg/mL puromycin was added to the media. Three days post-transfection, cells were trypsinized and ~2,000 cells were added per 10-cm dish to allow for colony formation; the remaining cells were used to test the efficiency of repair using Kpn1 digestion as follows.

To check the efficiency of desired mutagenesis, genomic DNA was prepared and the TPP1-TEL patch locus was PCR-amplified as already described for the Surveyor assay. Twenty microliters of the amplified DNA was incubated in a 30-µL reaction volume in the presence or absence of Kpn1 for 1 h. The reaction products were visualized using ethidium bromide staining of a 2% (wt/vol) GTG agarose gel. The amount of DNA

digested with Kpn1 was visible as smaller size DNA fragments (of predictable size), providing an estimation of the efficiency of mutagenesis.

2.5.8.4 Isolation and culture of TEL patch mutant clones.

After 14–16 d post-seeding (~2,000 cells were seeded on a 10-cm culture dish), colonies were readily observable under a light microscope. Each isolated colony was picked with the help of pipette tip under the microscope and transferred to a 96-well plate (master plate) and incubated for ~1 wk. At this time point each 96-well plate was trypsinized and half of the cells were transferred to a second plate (replica plate). Both the plates were incubated further for 4 d. Next, the replica plate was used for genomic DNA preparation using the ZR-96quick-gDNA kit (Zymo Research). Isolated genomic DNA from each well of the 96-well plate was subjected to PCR amplification and Kpn1 restriction digestion, as described above. Based on the Kpn1 sensitivity, wells with positive clones were marked in a master plate and expanded for genotyping, Sanger DNA sequencing, and further experiments.

2.5.8.5 Genotyping of TEL patch mutant clones.

PCR products spanning the TPP1 mutation site obtained using the genomic DNA of the edited cell lines as template were cloned into vectors using the T/A cloning strategy (#A1360, pGEM-T Easy Vector System I, Promega). At least 12 separate bacterial clones were sequenced using Sanger sequencing to obtain sequence information for all three TPP1 alleles in these HEK 293T clones.

For generating a TPP1 double KO (Δ/Δ/wt), we used a single KO clone (Δ/wt/wt) that we isolated during clonal isolation of WT* and K170Δ edited cells. The single KO cells were transfected with plasmids coding for guide RNAs 2 and 3, and the WT* ssODN.

Clones were isolated and analyzed as already described. In addition to isolating a TPP1 double KO clone, we were also able to isolate a second WT* clone (WT* clone #2) in this experiment.

2.5.9 Immunoblotting

Immunoblotting was performed using standard protocols in combination with the following antibodies at the specified dilutions: mouse monoclonal anti-FLAG M2-HRP conjugate (Sigma; A8592; 1:20,000), mouse monoclonal anti-c-myc antibody (Developmental studies hybridoma bank; 1:500) mouse monoclonal anti-β-actin antibody (Sigma; A5441; 1:10,000), and rabbit polyclonal TPP1 antibody (Bethyl laboratories; A303-069A; 1:2,500). Secondary horseradish peroxidase-conjugated goat antibodies against rabbit IgG and against mouse IgG (Santa Cruz Biotechnology; 1:10,000) were used to reveal the primary antibodies using chemiluminescence detection by ECL plus reagents (Pierce ECL Western Blotting Substrate; Thermo Scientific). The data were visualized and quantified using a gel-documentation system (ChemiDoc™ MP System; BioRad).

2.5.10 Immunofluorescence (IF) and fluorescence in situ hybridization (FISH) microscopy

IF-FISH experiments for telomerase recruitment were performed as described previously[130]. Briefly, IF was performed prior to FISH. Mouse monoclonal anti-FLAG M2 (Sigma; F1804; 1:500) in combination with Alexa Fluor 568-conjugated anti-mouse IgG (Life Technologies) was used to detect FLAG-tagged TPP1 proteins by IF. A mixture of three Cy5-conjugated TR probes[140] (30 ng of each probe per coverslip) was used to detect TR. For detecting myc-tagged proteins, we used the mouse

monoclonal anti-c-myc antibody (Developmental studies hybridoma bank; 1:250). Imaging was performed with a laser scanning confocal microscope (SP5; Leica, Germany) equipped with a 100X oil objective. Images were processed using ImageJ as well as Adobe Photoshop, and colocalizations were quantified manually by separate two individuals. Pseudocolored representative images are shown in figure panels. Mean and standard deviation of three experiments, each involving at least 100 telomeric foci, were plotted for each TPP1 stable cell line.

2.5.11 Telomere length analysis

Telomere length analysis was performed as described previously with a few modifications[130]. Genomic DNA was isolated from confluent 6 well plates of the FLAG-TPP1 expressing stable cell lines using the GenElute kit (Sigma). Genomic DNA (1 µg) was restriction digested with frequent cutters Hinf1 and Rsa1 overnight at 37°C. The DNA digests were run on a 0.8% 25 cm long Agarose-1X TAE gel at 80 V until the 250 bp marker migrated to the bottom of the gel. The gel was imaged using a florescent ruler and transferred to a sheet of dry Whatman filter paper, and dried at 55°C for one h. After drying the filter paper was removed and the gel was incubated first in buffer containing 0.25 M HCl followed by incubation in buffer containing 0.5 M NaOH, and finally shaken in solution containing 0.5 M Tris-Cl and 1.5 M NaCl (pH 7.5) for 30 min. The gel was then prehybridized in Church buffer (0.5 M sodium phosphate buffer [pH 7.2], 1% bovine serum albumin [BSA], 1 mM EDTA, 7% SDS) for 30 min at 60°C in a rotating hybridization oven. 5' ^{32}P-labeled (with T4 PNK; NEB) telomeric probe of sequence $(TTAGGG)_4$ was added (20 million cpm) and hybridization continued overnight at 55°C. The hybridization solution was discarded and the gel was washed

with buffer containing 0.1X SSC. The gel was then exposed to a phosphorimager screen for 24-72 h, and analyzed using the Imagequant TL software. The gel was calibrated using the known molecular weights of the DNA ladder, and the mean telomere length for each lane was plotted as a function of population doubling (PD) for each cell line. A linear regression (MS Excel) was used to calculate the rate of telomere elongation.

2.5.12 Telomere chromatin immunoprecipitation

Ten-centimeter culture dishes containing HeLa 1.2.11 cells were transfected with 9 µg TR-encoding plasmid, 3 µg TERT-encoding plasmid, and either 3 µg of TPP1 WT plasmid, 3 µg of TPP1 K170Δ plasmid, or a mixture containing 1.5 µg each of TPP1 WT and TPP1 K170Δ plasmids using Lipofectamine 2000 following the vendor's recommendations. Subsequent to cross-linking with formaldehyde and cell lysis, 25% of the lysates were kept aside as whole-cell extract samples. Immunoprecipitation was performed on the remaining 75% of the lysates using 4 µg of mouse anti-TRF2 4A794.15 (Novus Biological; NB100-56506) and 5 µL rabbit monoclonal TERT (C-term) antibody (Epitomics; 1531-1) antibodies. Hybridization was performed in Church buffer [0.5 M sodium phosphate buffer (pH 7.2), 1% BSA, 1 mM EDTA, 7% (wt/vol) SDS] using 32P-labeled (TTAGGG)4. Following hybridization, membranes were washed to reduce nonspecific binding of the probe, imaged using a phosphorimager (Storm; GE Life Sciences) and quantified using Imagequant TL (GE Life Sciences) software. The TERT-associated telomeric DNA signal for each sample was normalized with the TRF2-associated signal (obtained via immunoprecipitation using an anti-TRF2 antibody), which was assumed to remain constant across all samples.

2.6 Figures and Tables

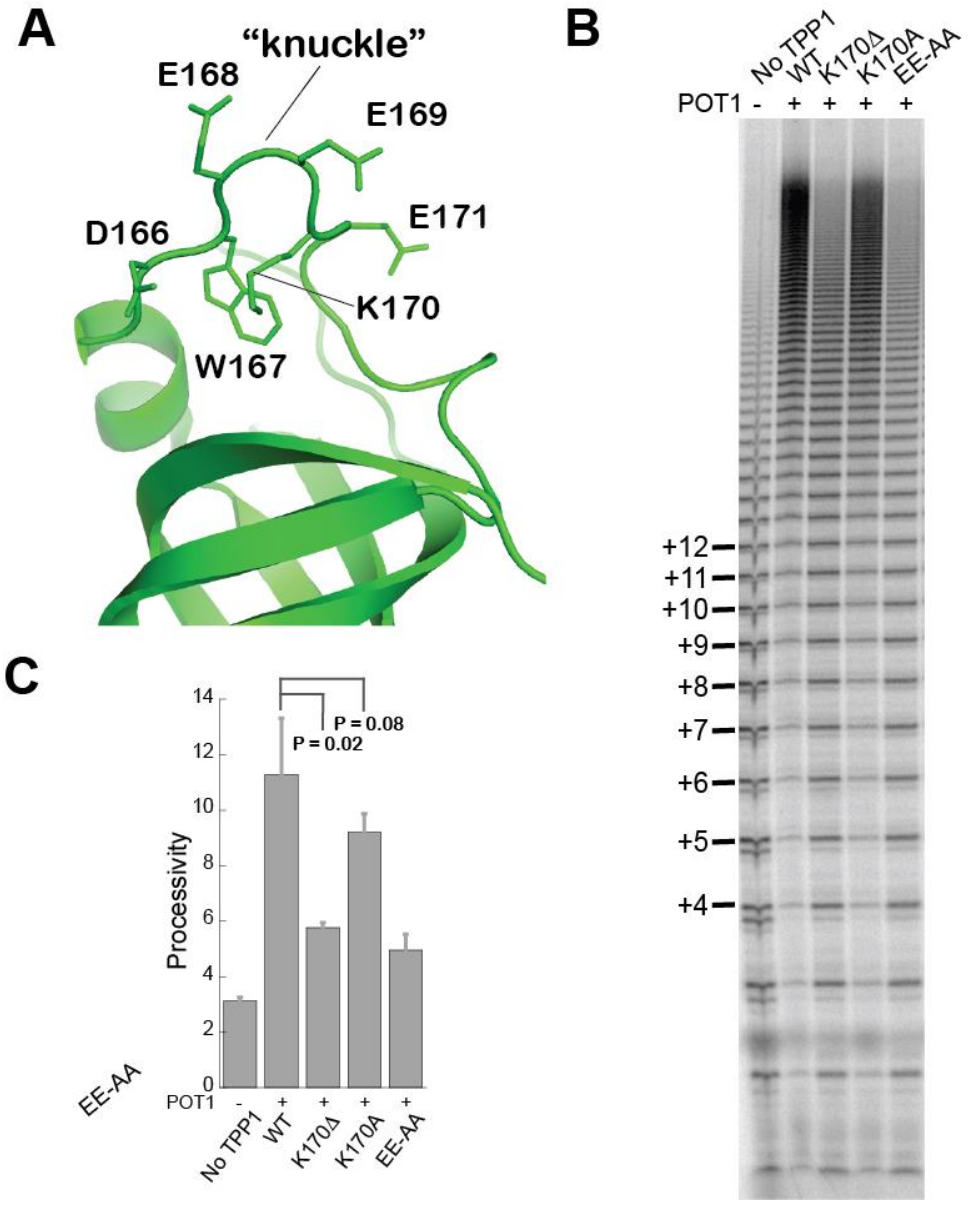

Figure 2.1 The main chain, but not the side-chain, of TPP1 K170 is important for stimulating telomerase processivity.
(A) Ribbon depiction of a part of the TPP1-OB wild-type crystal structure (PDB: 2I46) with the TEL patch loop (amino acids: 166-171) shown in stick representation. The protrusion in the loop is referred to here as a "knuckle". (B) Direct primer extension assays with telomerase extracts performed in the presence of purified POT1 (500 nM) and the indicated TPP1-N proteins (500 nM). "No TPP1" indicates a reaction lacking TPP1-N and POT1. The number of hexameric (GGTTAG) telomeric repeats is indicated on the left. (C) Quantification of telomerase processivity from triplicate experiments of which panel B is representative. Error bars represent standard deviation.

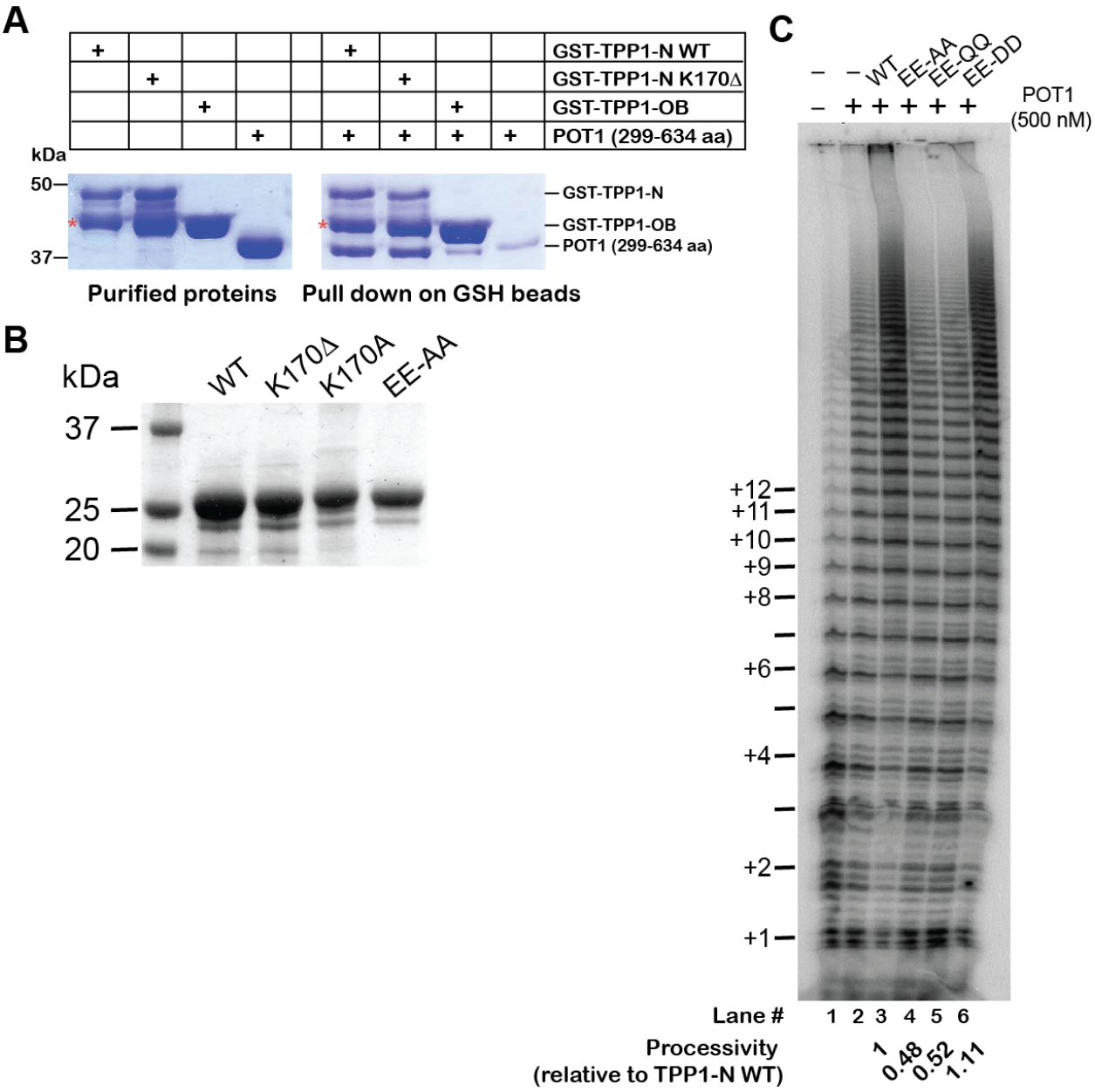

Figure 2.2 POT1-binding and telomerase stimulation analysis of TPP1 TEL patch mutants.
(A) Pull down of human POT1 (amino acids 299–634) on glutathione (GSH) beads containing the indicated GST–TPP1 fusions. The asterisk (*) indicates a prominent degradation product that copurifies with TPP1-N, which is approximately equal in size to GST–TPP1–OB. (B) Coomassie-stained SDS/PAGE showing uniform purity of the indicated TPP1-N protein constructs; EE-AA indicates E169A/E171A. (C) Primer extension assay with the indicated TPP1 mutants with quantification of processivity indicated at the bottom of the gel.

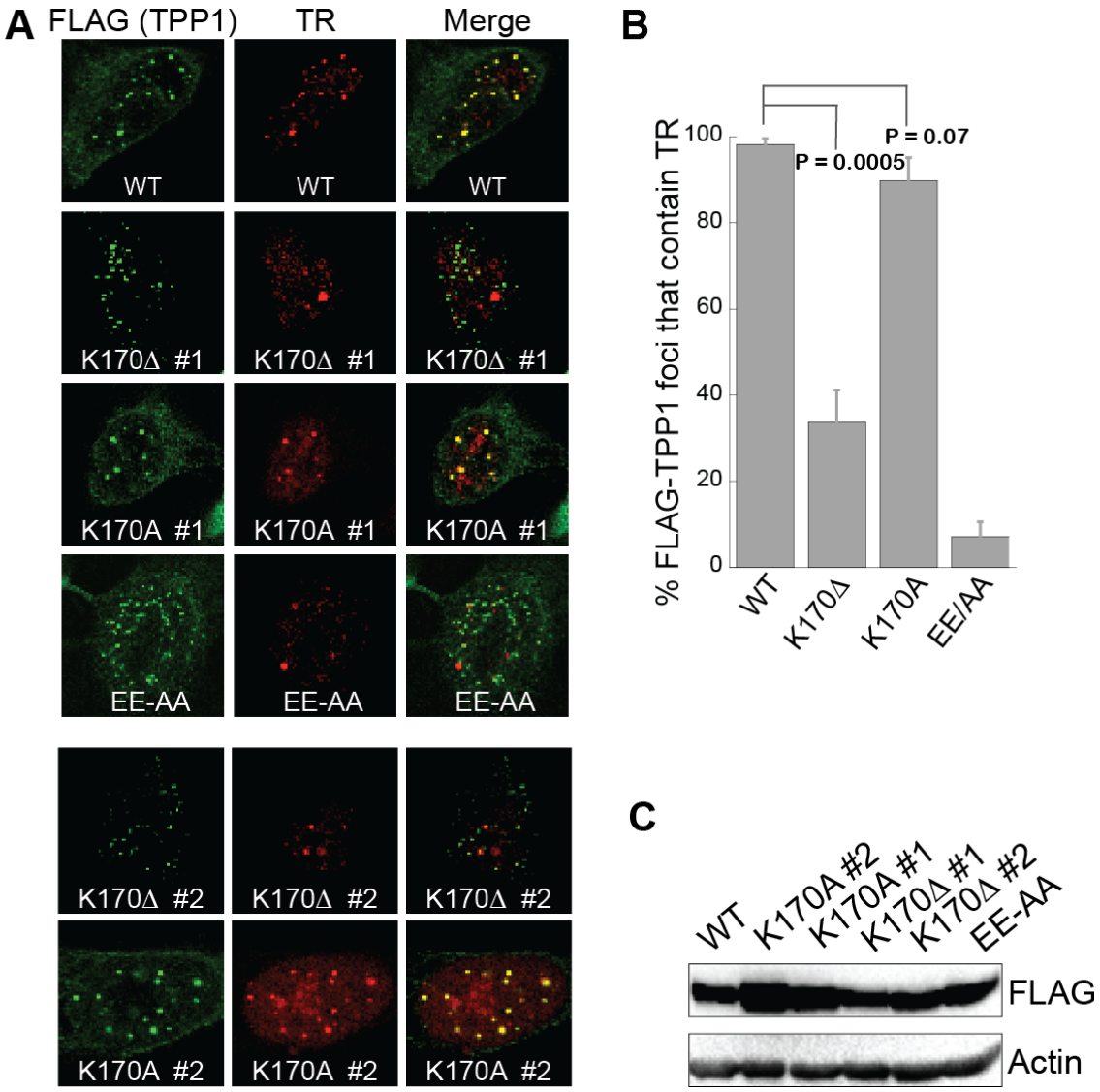

Figure 2.3 The main chain, but not the side-chain, of TPP1 K170 is important for telomerase recruitment.
(A) FISH was used to detect TR (red) and IF was used to detect the indicated FLAG-TPP1 proteins (green). Clonal cell lines of TPP1 K170Δ and K170A were analyzed in conjunction with previously characterized clones of TPP1 WT and E169A/E171A. Yellow spots in the "Merge" panel indicate recruitment of telomerase to telomeres. (Magnification: 100X) (B) Quantification of data of which D is representative. The average "% FLAG-TPP1 foci that contain TR" and SDs (error bars) of 10 fields of view (30–100 cells total) were plotted for the indicated stable cell lines. (C) Immunoblot showing comparable protein levels of FLAG-TPP1 in the indicated cell lines stably overexpressing WT or mutant TPP1 proteins.

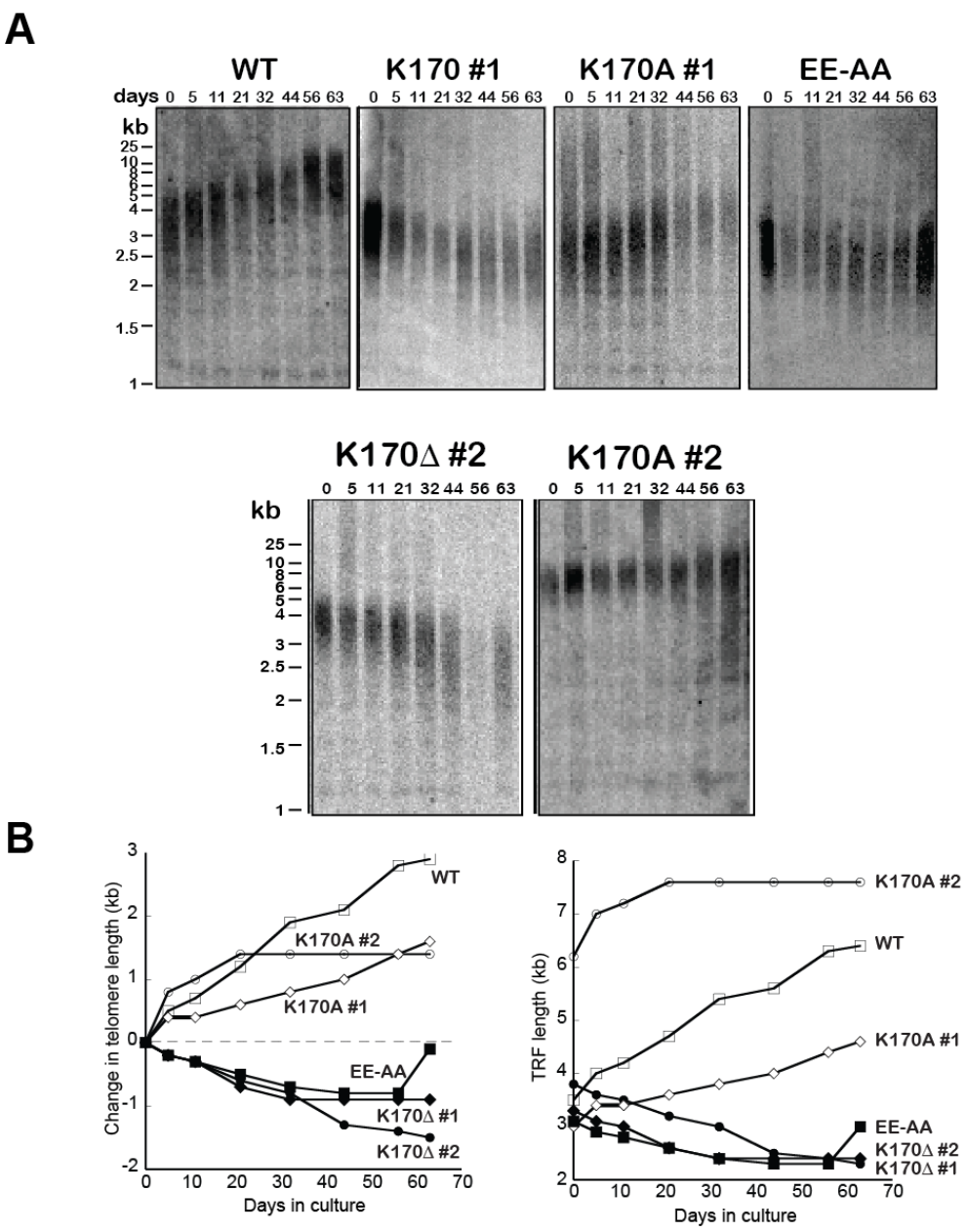

Figure 2.4 The main chain, but not the side-chain, of TPP1 K170 is important for maintaining telomere length.

(A) Telomere restriction fragment (TRF) Southern blot of genomic DNA from stable cell lines expressing the indicated TPP1 constructs. (B) Shown on the left is the quantification of data shown in panel A after subtracting the telomere length at "day 0." On the right is the quantification of mean TRF length from data shown in panel A.

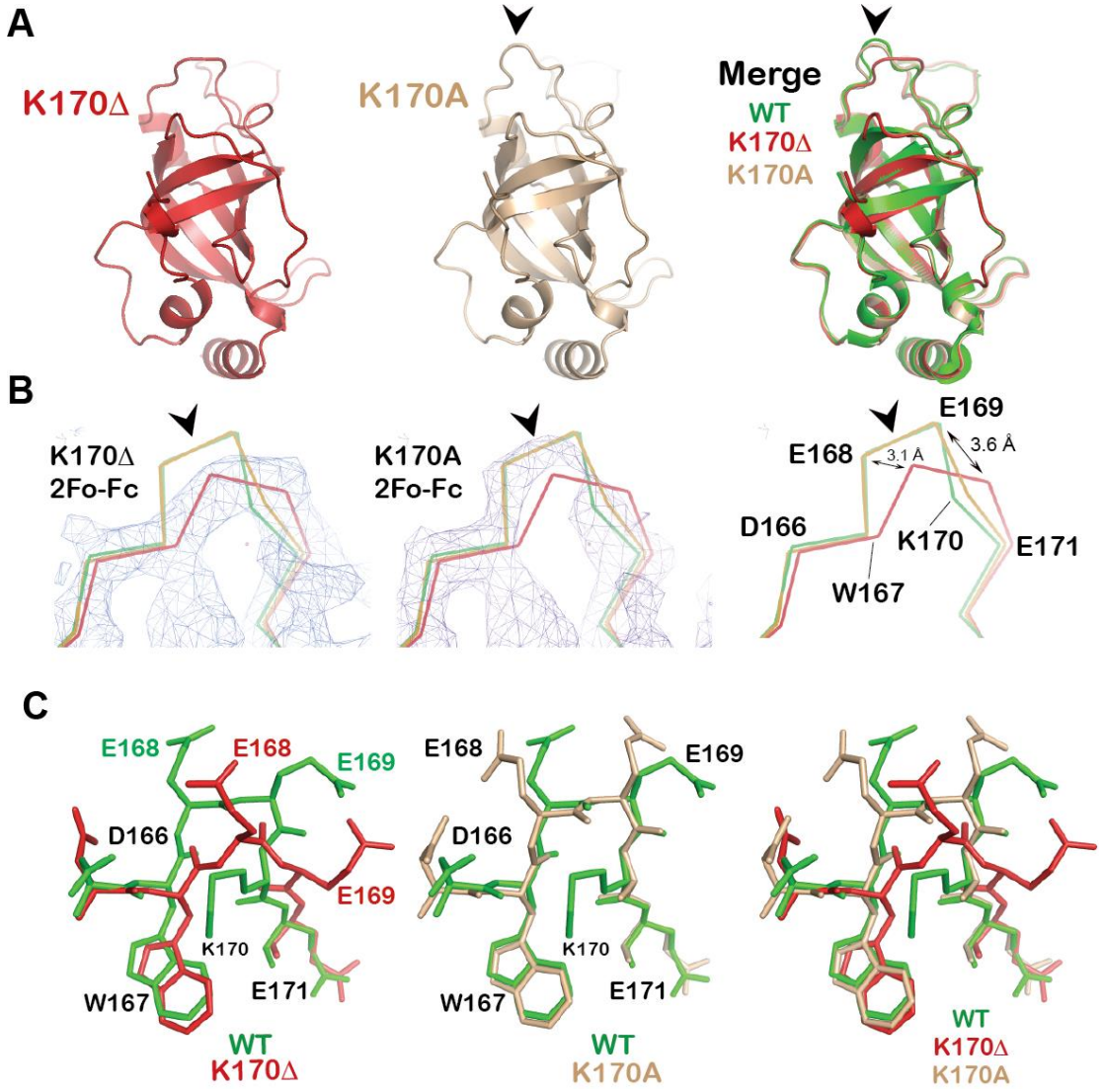

Figure 2.5 Deletion of K170 restructures the loop that harbors the critical glutamate residues of the TEL patch of TPP1.
(A) Ribbon diagrams of TPP1-OB K170Δ (red, Left) and TPP1–OB K170A (tan, Center) along with the overlay of these structures on the structure of TPP1–OB WT (WT in green, Right). (B) Overlay of the backbone traces for amino acids 166–171 of the three structures along with the 2Fo – Fc electron density for TPP1–OB K170Δ contoured at 1.1 σ (Left); or the 2Fo – Fc electron density for TPP1–OB K170A contoured at 1.1 σ (Center); or without any electron density displayed (Right). Single arrowheads indicate the TEL patch knuckle, and the double-headed arrows indicate the displacement of E168 and E169 in TPP1–OB K170Δ relative to their positions in the WT structure. The PDB code for the previously published TPP1–OB WT structure is 2I46. (C) Stick representations of the TPP1–OB mutant crystal structures. Overlay of the stick representations of amino acids 166–171 of TPP1–OB K170Δ and TPP1–OB WT (Left); TPP1–OB K170A and TPP1–OB WT (Center); and all three structures (Right).

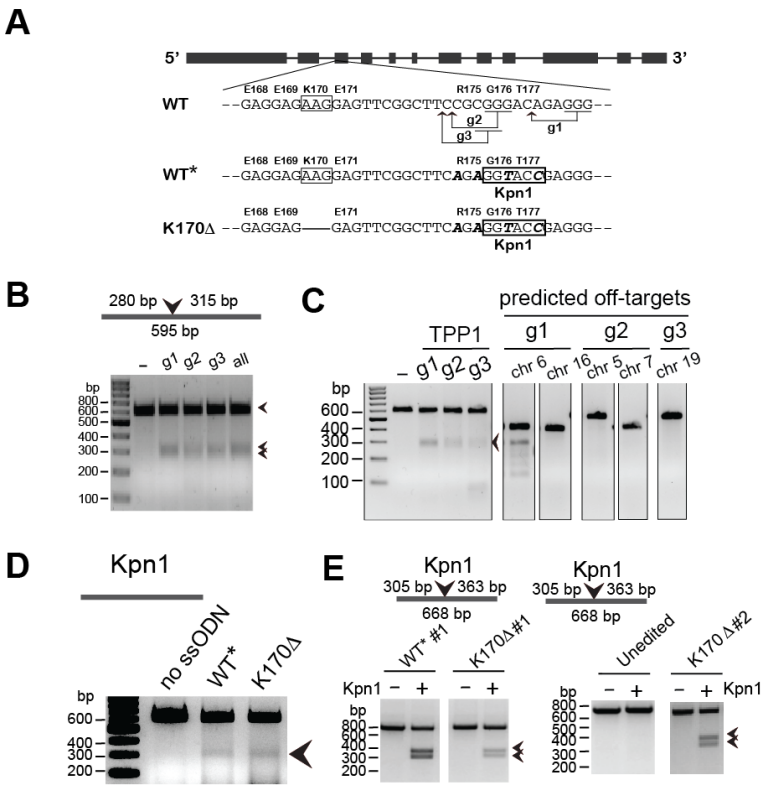

Figure 2.6 Introducing the TPP1 disease mutation in cells using CRISPR-Cas9 technology.

(A) The ACD gene coding for TPP1 protein is shown with exons as boxes and introns as lines. The sequence in exon #3 flanking the K170Δ codon is shown (WT) along with the "NGG" PAM sequences (underlined) and the cut sites (arrows) for the three guide RNAs (g1, g2, and g3). The mutagenic ssODN sequences to introduce WT* and K170Δ mutations are also shown; silent mutations to introduce the KpnI site (shown in a box) and to destroy Cas9 recognition are italicized and depicted in bold. (B) Results of the PCR-based Surveyor assay for assessing the efficiency of cleavage by Cas9 are shown for the indicated guide RNAs targeting the ACD gene. "all" indicates a transfection including all three guide RNA-encoding plasmids. The bar at the top shows the predicted product sizes upon Cas9-mediated cleavage, and the arrowheads alongside the gels indicate the uncleaved and cleaved PCR products. (C) Surveyor assay to analyze potential off-targeting of the three guide RNAs. The guide RNAs and the chromosomes that harbor the off-target are indicated. (D) PCR amplicons from genomic DNA templates of HEK 293T cells transiently cotransfected with plasmids encoding Cas9 and guide RNAs 2 and 3, and indicated ssODNs, were subjected to digestion by Kpn1 enzyme. The bar indicates the DNA digest sizes expected from successful integration of the Kpn1 site into the genome. The arrowhead indicates successful mutagenesis with WT* and K170Δ ssODNs. (E) KpnI-digests for clones of unedited, WT* (clone #1) and K170Δ (clone #1 and clone #2). The partial digestion of the PCR product is indicative of heterozygosity of the introduced mutations.

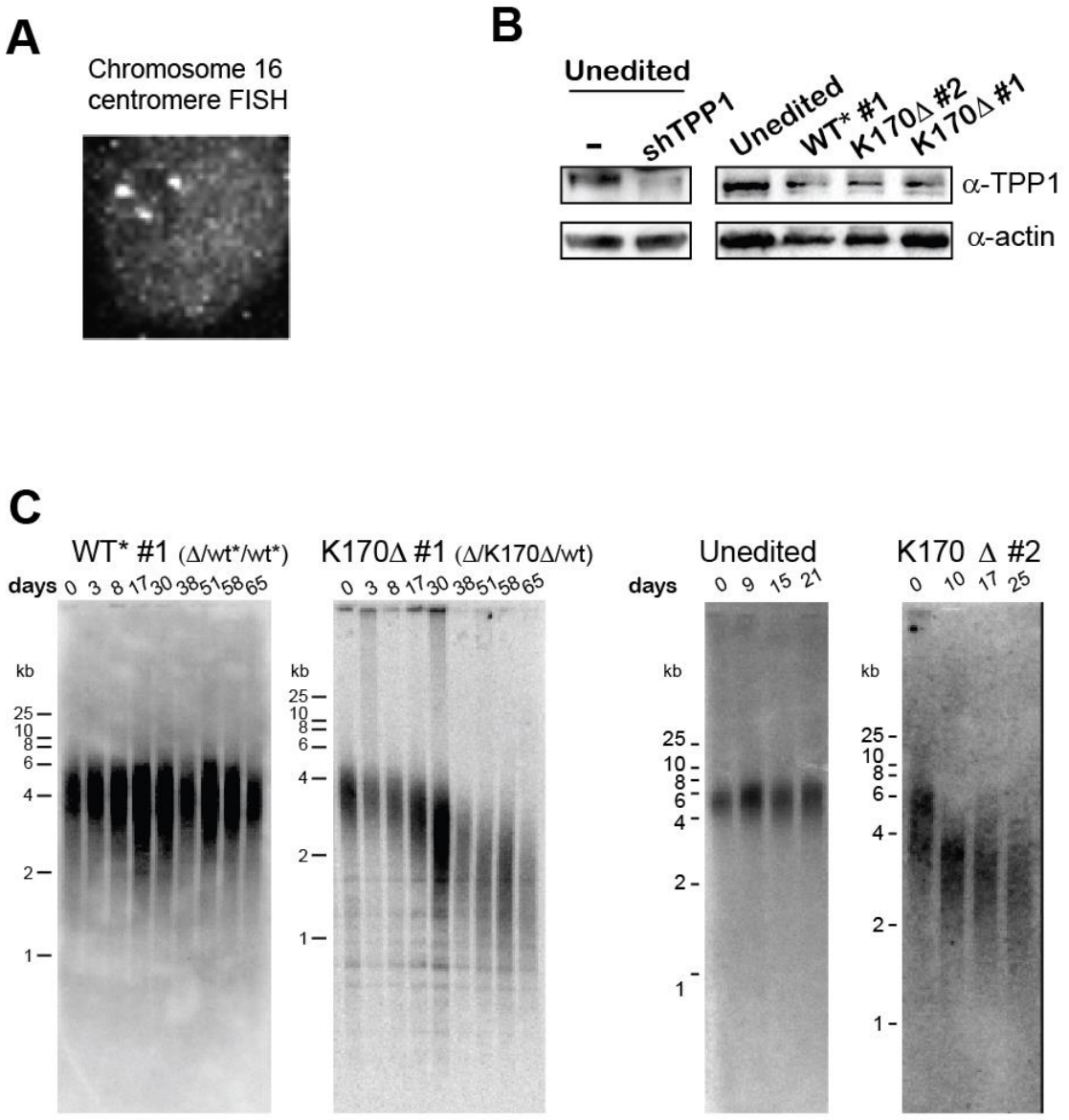

Figure 2.7 A single K170Δ allele is sufficient to cause telomere shortening in HEK 293T cells.
(A) Representative data for chromosome 16-specific centromere FISH in HEK 293T cells. The three bright spots indicate the FISH signals whereas the gray background indicates nuclear staining (DAPI). (Magnification: 100X) (B) Immunoblot of endogenous TPP1 from lysates of the indicated HEK 293T clonal cell lines (Right). The identity of the TPP1 band was verified by its effective knock down in HeLa cells transfected with a previously characterized shRNA against human TPP1 (Left). (C) TRF Southern blot of genomic DNA from the CRISPR-Cas9 derived clones of unedited, WT* (clone #1) and K170Δ (clone #1 and clone #2) at the indicated days in culture.

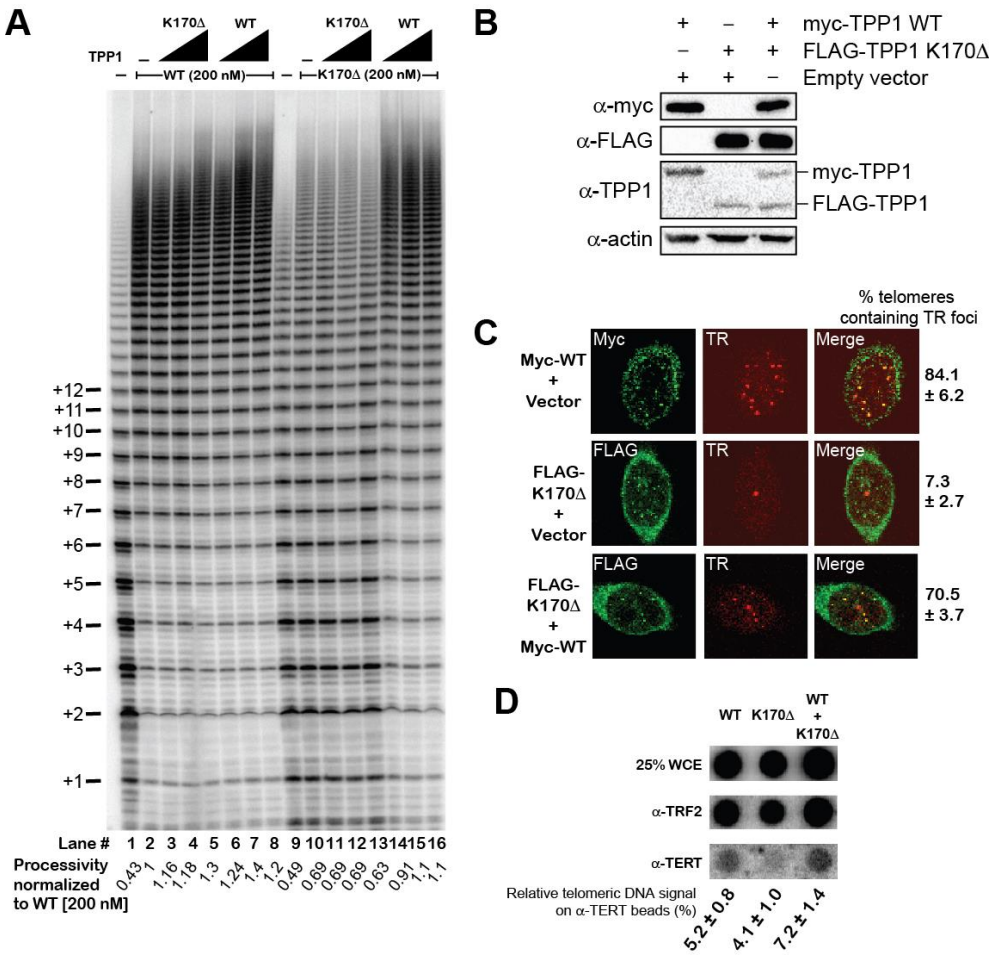

Figure 2.8 TPP1 K170Δ protein does not compromise the ability of WT TPP1 protein to facilitate telomerase function.

(A) Telomerase primer extension involving mutant mixing and titration performed in the presence of TPP1-N WT and the TPP1-N K170Δ. The filled triangles indicate 100 nM, 200 nM and 300 nM concentrations of the indicated TPP1-N construct. "–" in lanes 1 and 9 indicate no added POT1 or TPP1 proteins. Concentrations of DNA primer (1 μM) and POT1 protein (500 nM) were held constant. "Proc." indicates processivity relative to TPP1-N WT (200 nM). (B) Immunoblot analysis with the indicated antibodies of cell lysates obtained from the indicated transfections. (C) IF-FISH was performed on HeLa cells transfected with either myc-tagged TPP1 WT plasmid or FLAG-tagged TPP1 K170Δ plasmid or a mixture of the two. IF was performed with the anti-myc and anti-FLAG primary antibodies, and TR was detected by FISH as already described in Fig. 2. (Magnification: 100X) Quantification performed, as in Fig. 1, is shown on the right. (D) Telomere ChIP experiments using anti-TERT and anti-TRF2 antibodies. The "input" sample contains 25% of the whole-cell extract. Quantification of telomere ChIP experiments performed in duplicate with the SEM indicated with error bars is shown at the bottom. The "Relative telomeric DNA signal on α-TERT beads (%)" represents the ratio of the telomeric DNA signals of the TERT and TRF2 immunoprecipitations for each of the indicated transfections.

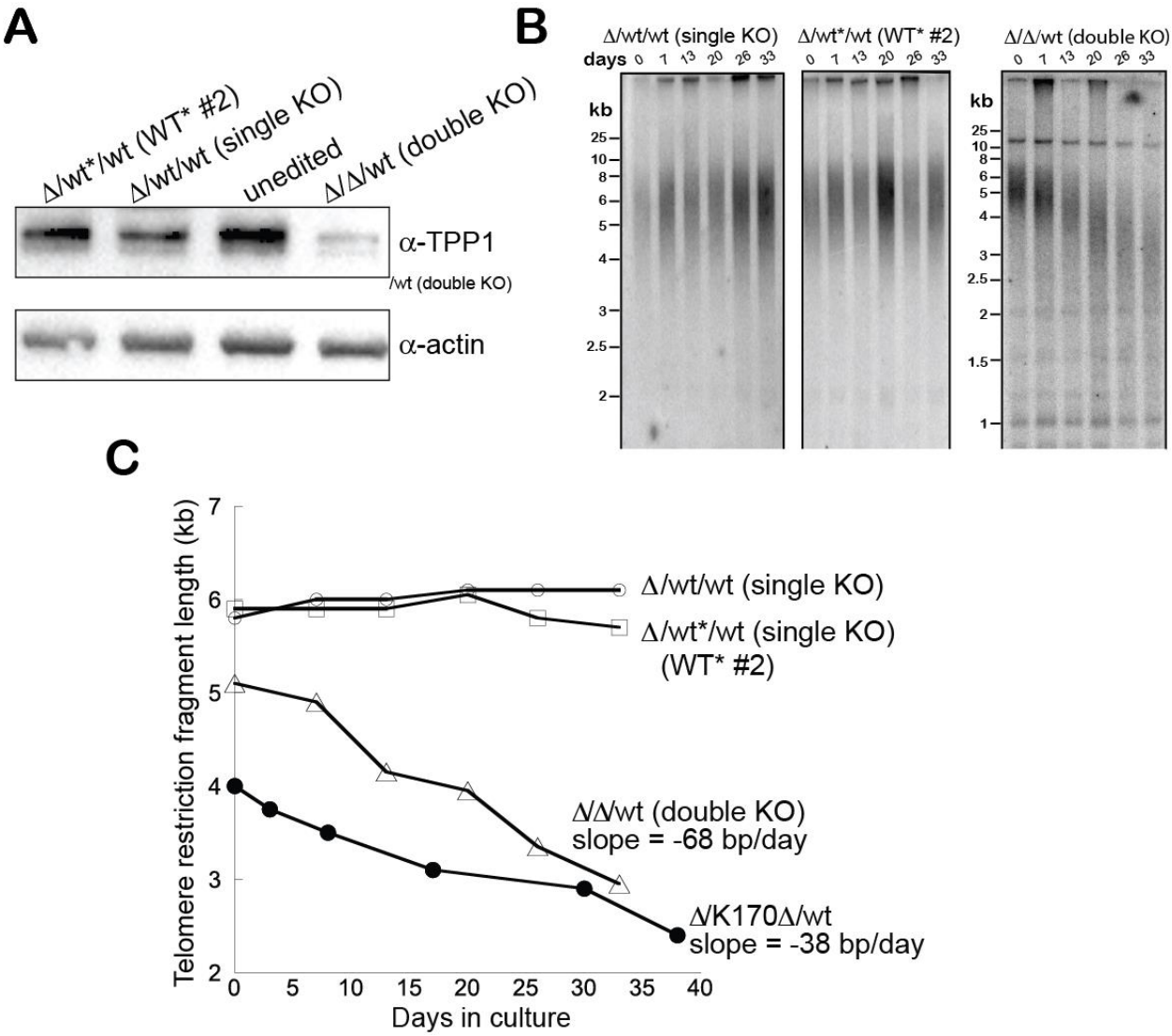

Figure 2.9 Telomere length analysis of single and double TPP1 knockout HEK 293T cells.

(A) Immunoblot to detect endogenous TPP1 protein in the indicated CRISPR-Cas9 derived TPP1 knockout HEK 293T cell lines. (B) TRF Southern blot of genomic DNA from the indicated CRISPR-Cas9 derived HEK 293T clones. (C) Quantification of TRF length data shown in panel B and Figure 2.7C.

Table 2.1 Table of crystallography statistics.

	TPP1-OB K170Δ	TPP1-OB K170A
Data collection		
Space group	$I4_122$	$I4_122$
Cell dimensions		
a, *b*, *c* (Å)	119.03, 119.03, 170.78	119.20, 119.20, 171.35
α, β, γ (°)	90.0, 90.0, 90.0	90.0, 90.0, 90.0
Resolution (Å)	50.0 – 3.0 (3.11 – 3.0)*	84.29 – 3.0 (3.16 – 3.0)*
R_{sym} or R_{merge}	14.8 (48.5)	21.1 (54.8)
$I / \sigma I$	7.1 (3.7)	7.5 (3.1)
Completeness (%)	99.7 (100)	98.9 (100)
Redundancy	6.9 (7.0)	6.6 (6.6)
Refinement		
Resolution (Å)	50.0 – 3.0 (3.08 – 3.0)	84.29 – 3.0 (3.08 – 3.0)
No. reflections	11321	11229
R_{work} / R_{free}	19.2 / 22.6 (27.5 / 30.1)	19.4 / 23.5 (28.1 / 32.1)
No. atoms	2233	2256
Protein	2178	2192
Water	55	64
B-factors		
Protein atoms	37.5	33.1
Water atoms	27.64	20.95
R.m.s. deviations		
Bond lengths (Å)	0.005	0.007
Bond angles (°)	0.988	1.125

*Values in parentheses are for highest-resolution shell.

Table 2.2 Sequencing of isolated clones.

Sanger sequencing results for the isolated WT* and K170Δ clones from CRISPR -
Cas9/ssODN mediated mutagenesis of the TPP1 locus in HEK 293T cells.

Unedited (wt/wt/wt)

GGAGGAGAAGGAGTTCGGCTTCCGCGGGACAGAGGGCGGCTGCTGCTGCTGCAG
E E K E F G F R G T E G R L L L L Q

K170Δ – clone #1 (Δ/K170Δ/wt)

Allele 1 GGAGGAGAAGGAGTTCGGCTTCAGAGGTACCGAGGGCCGGCTGCTGCTGCAG
E E K E F G F R G T E G R L L L L Q (WT)

Allele 2 GGAGGAG_ _ _GAGTTCGGCTTCAGAGGTACCGAGGGCCGGCTGCTGCTGCAG
E E X E F G F R G T E G R L L L L Q (K170Δ)

Allele 3 GGAGGAGAAG----------CGGGACAGAGGGCCGGCTGCTGCTGCAG
E E K R D R G P A A A A-10aa-STOP
(indel)

K170Δ – clone #2 (Δ/K170Δ/wt)

Allele 1 GGAGGAGAAGGAGTTCGGCTTCAGAGGTACCGAGGGCCGGCTGCTGCTGCAG
E E K E F G F R G T E G R L L L L Q (WT)

Allele 2 GGAGGAG_ _ _GAGTTCGGCTTCAGAGGTACCGAGGGCCGGCTGCTGCTGCAG
E E X E F G F R G T E G R L L L L Q (K170Δ)

Allele 3 GGAGGAG_ _ _GAGTTCGGCTTC-GCGGGACAGAGGGCCGGCTGCTGCTGCAG
E E X E F G F A G Q R A G C C C-44aa-STOP (indel)

WT* - clone #1 (Δ/wt*/wt*)

Allele 1 GGAGGAGAAGGAGTTCGGCTTCAGAGGTACCGAGGGCCGGCTGCTGCTGCAG
E E K E F G F R G T E G R L L L L Q (WT*)

Allele 2 GGAGGAGAAGGAGTTCGGCTTCAGAGGTACCGAGGGCCGGCTGCTGCTGCAG
E E K E F G F R G T E G R L L L L Q (WT*)

Allele 3 GGAGGAGAAGGAGT----------CAGAGGGCCGGCTGCTGCTGCAG
E E K E S X X X X X E G R L L L L Q (indel)

Single KO (Δ/wt/wt)

Allele 1 GGAGGAGAAGGAGTTCGGCT-CCGCGGGACAGAGGGCGGCTGCTGCTGCTGCAG
E E K E F G S A G Q R A G C C C C-14aa-STOP(indel)

Allele 2 GGAGGAGAAGGAGTTCGGCTTCCGCGGGACAGAGGGCGGCTGCTGCTGCTGCAG
E E K E F G F R G T E G R L L L L Q (WT)

Allele 3 GGAGGAGAAGGAGTTCGGCTTCCGCGGGACAGAGGGCGGCTGCTGCTGCTGCAG
E E K E F G F R G T E G R L L L L Q (WT)

WT* - clone #2 (Δ/wt*/wt)

Allele 1 GGAGGAGAAGGAGTTCGGCT-CCGCGGGACAGAGGGCCGGCTGCTGCTGCTGCAG
E E K E F G S A G Q R A G C C C C-14aa-STOP(indel)

Allele 2 GGAGGAGAAGGAGTTCGGCTTCAGAGGTACCGAGGGCCGGCTGCTGCTGCTGCAG
E E K E F G F R G T E G R L L L L Q (WT*)

Allele 3 GGAGGAGAAGGAGTTCGGCTTCCGCGGGACAGAGGGCCGGCTGCTGCTGCTGCAG
E E K E F G F R G T E G R L L L L Q (WT)

Double KO (Δ/Δ/wt)

Allele 1 GGAGGAGAAGGAGTTCGGCT-CCGCGGGCAGAGGGCCGGCTGCTGCTGCTGCAG
E E K E F G S A G R G P A A A A -17aa-STOP(indel)

Allele 2 GGAGGAGAAGGAGTTCGGCT---------- CAGAGGGCCGGCTGCTGCTGCTGCAGGACT
E E K E F G X X X S E G R L L L L Q D (indel)

Allele 3 GGAGGAGAAGGAGTTCGGCTTCCGCGGGACAGAGGGCCGGCTGCTGCTGCTGCAG
E E K E F G F R G T E G R L L L L Q (WT)

Note that both in the WT* clone #1 and in the double KO cell line, one of the indels is an in-frame deletion that introduces new residues in addition to deleting residues normally present in WT TPP1 protein. These alleles can in principle give rise to truncated TPP1 polypeptides. However, the reduction of TPP1 protein levels observed in the immunoblots of these cells is consistent with these alleles being KO alleles.

Chapter 3[3]

Mapping the TPP1-Telomerase interface

3.1 Abstract

The telomeric protein TPP1 recruits telomerase to the telomere through its N-terminal OB domain. The surface of this domain has been extensively studied and two separate surfaces called the TEL patch and NOB region were identified as necessary for TPP1 to recruit telomerase to the telomere. While the surfaces on TPP1 that is involved in telomerase recruitment are well defined, the corresponding interaction surface on TERT has yet to be fully characterized. Both the TEN domain and IFD of TERT have been implicated in interacting with TPP1, with one direct interaction between the TEN domain of TERT and the TEL patch of TPP1 being identified. Here we use an alanine scanning mutagenesis screen to define two regions, one in the TEN domain and one in the IFD, that are necessary for telomerase recruitment to the telomere. We then show with an *in vitro* primer extension assay that mutating residues in these regions affect the ability of TPP1 to stimulate telomerase processivity. Finally, we utilize a co-FISH based assay to show that these mutations affect the ability of telomerase to extend telomeres *in vivo*.

[3] Oana Danciu helped perform site directed mutagenesis to create several IFD mutant constructs and aided in performing IF-FISH assays. I carried out all other experiments shown in this chapter.

3.2 Introduction

Telomerase facilitates the continued division of stem and germ line cells by maintaining telomere length over time. Telomerase is recruited from structures called Cajal bodies in the nucleus to telomeres by the shelterin component TPP1. As aberrant telomerase expression is a hallmark of an overwhelming majority of cancers, the interface between the TPP1 and telomerase is a prime target for anti-cancer therapeutics. TPP1 is able to recruit telomerase through two specific regions found on its N-terminal OB domain, called the TEL patch and the NOB region (Figure 3.1A and B) [60,66,69,68]. We and others have highlighted the role of the TEL patch in telomerase recruitment by identifying and characterizing an in frame deletion of lysine 170 in the OB domain of TPP1 in patients suffering from telomeropathies. Lysine 170 is found directly in between two critical glutamates of the TEL patch and affected the ability of telomerase to maintain telomeres in these patients [127,125,124]. While much has been discovered about this interface from the side of TPP1 it is still not known which residues on telomerase are responsible for interacting with TPP1. To date only one direct interaction has been demonstrated by charge swap experiments between K78 of the TEN domain of TERT and E215 of the TEL patch of TPP1 [70]. Here we use an alanine mutagenesis screen to identify two stretches of amino acids: one in the TEN domain and another in the insertion in the fingers domain (IFD) of TERT that are important for telomerase recruitment to the telomere. The mutagenesis screen utilized an immunofluorescence-fluorescence *in situ* hybridization (IF-FISH) assay to determine which mutations affected recruitment of telomerase to the telomere without abolishing telomerase RNP assembly. Hits from the screen were further validated *in vitro* with a

direct primer extension assay for telomerase processivity stimulation by POT1-TPP1, and *in vivo* with a co-FISH assay used to detect newly synthesized telomeres in HeLa cells.

3.3 Results

3.3.1 Design of a mutagenesis screen to identify the TERT surface that binds TPP1

Previous work has established that the TEN and IFD domains of TERT are important for telomerase recruitment to the telomere through the TEL patch and NOB regions of the shelterin component TPP1. The primary structural insights into this process came from the *Tetrahymena* telomerase cryo-EM structures (Figure 3.2A). These structures were the first to reveal the proximity of TEN and IFD to each other and to the p50 subunit (the *Tetrahymena* homolog of TPP1). To begin to understand what role these domains play in telomerase recruitment we first attempted to express protein constructs for the TEN domain and IFD in human cells. Interestingly, a construct that linked the TEN domain with the IFD using a 20 amino acid serine/glycine linker expressed at a much higher level than either the TEN domain or IFD construct alone (Figure 3.1C). This result agrees with the recently published 4.8 Å resolution structure of *Tetrahymena* telomerase. In it the TEN domain and IFD interact through a surface described as a three-stranded β-sheet named the IFD TRAP (Figure 3.2A). From these observations, we hypothesized that the TEN and IFD come together to form structural platform that interacts with the TEL patch and NOB region of TPP1. To map the regions in TERT that are critical for telomerase recruitment by TPP1 we engineered an alanine scanning mutagenesis screen limited to only the TEN and IFD regions of human TERT.

We used the crystal structure of the *Tetrahymena* TEN domain, the cryo-EM structure of *Tetrahymena* telomerase, and sequence alignments between human and *Tetrahymena* telomerase (Figure 3.2B and C) to generate a homology model of the human TERT TEN and IFD regions. We selected residues to mutate that were well conserved and predicted to be on the surface of the TEN and IFD regions. The screen was composed of eighteen mutations in the TEN domain (3 double mutants, 15 single mutants) and twelve mutations in the IFD (9 double mutants, 3 single mutants) (Figure 3.2B and C and Figure 3.3). We also utilized the previously identified K78E mutation in the TEN domain as a positive control for defective interaction with TPP1 [70].

3.3.2 Scanning alanine mutagenesis reveals residues on TEN and IFD that are important for telomerase recruitment to the telomere

To identify residues on telomerase that interact with TPP1 we transiently transfected WT or mutant TERT along with TR into a HeLa-EM2-11ht derived cell line that stably expresses FLAG-TPP1. We then performed immunofluorescence (IF) and fluorescence *in situ* hybridization (FISH) to determine how mutations in TERT affected the ability of hTR (telomerase) to colocalize with FLAG-TPP1 (telomeres). In agreement with previous data, we found that WT TERT was effectively recruited to telomeres, with 97% of TR foci colocalized with FLAG-TPP1 foci, while TERT K78E showed only 46% of TR foci colocalized with FLAG-TPP1 foci (Figure 3.4). Eighteen TERT constructs from our mutagenesis screen with mutations in the TEN domain (A46I/F47Y, R48A, Q73A/S75A, E79A, R83A, Q86A/R87A, F115A, V119A, R120A, L141A and V162A) and IFD (Q722A/R72A, L725A/E727A, V747A, K757A/F759A, Q781A, R787A, and F809A/R811A) had 80-96% of their TR foci colocalize with FLAG-TPP1, suggesting

these mutations do not affect telomerase recruitment to the telomere (Figure 3.5 and 3.7). In sharp contrast, five TERT constructs with mutations in the TEN domain (N125A, T128I, L139A, L140A, and R143A) had only 2%-10% of their TR foci colocalize with FLAG-TPP1 foci (Figure 3.4A and B). Using the model developed from the *Tetrahymena* telomerase cryo-EM structures and protein sequence alignment of the *Tetrahymena* and human proteins, N125 and T128 can be mapped to an α-helix (α5) of the TEN domain which is in close proximity to p50 suggesting that these residues may interact with TPP1 (Figure 3.3). Residues L139, L140, and R143 all map to α6 which is in the core of the TEN domain suggesting that these residues may play a structural role instead of, or in addition to, interacting with TPP1. Additionally, six mutants in the IFD (V790A/I792A, E793A/Q794A, S802A/S803A, L805A/F806A, and V818A/R819A) had only 5%-22% of TR foci colocalize with FLAG-TPP1 foci (Figure 3.6A and B). Based on the same *Tetrahymena* telomerase cryo-EM structure, residues V790 and I792 are found at the interface between β3 of the IFD and TEN (Figure 3.3). Residues E793 and Q794 are found at the interface of IFD, TEN and p50 suggesting that at least one of these two residues may interact with TPP1. Residues S802, S803, L805, and F806 are all found in the C-terminal α-helix of the IFD that along with the N-terminal α-helix of IFD forms the short arm of the L-shaped structure (Figure 3.3). It is possible that the short arm interacts with TPP1 as it is in close proximity to the N-terminus of p50 in the *Tetrahymena* telomerase structure. Our primary screen of TEN and IFD mutants revealed that eleven mutants were significantly defective in telomerase recruitment to the telomere, and mapping their location on the *Tetrahymena* structure suggests that several of these residues could be involved in a direct interaction with TPP1. As a

corollary, most of the mutations that did not affect telomerase recruitment to telomeres are predicted to be located farther away from the telomerase-TPP1 interface based on our homology model of human telomerase (Figure 3.3; yellow residues).

3.3.3 Telomerase recruitment defects of many TEN and IFD mutants occur downstream of telomerase assembly

Previous experiments with TPP1 TEL patch mutants defective in telomerase recruitment have demonstrated that telomerase remains in Cajal bodies when not recruited to the telomere [124,66]. Indeed, all mutants in both the TEN domain and IFD that are defective in telomerase recruitment to the telomere show large TR foci, indicative of telomerase residing in the Cajal body. While this suggests defective telomerase recruitment by TPP1, it is also possible that some of these mutations disrupt the TERT structure in a way that would adversely affect expression. We were able to check TERT expression by immunoblot and found TERT constructs harboring mutations in the TEN or IFD were expressed (Figure 3.5C). It is also possible these mutations affect the ability of TERT to assemble with TR. As it is known that transfecting TR alone leads to large TR foci in Cajal bodies (Figure 3.8), it is possible that Cajal body localization of TR in the telomerase recruitment assay is a result of failed assembly of TR with TERT rather than due to failed recruitment to telomeres. To determine if the disruptive mutations identified in the recruitment assay grossly affected the ability of TERT and TR to assemble, a second set of IF-FISH experiments was performed. In these experiments HeLa-EM2-11ht cells were transiently transfected with either wild type or mutant FLAG-TERT along with TR. TR foci were visualized with FISH and immunofluorescence was used to detect FLAG-TERT. The extent to which TR

colocalized with FLAG-TERT was used to confirm correct telomerase assembly. When the HeLa cells were transfected with WT TERT or TERT K78E 91% and 84% of TR foci colocalized with FLAG-TERT foci respectively (Figure 3.8). In sharp contrast to the drastic reduction in telomerase recruitment to telomeres, most of these mutants (N125A, T128I, L139, L140A, V790A/I792A, E793A/Q794A, S802A/S803A, L805A/F806A) showed substantial TERT-TR colocalization in Cajal bodies (quantitation showed ~50% or higher level of assembly), suggesting that the telomerase recruitment defects could not be attributed to faulty RNP assembly (Figure 3.8 and Figure 3.9). It should be noted that the FLAG-TERT V790A/I792A used in the assembly assay, but not the untagged TERT V790A/I792A construct used in telomerase recruitment assays, has been fully sequenced and found to have DNA mutation encoding L55M in the TEN domain. Although, this unintended mutation does not appear to have a negative effect on RNP assembly we are working to perform these assays with the correct TERT V790A/I792A construct. While many TERT mutations did not affect assembly, two exceptions were V818A/R819A (36% TERT-TR colocalization) and R143E (no TERT signal), which showed large reductions in both telomerase recruitment to telomeres and telomerase assembly (Figure 3.8 and Figure 3.9). It is therefore possible that for these two mutants, the observed telomerase recruitment defect is primarily derived from the inability of TERT to assemble with TR, although an additional TPP1-binding role for the mutated residues cannot be ruled out. Taking both the recruitment and assembly data together we have been able to identify four mutants each in the TEN and IFD that are greatly defective in telomerase recruitment to telomeres *per se* (TEN: N125A, T128I, L139A, L140, IFD: V790A/I792A, E793A/Q794A, S802A/S803A, and L805A/F806A).

3.3.4 Mutations in TEN and IFD that disrupt telomerase recruitment also affect the stimulation of repeat addition processivity

It has been well established that POT1-TPP1 act to stimulate telomerase repeat addition processivity [64]. Two specific regions on the OB domain of TPP1 called the TEL patch and the NOB region have been shown to be responsible for both recruiting telomerase and stimulating its processivity [69,66]. To better understand if the telomerase residues identified here are responsible for interacting with the TEL patch and NOB regions of TPP1 we utilized a direct primer extension assay taking note of the caveat that any mutations that disrupt telomerase assembly and/or catalytic activity will obviate our ability to assess stimulation by POT1-TPP1. This assay has been used previously to show that K78 of TERT and E215 in the TEL patch of TPP1 interact using a charge swap [70]. Two other studies have utilized this assay to illustrate the importance of the interaction between TPP1 and the IFD [112,113]. As expected, POT1-TPP1 stimulated telomerase consisting of WT TERT by ~three fold over reactions without POT1 or TPP1 supplementation (Figure 3.10A and B). When we performed reactions that contained TERT that harbored an N125A, T128I, L139A or E793A/Q794A mutations, POT1-TPP1 was not able to stimulate their processivity. This, along with the recruitment data, suggests that these TERT residues are essential for a TPP1 interaction. When we tested the L805A/F806A mutants we found that POT1-TPP1 was able to stimulate processivity ~2 fold, suggesting that the residues may play a less critical role in binding TPP1 (Figure 3.10A and B). The S802A/S803A TERT mutant failed to show any activity in primer extension assays.This prevented analysis of this mutant with POT1-TPP1 (Figure 3.10A and B). More surprising however, TERT

harboring either an L140A or the V790A/I792A mutations also displayed no activity in our primer extension assays despite proper telomerase assembly (Figure 3.10A and B). Based on the crystal structures of the TEN domain from *Hansenula polymorpha* and *Tetrahymena* L140 is predicted to contribute to the core of the TEN domain, so mutating it to alanine might alter the structure of the TEN domain in addition to disrupting a potential interaction with TPP1 [99,100]. A residue in *Tetrahymena* TEN domain corresponding to human V791 (previously implicated in TPP1 binding) was mapped to the TEN-IFD interface in the recent cryo-EM structure of *Tetrahymena* telomerase. Thus the V790A/I792A mutation may result in a loss of activity because these residues are important for the integrity of the TEN-IFD interface and therefore holoenzyme stability (Figure 3.3) [113,121]. Based on the same structure N125, T128, E793, and Q794 of human TERT are all expected to interact with TPP1 (Figure 3.3).

3.3.5 TEN and IFD mutations compromised in telomerase recruitment are unable to extend telomeres *in vivo*

To assess the effects of TERT mutations on telomere elongation in living cells, we transiently transfected the FLAG-TPP1 HeLa stable cell line with wild type or mutant TERT and a telomerase RNA (TR) mutant that contains a non-telomeric sequence in its template (3'-GCCAAC-5'). This allows us to visualize newly added mutant telomere repeats by performing FISH with a Cy3 labeled DNA probe that cannot hybridize to the canonical GGTTAG repeat, but rather binds the newly added mutant 5'-GTTGCG-3' repeat. We simultaneously determined the localization of FLAG-TPP1 (telomeres) by IF, and the localization of the mutant TR (telomerase) by FISH. We found that the Cy3 labeled DNA probe not only hybridizes to the newly synthesized telomeric repeats, but

also non-specifically to RNA found in the nucleolus (Large red spots, Figure 3.11). The protocol this experiment was adapted from called for the use of an RNase, but as our experiment relied on visualizing TR foci to determine which cells were transfected with telomerase, we omitted RNase treatment. As the nucleolar staining is spatially separated from telomeric foci, it did not interfere with our analysis.

With transfections containing WT TERT and mutant TR, approximately 75% of HeLa cells that contained telomerase also contained newly synthesized mutant telomeres. However when TERT K78E was transfected we found that 28% of cells contained both TR and mutant telomeric repeats. Based on the defects in recruitment and the inability of POT1-TPP1 to stimulate telomerase repeat addition processivity, it is not surprising that transfections with TERT containing TEN domain or IFD mutations had significantly less cells that contained mutant telomeres than transfections with WT TERT (Figure 3.11 and Figure 3.12). When TERT containing N125A, T128I, or L139A were transfected into cells we found that between 13% and 15% of cells contained both TR foci and foci corresponding to newly synthesized telomeres, while L140A, V790A/I792A, E793A/Q794A, S802A,S805A, and L805A/F806A all displayed between 6% and 9% of cells containing both TR foci and newly synthesized telomeres (Figure 3.11 and Figure 3.12). These data confirm that mutations in telomerase that adversely impact telomerase recruitment by TPP1 also fail to extend telomeres *in vivo*.

3.4 Discussion

Telomerase is a unique ribonucleoprotein that is able to both provide the template for and catalyze the synthesis of telomeric repeats at the extreme ends of linear chromosomes. This action facilitates continued division of stem cells by counteracting

the erosion of telomeres that would occur due to the end replication problem. The telomerase RNP is assembled from TERT, TR and other associated factors in the nucleus and trafficked to Cajal bodies in preparation for telomerase recruitment. Telomerase is then recruited to telomeres by TPP1 to facilitate chromosome end replication. Here I show that mutating residues in both the TEN and the IFD can result in a defect in telomerase recruitment, a loss of POT1-TPP1 facilitated repeat addition processivity *in vitro*, and an inability to extend telomeres *in vivo*. This allows us to define two separate stretches of amino acids, one in the TEN domain and one in the IFD that are necessary for telomerase recruitment to the telomere (Figure 3.13).

Here we set out to define regions of TERT, specifically in the TEN domain and IFD, that are important for telomerase recruitment to the telomere through the established interaction with TPP1. We were able to use an alanine scanning mutagenesis screen in conjunction with a series of IF-FISH experiments to define two stretches of amino acids, one in the TEN domain and one in the IFD, that when mutated affect telomerase recruitment to the telomere. We were further able to show that many of these mutations didn't affect the ability of TERT and TR to assemble, confirming that the telomerase recruitment defect was not a consequence of compromised RNP assembly. Additionally, using a direct primer extension assay we were able to show that the repeat addition processivity of telomerase harboring telomere recruitment-defective mutations (N125A, T128I, L139A and E793A/Q794A) was not able to be stimulated by POT1-TPP1 further suggesting that the mutated residues directly interact with TPP1. Ultimately we were also able to demonstrate that mutations in the TEN and IFD affected the ability of telomerase to extend telomeres *in vivo.*

Creating a homology model of human telomerase based off of the *Tetrahymena* telomerase cryo-EM structure allows us to map the mutations that we found in the TEN and IFD to their predicted location in TERT and relative to the OB domain of TPP1 (Figure 3.13). In the TEN domain this region starts with a predicted α-helix, which begins with N125 and contains T128. This region continues with a short flexible linker that contains R132 and continues into another predicted helix that contains L139, L140, and R143. In the IFD we identified a region that begins with a long loop/β-strand (shown to be a β-sheet in the *Tetrahymena* cryo-EM structure). This loop is in close proximity to the TEN domain and a portion of the loop forms part of the IFD-TRAP defined by Jiang et al. *Cell* 2018. The region of the IFD that we found to be important for telomerase recruitment continues into a predicted C-terminal α-helix (Figure 3.13). Together the stretches of residues in the TEN domain and the IFD are predicted to form a contiguous surface that is oriented toward TPP1 in our model. The crystal structure of the OB domain of TPP1 was placed in our homology model using the orientation of p50 in the cryo-EM structure along with the K78-E215 interaction as a guide. The NOB region of TPP1 is predicted to be in close proximity to the IFD residues and the TEL patch is in close proximity to the two predicted α-helices we found to be important for telomerase recruitment. While these predictions may provide a reasonable approximation of how TPP1 and TERT interact, a crystal structure or a high resolution cryo-EM map of the two proteins in complex is still required to fully define the interface between the two proteins.

3.5 Materials and methods

3.5.1 Molecular cloning and site-directed mutagenesis

All mutations in TERT were introduced into p3X-FLAG-TERT-cDNA6/myc-HisC and pTERT-cDNA6/myc-HisC using the QuikChange® Site-Directed Mutagenesis Kit (Agilent Technologies) and complementary mutagenic primers (Integrated DNA Technologies). The resulting plasmids were sequenced to confirm both the presence of the intended mutation and the absence of unwanted errors introduced during PCR amplification/cloning.

3.5.2 Cell culture

HeLa-EM2-11ht cells were used in all IF-FISH experiments. HEK 293T cells were used to create super telomerase extracts following previously published protocols [127,66]. Cells were grown at 37°C in the presence of 5% CO2 and grown in media containing modified DMEM (Gibco; Dulbecco's Modified Eagle Medium; 11995-065), 100 U/mL penicillin, 100 µg/mL streptomycin, and 10% FBS. For experiments where induction was necessary, doxycycline was added to a final concentration of 200 ng/mL to drive a tetracycline-inducible promoter within the p6X-FLAG-BI4 plasmids (FLAG-TPP1).

3.5.3 Immunoblots

Immunoblotting was performed using previously published protocols with the following antibodies: mouse monoclonal anti-FLAG M2-HRP conjugate (Sigma; A8592; 1:10,000), mouse monoclonal anti-FLAG M2 (Sigma; F3165; 1:10,000) . Secondary horseradish peroxidase-conjugated goat antibodies against mouse IgG (Santa Cruz

Biotechnology; 1:10,000) were used to observe primary antibodies using chemiluminescence detection by ECL plus reagents (Pierce ECL Western Blotting Substrate; Thermo Scientific). The data were visualized using a gel-documentation system (ChemiDoc MP System; Bio-Rad).

3.5.4 IF-FISH to monitor telomerase recruitment to telomeres and telomerase assembly

IF-FISH experiments for telomerase recruitment were performed exactly as described previously [127]. For telomerase assembly ~1.2 million HeLa-EM2-11ht cells in 6-well plates were transiently transfected using Lipofectamine 2000 (Fisher; 11668019) with 1 µg of p3X-FLAG-TERT-cDNA6/myc-HisC and 3 µg of phTRmut-Bluescript II SK (+) plasmids using the manufacturer recommended protocol. 24 h post transfection cells were fixed with 4% formaldehyde in PBS for 10 min at room temperature, washed with PBS three times. The cells were permeabilized with PBS containing 0.3% Triton X-100 for 5 min and subsequently blocked in PBS containing 0.1% Triton X-100, and 3% BSA for 30 min. Cells were incubated with mouse monoclonal anti-FLAG M2 (Sigma; F1804; 1:500) in PBS containing 0.1% Triton X-100, and 3% BSA for 1 h. The cells were then washed three times in PBS for 5 min each wash, and incubated with Alexa Fluor 568-conjugated anti-mouse IgG (Life Technologies). The cells were then washed three times in PBS and fixed with 4% formaldehyde in PBS for 10 min at RT. After washing the cells three times with PBS the cells were consecutively dehydrated for 5 min each with 70%, 95%, and 100% ethanol. Cells were air dried for 3 min and then rehydrated with 2X SSC 50% formamide for 5 min prior to pre-hybridizing for 1 h with hybridization buffer containing 100 mg/ml

dextran sulfate, 0.125 mg/ml yeast tRNA, 1 mg/ml BSA, 0.5 mg/ml salmon sperm DNA, 1 mM vanadyl ribonucleoside complexes (VRC), and 50% formamide in 2X SSC. After pre-hybridization cells were transferred to hybridization solution containing a mixture of three Cy5-conjugated probes against TR and then incubated at 37°C for ~16 h. After incubation cells were washed with 2X SSC 50% formamide for 30 min each wash and mounted on microscope slides using ProLong Gold mounting medium with DAPI (Life Technologies). Imaging was performed using a laser scanning confocal microscope (SP5; Leica, Germany) equipped with a 100X oil objective. ImageJ and Adobe Photoshop were used to process all images.

3.5.5 Protein expression and purification

TPP1-N and POT1 proteins were prepared as described previously [127]. Briefly, lysates from isopropyl β-d-thiogalactopyranoside-induced BL21(DE3) cells were passed through a nickel-agarose (Ni-NTA) column. Following elution the proteins were treated with Ulp1 protease (material transfer agreement with Cornell University for pUlp1 vector) to cleave the Smt3 tag. The final step of purification was Size-exclusion chromatography (Superdex 75; GE Life Sciences). The baculoviral expression plasmid for His-Sumostar-hPOT1 was described previously [127]. This plasmid was used to express POT1(1-634) in High Five cells (Life Technologies) that were infected with a baculovirus using vendor recommendations. Insect cell lysates were passed over a nickel-agarose column. After elution the sumostar tag on full length POT1 was cleaved with SUMOstar protease (Life Sensors) and the POT1 protein was first purified by anion exchange (HiTrap Q HP; GE Life Sciences), and subsequently size-exclusion chromatography (Superdex 200; GE Life Sciences).

3.5.6 Preparation of telomerase extracts

Telomerase extracts were prepared as published previously [66]. First HEK 293T cells were seeded into a 6 cm dish at a density of approximately 800,000 cells and transfected about 42 h later using Lipofectamine 2000 (Invitrogen) using the manufacturer's recommended protocol. 1 µg of each p3X-FLAG-TERT-cDNA6/myc-HisC construct, and 3 µg phTR-Bluescript II SK(+)18 were added for each transfection. After 24 h cells were trypsinized and plated in a 10 cm dish, and 48 h after transfection the cells were trypsinized and consecutively washed with DMEM containing 10% FBS and PBS. The detached cells were spun down at 800 rpm after each wash step. Cells were then resuspended in 300 µl CHAPS buffer (10 mM Tris-HCl (pH 7.5), 1 mM MgCl2, 1 mM EGTA, 0.5% CHAPS, 10% glycerol, 5 mM BME, 1X complete, Mini, EDTA-free Protease Inhibitor Cocktail (Rouche, 11836170001) and 2.5 ul 20 U/ul SupernaseIn (Ambion, AM2694). Resuspended cells were nutated for 20 min at 4°C, and following nutation, centrifuged at 14,000 x g for 10 min at 4°C. The supernatant was flash frozen as 30 µl aliquots in liquid nitrogen before being stored at -80°C.

3.5.7 Direct telomerase activity assays

Telomerase assays were performed as described previously [66,127]. Super telomerase extracts from HEK 293T cells were prepared as described above. Before starting telomerase reactions immunoblots were performed using a FLAG antibody of WT and mutant extracts to ensure equal amounts of telomerase were added to each reaction. In each reaction, the total amount of HEK 293T cell extract was 6 µl. Each reaction contained 500 nM POT1 and 500 nM TPP1-N (87-334) as well as 50 mM Tris–Cl (pH 8.0), 1 mM MgCl2, 1 mM spermidine, 30 mM KCl, 5 mM β-mercaptoethanol, 1

µM of primer a5 (TTAGGGTTAGCGTTAGGG), 500 µM dATP, 500 µM dTTP, 2.92 µM unlabeled dGTP, and 0.17 µM radiolabeled dGTP (3000 Ci/mmol). Reactions proceeded for 1 hour at 30°C. 100 µl of buffer containing 3.6 M ammonium acetate and 20 µg of glycogen was used to quench each reaction, and the DNA products were precipitated with 70% ethanol at -80°C overnight. The pellets were resuspended in 7 µl H_2O, then mixed with 7 µl loading buffer containing 95% formamide, and heated at 95°C for 5 min. Samples were resolved on a 10% acrylamide, 7 M urea, 1X TBE sequencing-size gel, which was then dried and imaged on a phosphorimager (Storm; GE). All assays were analyzed using Imagequant TL (GE Life Sciences) software. Processivity calculations were performed as previously described [127].

3.5.8 Detection of *in vivo* telomere synthesis using mutant TR IF-coFISH

To monitor the synthesis of mutant telomeric DNA in HeLa-EM2-11ht derived FLAG-TPP1 stable cell lines, cells were induced with 200 ng/µl doxycycline for 48 h prior to transfection with TERT and TR. After 48 h induction, 1 µg of p3X-FLAG-TERT-cDNA6/myc-HisC and 3 µg of template mutated phTRmut-Bluescript II SK (+) plasmids were transfected into 6-well plates with approximately 1.2 million cells with Lipofectamine LTX (Fisher; 15338100) using the manufacturer recommended protocol. 24 h post transfection cells were fixed with 4% formaldehyde in PBS for 10 min at room temperature and washed three times with PBS. The cells were fixed 24 h post transfection to both allow enough time for telomere elongation, but not allow for cell death presumed to be caused from end deprotection by the addition of a non-canonical telomeric sequence. The cells were permeabilized with PBS containing 0.3% Triton X-100 for 5 min and subsequently blocked in PBS containing 0.1% Triton X-100, and 3%

BSA for 30 min. Cells were incubated with mouse monoclonal anti-FLAG M2 (Sigma; F1804; 1:500) in PBS containing 0.1% Triton X-100, and 3% BSA for 1 h. The cells were then washed three times in PBS for 5 min each wash, and incubated with Alexa Fluor 568-conjugated anti-mouse IgG (Life Technologies). The cells were then washed three times in PBS and fixed with 4% formaldehyde for 10 min at RT. After washing the cells three times with PBS the cells were consecutively dehydrated for 5 min each with 70%, 95%, and 100% ethanol. Cells were then rehydrated with 2X SSC 50% formamide for 5 min prior to pre-hybridizing for 1 h with a hybridization buffer containing 100 mg/ml dextran sulfate, 0.125 mg/ml yeast tRNA, 1 mg/ml BSA, 0.5 mg/ml salmon sperm DNA, 1 mM vanadyl ribonucleoside complexes (VRC), and 50% formamide in 2X SSC. After pre-hybridization cells were transferred to hybridization solution containing a mixture of three Cy5-conjugated probes against TR and a Cy3-conjugated PNA-$(CCGCAA)_3$ probe. The cells were heated at 80°C for 5 min for denaturation then incubated at 37°C for ~18 h. After incubation cells were washed with 2X SSC 50% formamide for 30 min and mounted on microscope slides using ProLong Gold mounting medium with DAPI (Life Technologies). Imaging was performed using a laser scanning confocal microscope (SP5; Leica, Germany) equipped with a 100X oil objective. ImageJ and Adobe Photoshop were used to process all images.

3.6 Figures

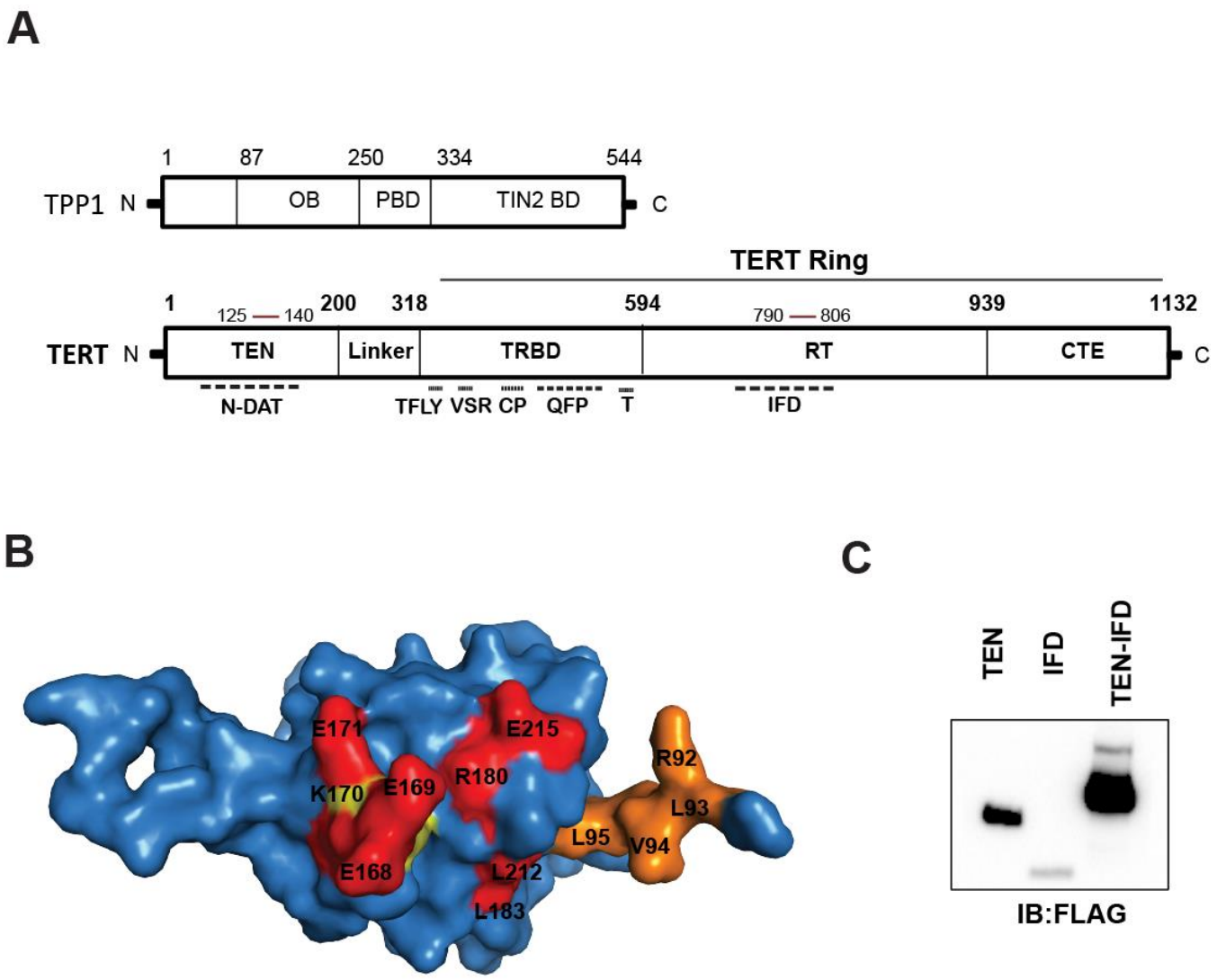

Figure 3.1 Domains involved in the telomerase-TPP1 interaction.
(A) Domain diagrams of TPP1 and TERT. TEN: telomerase N-terminal domain, TRBD: telomerase RNA binding domain, RT: reverse transcriptase domain, CTE: C-terminal extension, N-DAT: N-terminal dissociates activities of telomerase, VSR: vertebrate-specific recognition motif, IFD: insertion in the fingers domain. (B) The solved crystal structure of the OB domain of TPP1 (PDB: 2I46) with TEL patch residues in red, NOB residues in orange, and K170 in yellow. (C) FLAG immunoblot depicting the expression levels of FLAG-TEN, FLAG-IFD, and the fusion construct FLAG-TEN-$(SG)_{20}$-IFD. Experiment was performed in duplicate.

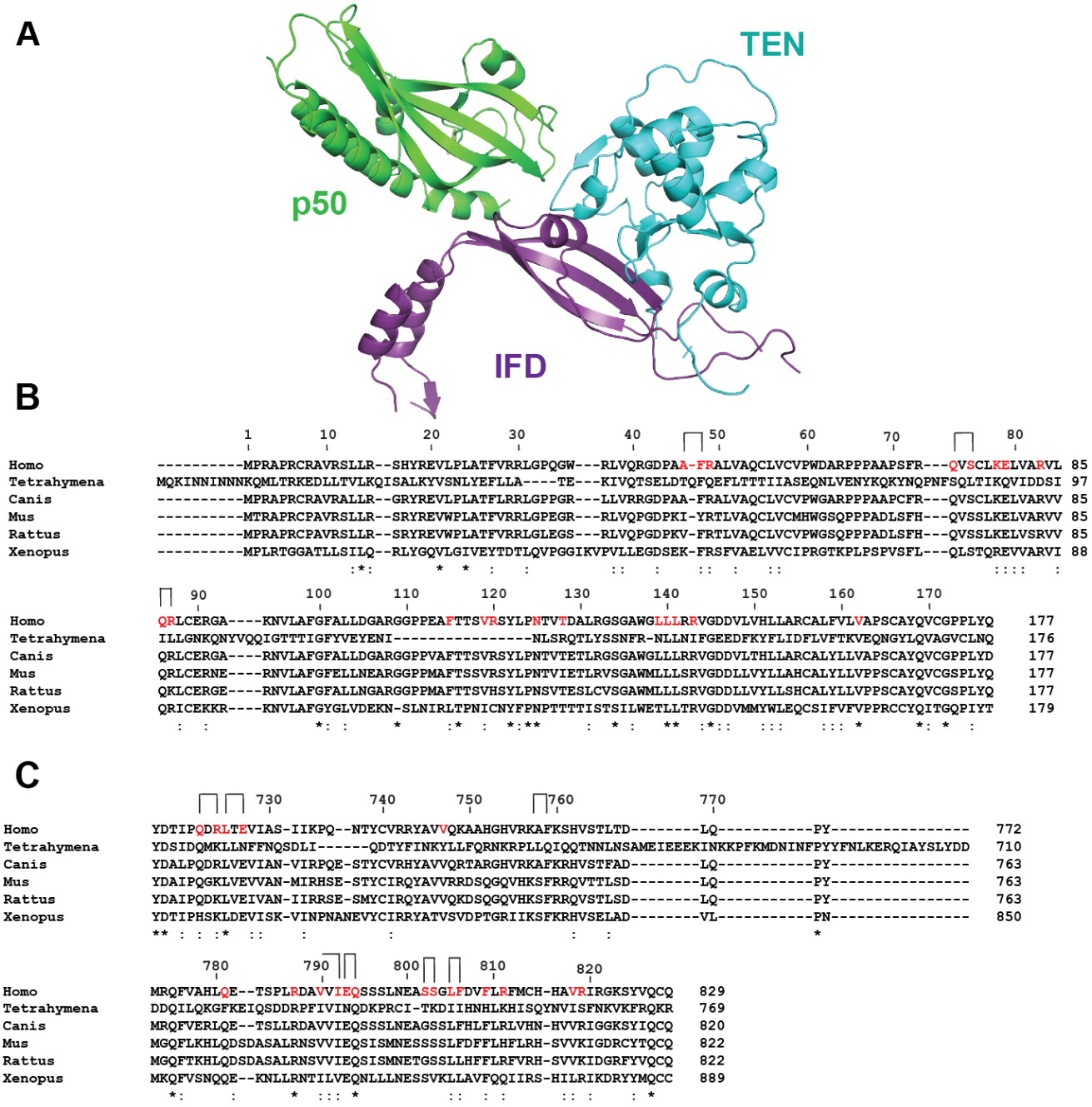

Figure 3.2 Structural model-based mutagenesis screen of TEN and IFD.
(A) CryoEM model of Tetrahymena telomerase (PDB ID: 6D6V) (B) Sequence alignment of the TEN domain from indicated eukaryotic TERT homologs. Sequence alignments were performed with ClustalW and refined manually. The alignment in Schmidt et al. *eLife* 2016 was used as a guide. (C) Sequence alignment of the IFD sequences from indicated eukaryotic TERT homologs. Initial alignment was performed by MUSCLE and refined manually. In B and C, mutated residues are shown in red; double mutants are denoted with brackets.

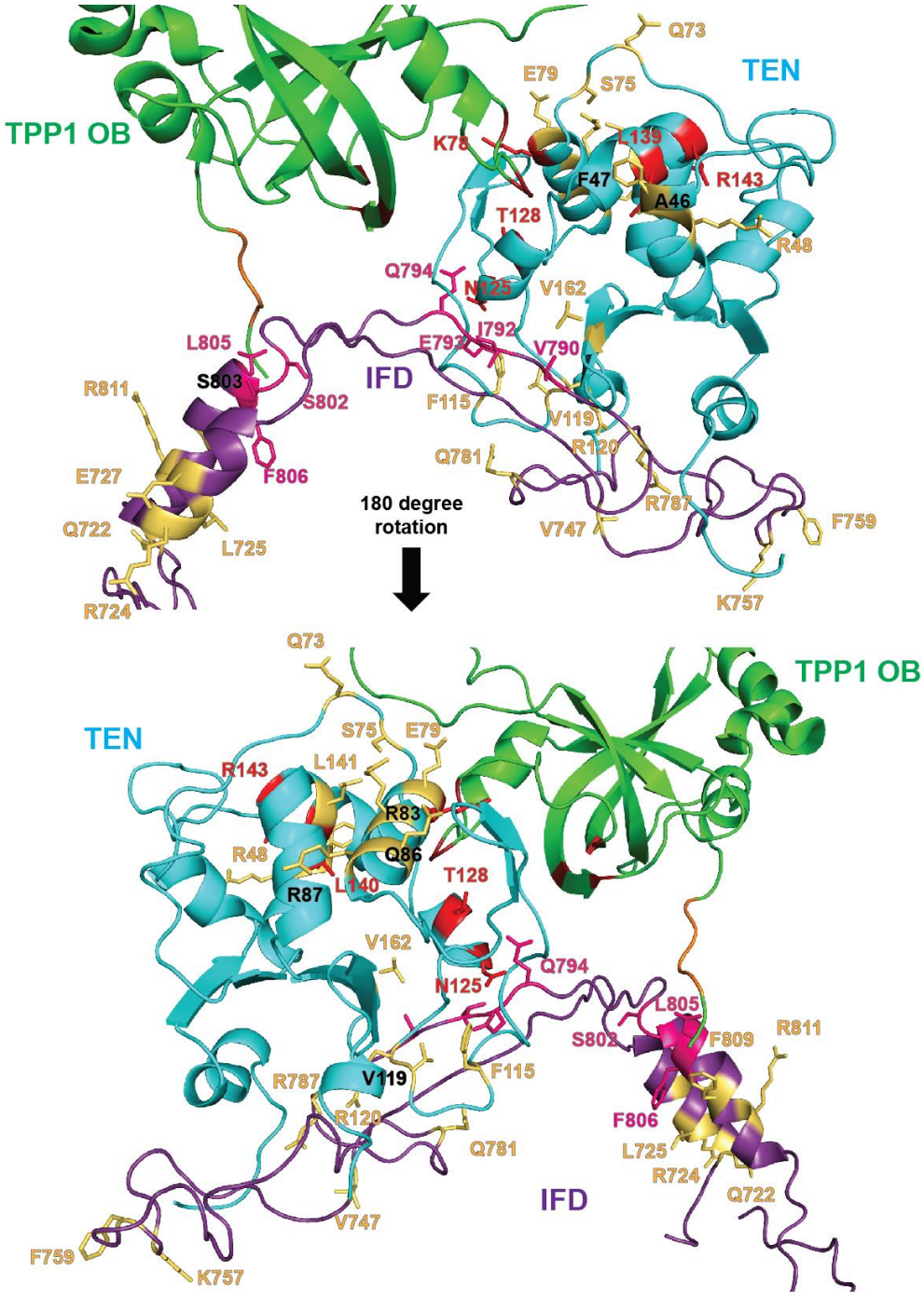

Figure 3.3 A model of human TEN and IFD with the TPP1 OB Domain.
Two views of a model of human telomerase generated with SWISS-MODEL using the *Tetrahymena* telomerase structure (PDB ID: 6D6V) along with the sequence alignments in Figure 3.2B and C. In green is the TPP1 OB domain (PDB ID: 2146). TEL patch residues are in red and NOB residues in orange. The TEN domain (cyan) and IFD (violet) are both homology models. Residues in yellow are mutated residues in hTERT that had no effect on telomerase recruitment. Residues in red (TEN) or pink (IFD) are residues that are important for telomerase recruitment to the telomere.

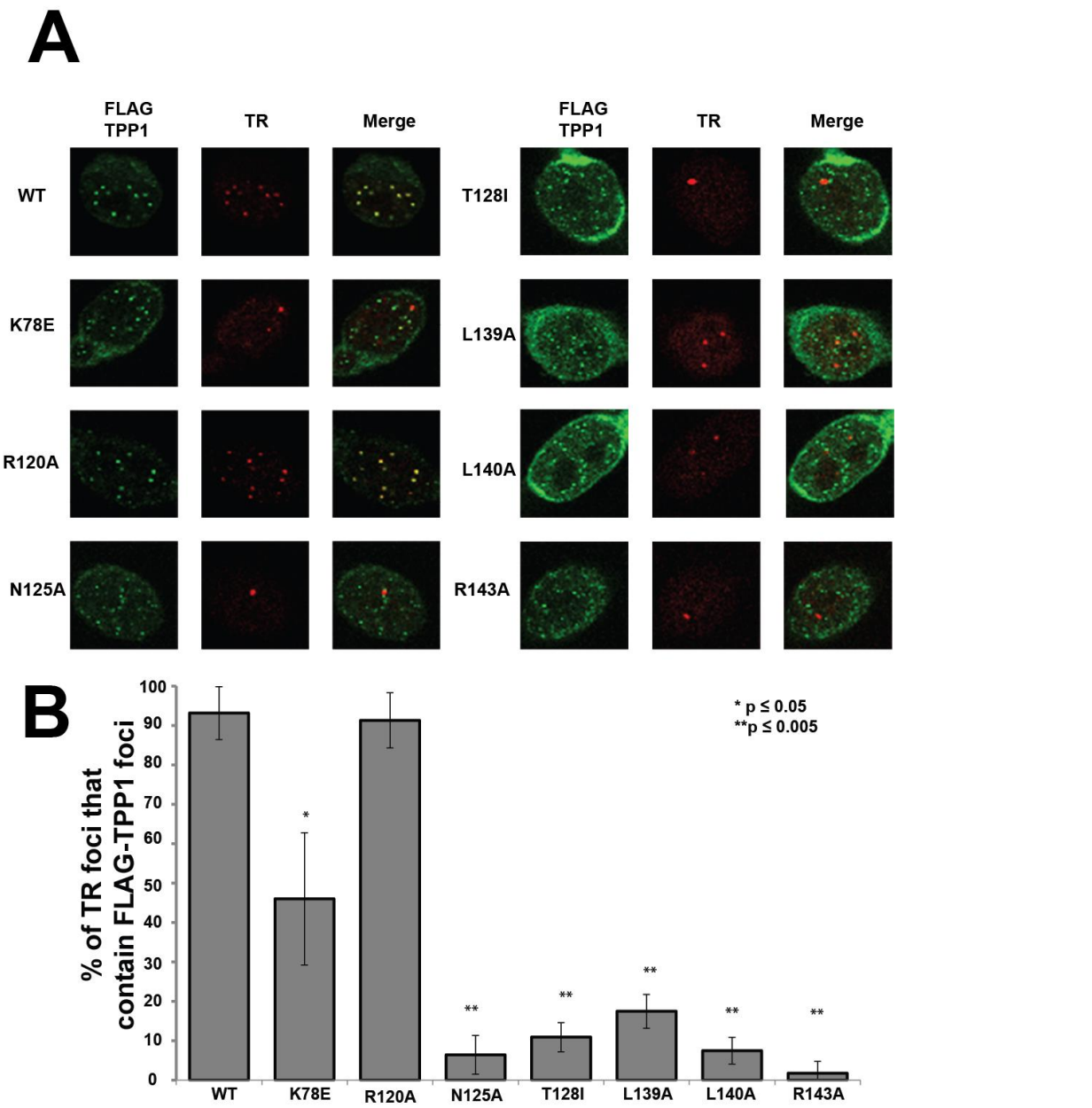

Figure 3.4 Several mutations in the TEN domain affect recruitment of telomerase to telomeres.

(A) Stable HeLa-EM2-11ht clones overexpressing FLAG-TPP1 and transiently transfected with TR and the indicated TERT mutant were analyzed for telomerase recruitment to telomeres using immunofluorescence-fluorescence *in situ* hybridization. TPP1 foci (green) were detected by immunofluorescence. Telomerase RNA (TR; red) was detected by fluorescence *in situ* hybridization. Yellow/orange coloration in the *Merge* panels signifies recruitment of TR foci to telomeres. (B) Quantitation of telomerase recruitment data of which panel A is representative. The mean percentage of TR foci containing TPP1 foci was calculated and standard deviation for triplicate measurements (>100 TR foci scored in total) were plotted.

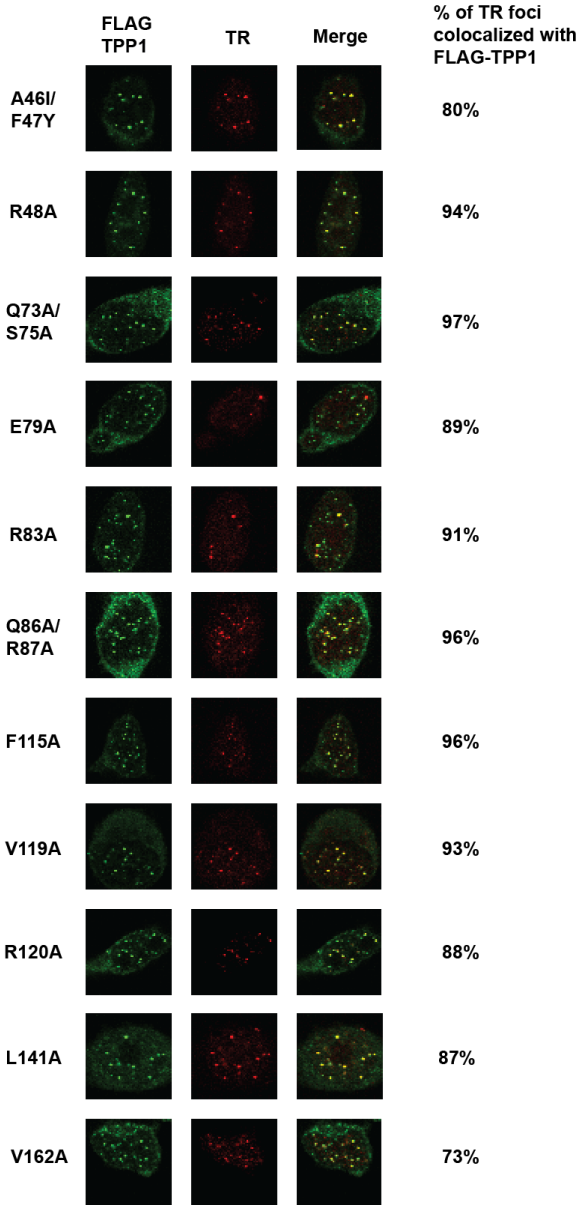

Figure 3.5 Several mutations in The TEN domain are permissive towards telomerase recruitment to telomeres.
Stable HeLa-EM2-11ht clones overexpressing FLAG-TPP1, and transiently transfected with TR and the indicated TERT mutant were analyzed for telomerase recruitment to telomeres using immunofluorescence-fluorescence *in situ* hybridization. TPP1 foci (green) were detected by immunofluorescence. Telomerase RNA (TR; red) was detected by fluorescence *in situ* hybridization. Yellow/orange coloration in the *Merge* panels signifies recruitment of TR foci to telomeres. Quantitation of telomerase recruitment data of which images are representative is shown to the right.

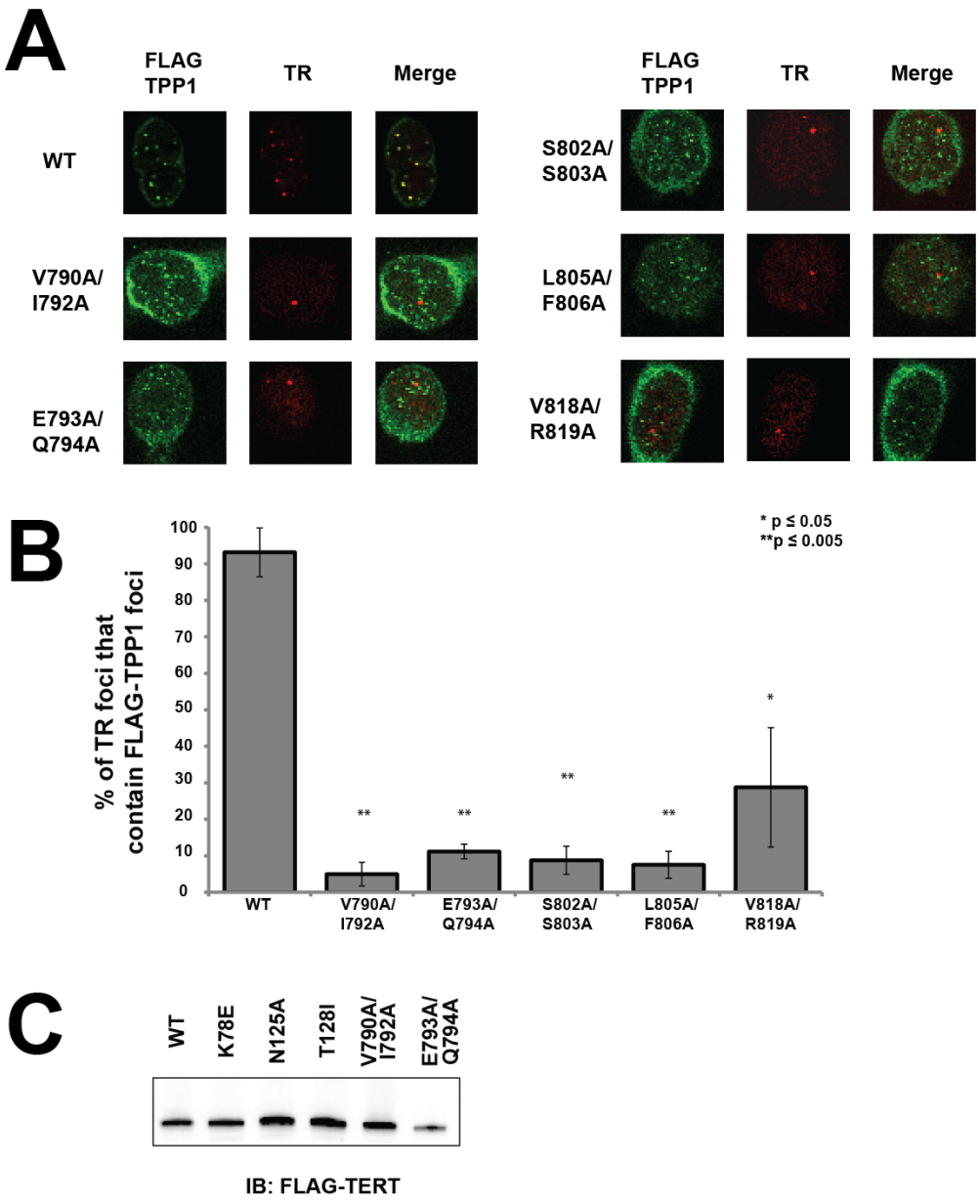

Figure 3.6 Several mutations in the IFD affect recruitment of telomerase to telomeres.
(A) Stable HeLa-EM2-11ht clones overexpressing FLAG-TPP1 and transiently transfected with TR and the indicated TERT mutant were analyzed for telomerase recruitment to telomeres using immunofluorescence-fluorescence *in situ* hybridization. TPP1 foci (green) were detected by immunofluorescence. Telomerase RNA (TR; red) was detected by fluorescence *in situ* hybridization. Yellow/orange coloration in the *Merge* panels signifies recruitment of TR foci to telomeres. (B) Quantitation of telomerase recruitment data of which panel A is representative. The mean percentage of TR foci containing TPP1 foci was calculated and standard deviation for triplicate measurements (>100 TR foci scored in total) were plotted. (C) Immunoblot of the indicated FLAG-TERT constructs expressed in HEK293T cells.

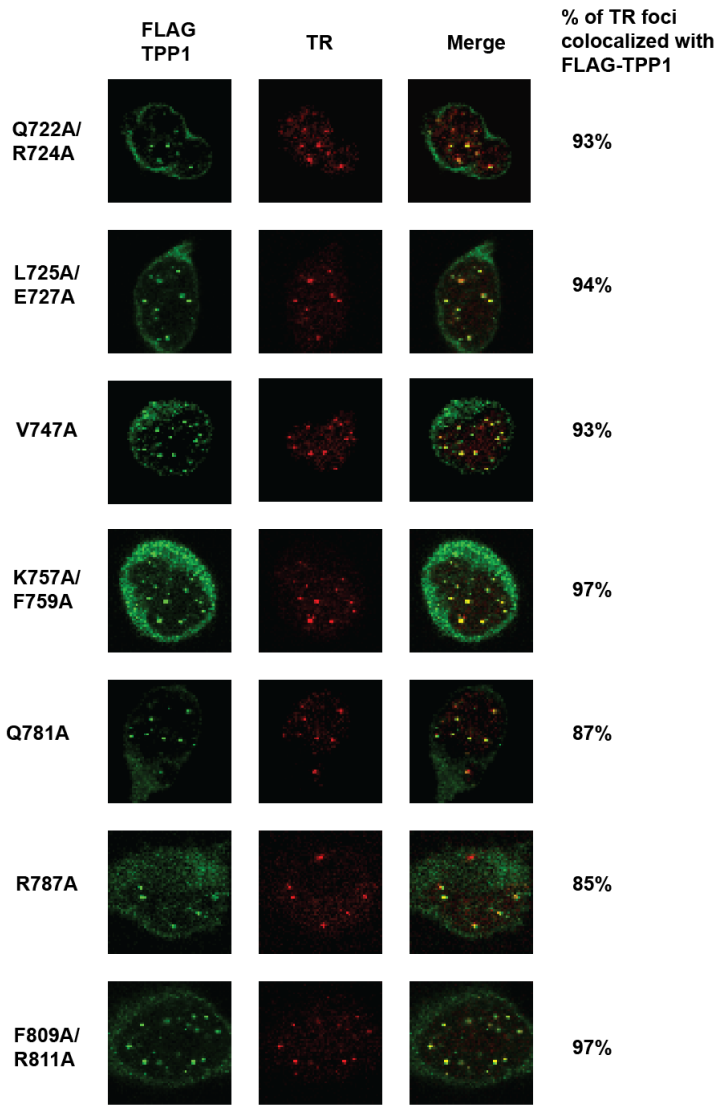

Figure 3.7 Several mutations in The IFD are permissive towards telomerase recruitment to telomeres.
Stable HeLa-EM2-11ht clones overexpressing FLAG-TPP1 and transiently transfected with TR and the indicated TERT mutant were analyzed for telomerase recruitment to telomeres using immunofluorescence-fluorescence *in situ* hybridization. TPP1 foci (green) were detected by immunofluorescence. Telomerase RNA (TR; red) was detected by fluorescence *in situ* hybridization. Yellow/orange coloration in the *Merge* panels signifies recruitment of TR foci to telomeres. Quantitation of telomerase recruitment data of which panel A is representative is shown to the right. The mean percentage of TR foci containing TPP1 foci was calculated (>100 TR foci scored in total).

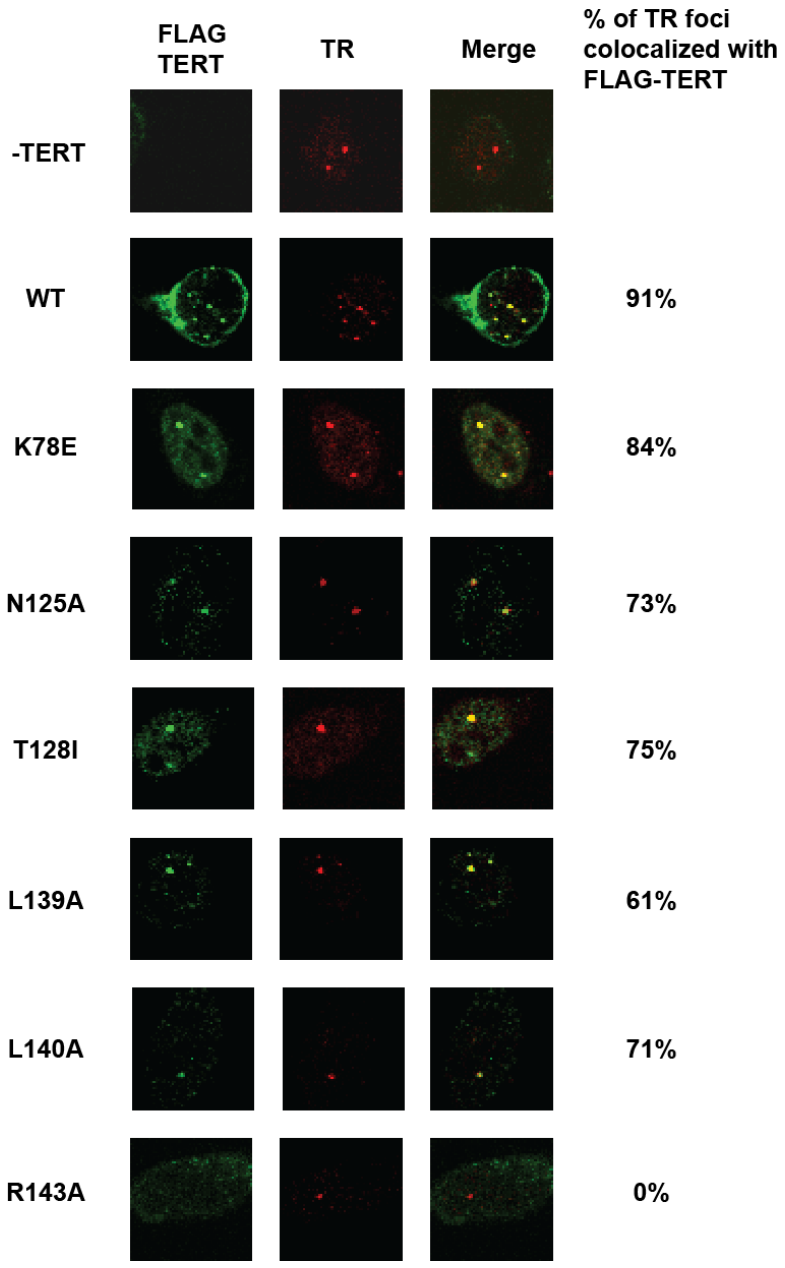

Figure 3.8 Analysis of telomerase assembly of mutants in the TEN domain. HeLa cells were transiently transfected with TR and the indicated FLAG-TERT constructs and assembly was analyzed using immunofluorescence-fluorescence *in situ* hybridization. “-TERT“ implies cells were not transfected with TERT. TERT foci (green) were detected by immunofluorescence. Telomerase RNA (TR; red) foci were detected by fluorescence *in situ* hybridization. Yellow/orange coloration in the *Merge* panels signifies colocalization of TERT and TR. Quantitation of telomerase assembly data of which images are representative is shown to the right. The mean percentage of TR foci containing TERT foci was calculated (>50 TR foci scored in total).

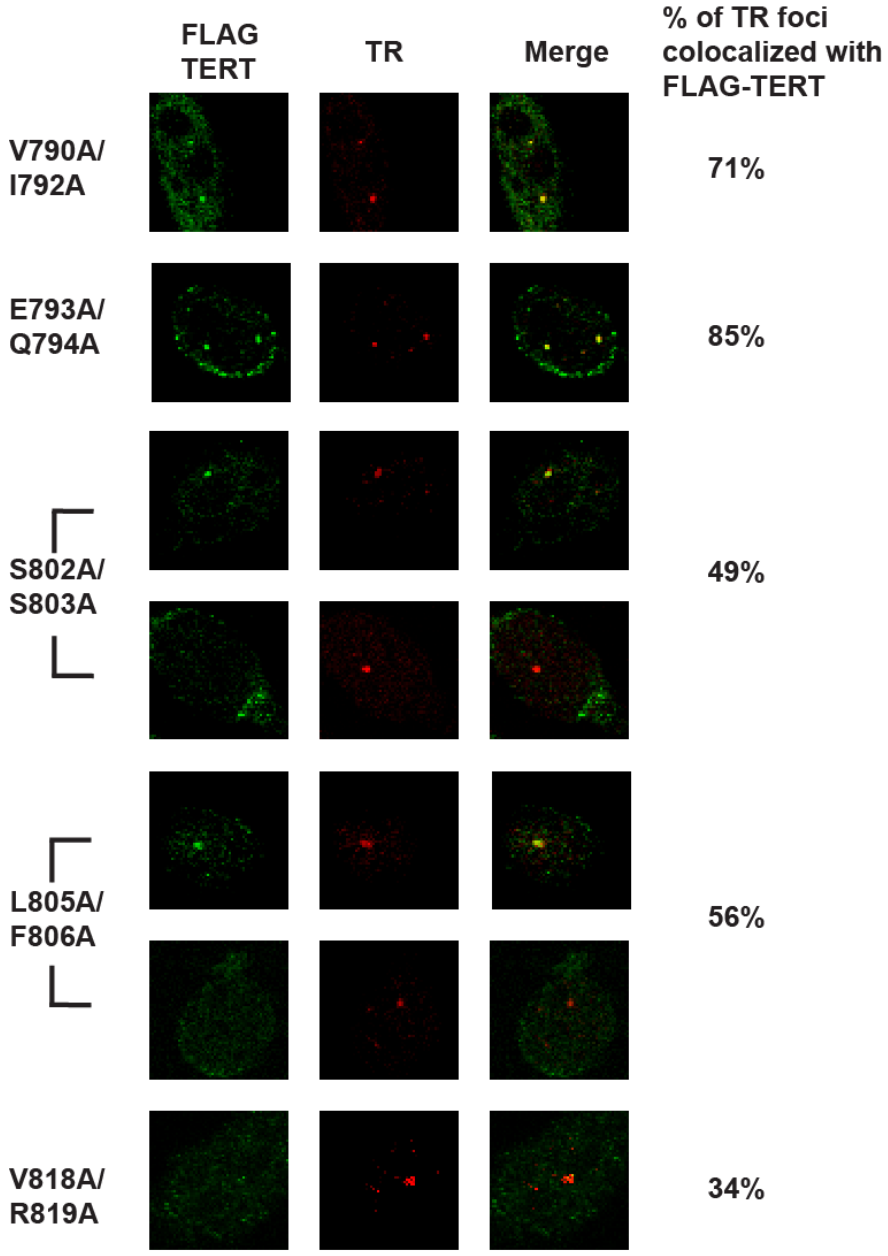

Figure 3.9 Analysis of telomerase assembly of mutants in the IFD.
HeLa cells were transiently transfected with TR and the indicated FLAG-TERT constructs assembly was tested using immunofluorescence-fluorescence *in situ* hybridization. TERT foci (green) were detected by immunofluorescence. Telomerase RNA (TR; red) foci were detected by fluorescence *in situ* hybridization. Yellow/orange coloration in the *Merge* panels signifies colocalization of TERT and TR. Quantitation of telomerase assembly data of which images are representative is shown to the right. The mean percentage of TR foci containing TERT foci was calculated (>50 TR foci scored in total).

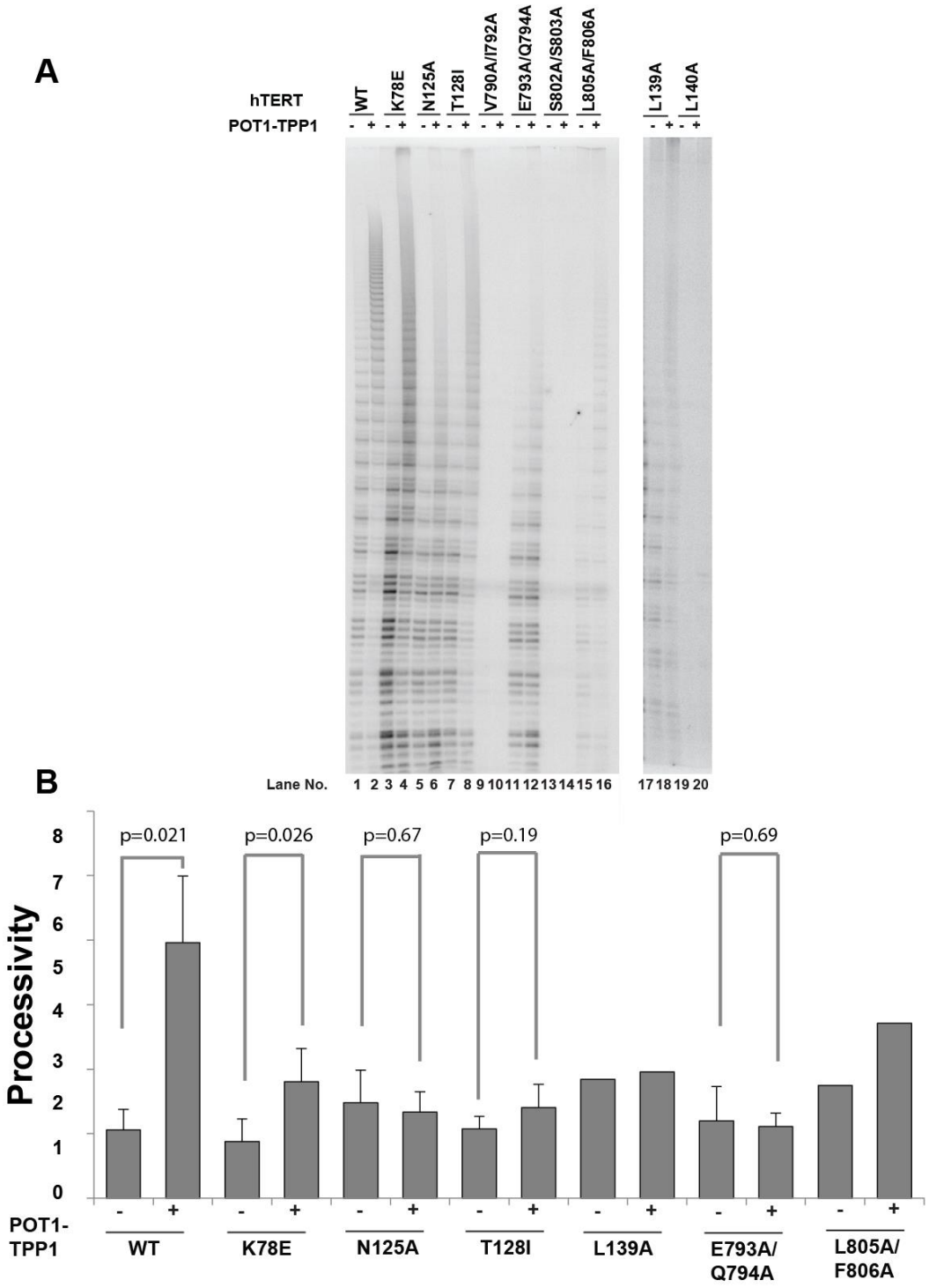

Figure 3.10 Several mutations in the TEN domain and IFD affect telomerase repeat addition processivity.

(A) Direct primer extension assay using primer a5. Lanes positive for POT1-TPP1 contain 500 nM each of purified TPP1-N and POT1. (B) Quantification of direct primer extension assays. n = 3 for WT, K78E, N125A, T128I, and E793A/Q794A. n = 2 for L139A and L805A/F806A; average values are shown. p-values were calculated using a two tailed student's t-test.

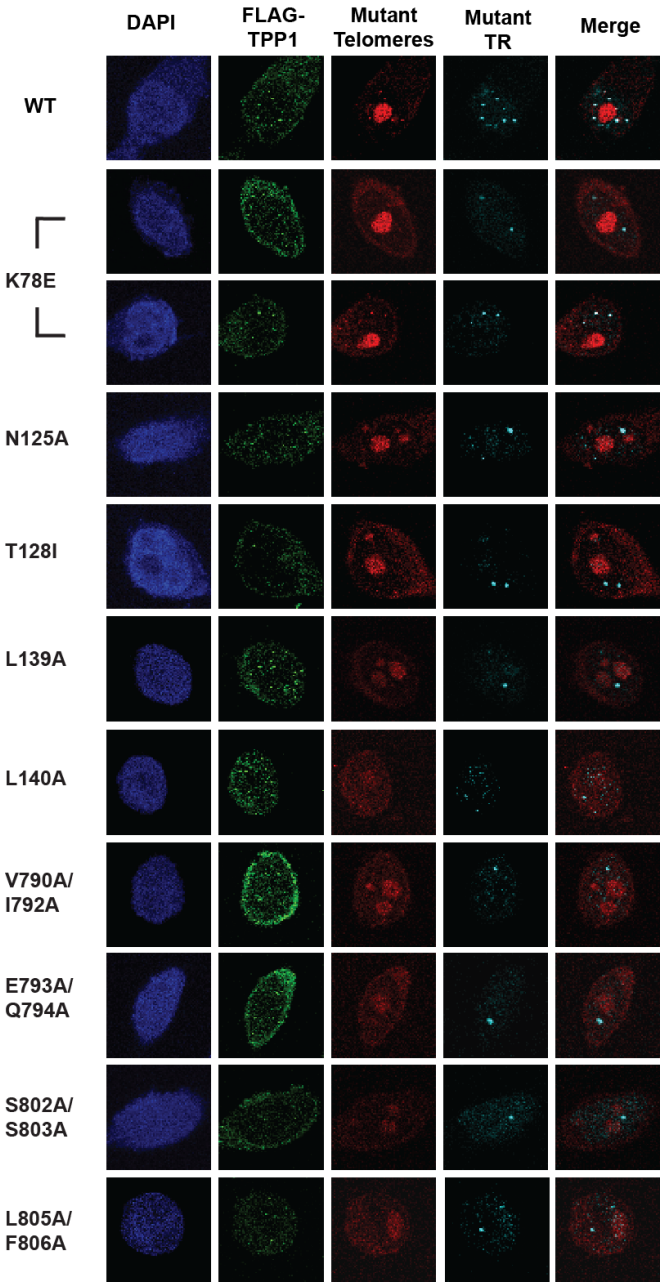

Figure 3.11 Mutations in the TEN domain and IFD compromise telomeric repeat synthesis *in vivo.*
A HeLa cell line that stably expressed FLAG-TPP1 was transiently transfected with the indicated TERT constructs and mutant TR that contains a non-telomeric template sequence. Immunofluorescence-fluorescence *in situ* hybridization was used to visualize newly synthesized mutant telomeric repeats. Channels detecting DAP1 (blue), FLAG-TPP1 (green), newly synthesized telomeres (red), and TR foci (cyan) are shown. Merge panel illustrates an overlay of mutant telomere and TR panels. Non-specific binding of the mutant telomere probe to RNA in the nucleolus occurred in all cells (even in the absence of transfected mutant TR; data not shown).

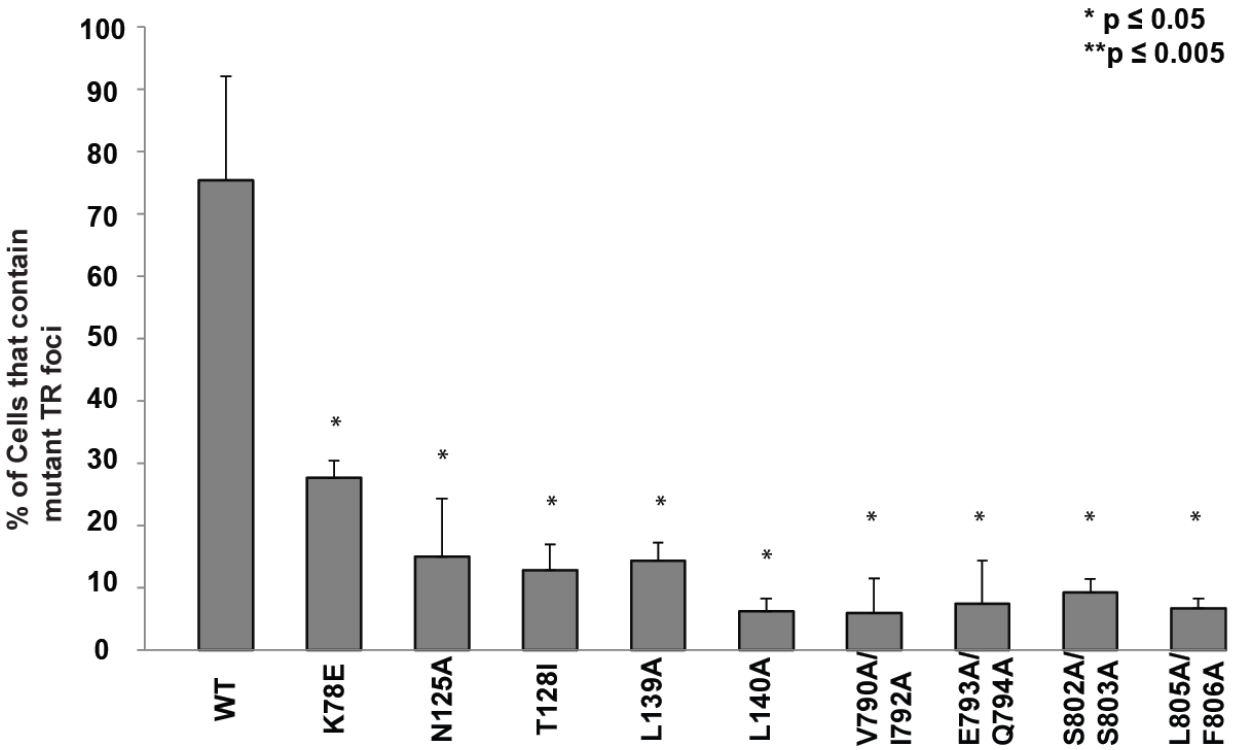

Figure 3.12 Quantitation of cells that contain mutant telomeres.
Quantitation of images for which figure 3.10 is representative. For each experiment >50 cells were counted and the mean percentage of cells with foci containing both TR and mutant telomere sequence is shown for triplicate measurements. p-values were calculated using a two tailed student's t-test comparing each mutant to WT.

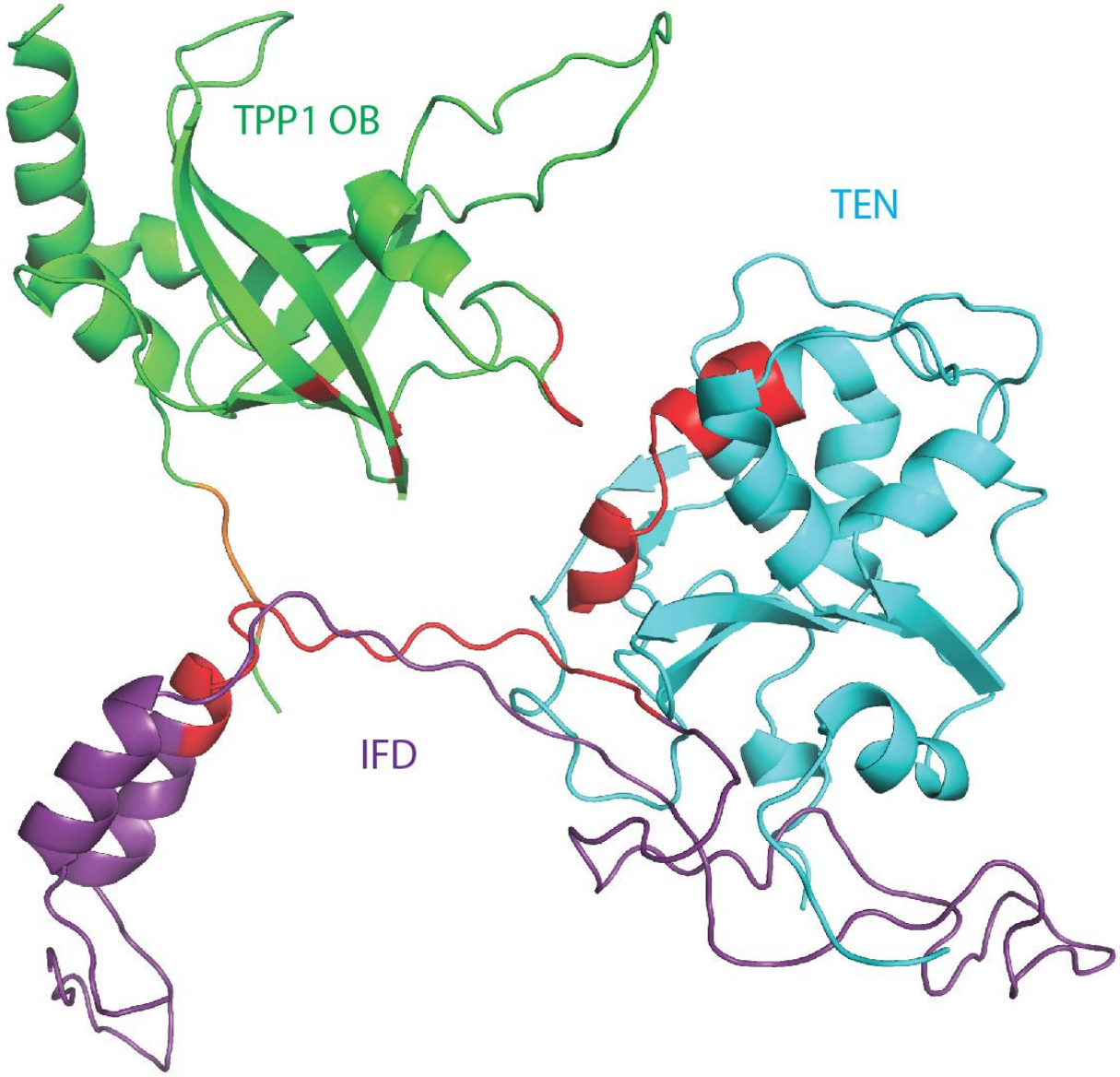

Figure 3.13 Two regions on TERT are predicted to interact with TPP1.
Homology model of human telomerase (SWISS-MODEL) using the alignment in Figure 3.2 along with the cryo-EM structure of *Tetrahymena* telomerase (PDB ID: 6D6V). The solved crystal structure of the OB domain of TPP1 (PDB ID: 2I46) is shown in green. TEL patch residues are shown in red and NOB region residues are shown in orange. The IFD is shown in purple and the TEN domain in cyan. The regions in TEN and IFD involved in telomerase recruitment are highlighted in red.

Chapter 4

Conclusions and future directions

4.1 Introduction

Throughout this dissertation the mechanisms by which telomeres and telomerase are able to work together to solve the end protection and end replication were discussed in detail (Chapter 1). The structural and functional consequences of a dyskeratosis congenita associated mutation in the shelterin component TPP1 were elucidated (Chapter 2). Two regions on TERT important for the recruitment of telomerase to the telomere were defined (Chapter 3). This Chapter is centered on a brief discussion of the conclusions we can draw from the studies presented here, questions that still remain, and the future directions for research on these topics.

4.2 The dichotomous roles of POT1-TPP1

As discussed in Chapter 1, POT1 and TPP1 play two essential roles at telomeres. First, TPP1 is able to recruit POT1 to the single stranded portion of the telomere through its POT1 binding domain. Once there, POT1 protects single stranded telomeric DNA from being misrecognized by ATR mediated DNA damage response proteins by binding the DNA with high affinity and specificity (Kd~ 10 nM) [49,1,64]. Biochemical experiments have shown that TPP1 helps increase the affinity of POT1 for

single stranded DNA by about tenfold [64]. The POT1-TPP1 heterodimer also works to recruit telomerase and stimulate repeat addition processivity [64]. So it must allow telomerase to access the same end that it is actively protecting. How the complex is able to achieve these seemingly opposing roles is a question that still remains. Structurally what is known about this complex largely comes from small angle X-ray scattering (SAXS) data that depicts the TPP1-POT1-DNA complex forming a V-shape with the OB domain placed away from the 3' end of the telomeric DNA [56]. This model does not agree with the solved structure of the POT1-TPP1 homolog from *Sterkiella nova* TEBP-α-β-DNA complex which forms a heart shape with TPP1 homolog TEBP-β interacting with the 3' end of the DNA [48]. Future work is necessary to determine how the full POT1-TPP1 complex is able to bind telomeric DNA and how POT1 orients the OB domain to recruit telomerase (discussed in appendix A). The mechanism by which POT1 allows telomerase access has been investigated by single molecule FRET studies which have suggested that POT1-TPP1 may slide on the DNA allowing telomerase access [141]. Others hypothesize that during S-phase, telomeres may become more accessible to telomerase due to reorganization of shelterin [142]. With the publication of a cryo-EM structure of human telomerase future work should be directed at improving on the current structure by including POT1, TPP1, and other shelterin components along with a telomeric DNA substrate. This would provide a clearer picture of how shelterin occupies chromosome ends while allowing telomerase access to that same end. These cryo-EM studies would also help understand how POT1 is able to orient TPP1 to recruit telomerase.

4.3 Telomerase recruitment

It is evident from our study presented in Chapter 2 that telomerase recruitment to, and subsequent action at, telomeres is essential for the continued renewal of vital cell populations like hematopoietic stem cells. In stark contrast, it is known that aberrant telomerase activation in somatic cell populations allows cancer cells to maintain their telomeres, leading to replicative immortality, a hallmark of cancer. Because recruitment is one of the major steps in both of these scenarios, the telomerase-telomere interface is an attractive target for therapeutics.

4.3.1 The role of TPP1 in telomerase recruitment

In Chapter 2 I demonstrated how a previously discovered mutation in the telomeric protein TPP1 caused telomere shortening and the telomeropathy dyskeratosis congenita in a patient. The TEL patch and the recently discovered NOB regions of TPP1 were shown to be imperative to telomerase recruitment to the telomere, suggesting that mutations in these regions would cause telomerase deficiency diseases such as dyskeratosis congenita [69,66,68]. Indeed, we showed that an in-frame deletion of lysine 170 found in the TEL patch loop displaced the C-α backbone of two critical glutamates causing telomere shortening and telomeropathies in two unrelated patients. We were able to use CRISPR-Cas9 gene editing to introduce this mutation into HEK 293T cells in a heterozygous context to show that this mutation caused the telomere shortening seen in the patient. Our genetic analysis revealed that the dosage of a functional TEL patch was important for telomerase to maintain telomeres as a cell line with only one copy of WT TPP1 shortened at a faster rate than a cell line with one copy each of K170Δ and WT TPP1. Our study encourages the use of small molecules to

rescue the TPP1-telomerase interaction. Reestablishing this interaction with a small molecule could help facilitate telomere length maintenance in stem cell pools throughout the body. Alternatively our study also suggests gene therapy could be used to correct mutations in TPP1 to treat patients with TPP1 TEL patch mutations, as currently bone marrow transplant is the only disease management option for these individuals.

4.3.2 Regions on the TEN domain and the IFD are involved in telomerase recruitment

In Chapter 3 I designed an alanine scanning mutagenesis screen to discover what residues on the TEN domain and IFD are important for telomerase recruitment to the telomere. I used the recently published high resolution structure of *Tetrahymena* telomerase along with my sequence alignment to make a homology model of human telomerase [121]. The residues I found to be important on the TEN domain span two helices connected by a short linker. These helices are facing the OB domain of TPP1 in our model and are in close proximity to the TEL patch loop that contains three critical glutamates (E168, E169, and E171). This region seems to be structurally conserved as it is not only helical in the *Tetrahymena* TEN domain crystal structure, but is also shown to be helical in the crystal structure of the TEN domain of *Hansenula polymorpha* TERT [100,99]. The region I found to be important in the IFD begins in what is predicted to be a flexible linker in our homology model, but is part of a β-sheet that continues into a short linker region in the homologous *Tetrahymena* structure. In both scenarios the β-sheet continues in to a C-terminal helix that has residues that both face the TPP1 OB domain and interact with an N-terminal helix of the IFD. The IFD is in close proximity to the NOB region of TPP1, and I would predict that the two to interact. Together, both of

these stretches of residues are predicted to form one surface that interacts with the OB domain of TPP1, while the previously identified K78 residue is just outside of this surface, but still in close proximity to its biochemically identified binding partner, E215 of the TEL patch. In the future we plan to crystallize the OB domain in complex with peptides from the regions in the TEN domain and IFD that I identified in my alanine scanning mutagenesis screen. If the IFD does indeed bind the N-terminus of TPP1, I would expect the OB domain to crystallize in a different lattice than it does alone, as it uses its N-terminus to make a non-physiological dimer in the asymmetric unit of the apo-OB domain structure. A high resolution crystal structure of the OB domain of TPP1 in complex with a peptide of the TEN domain, IFD, or a combination of the two would allow us to uncover the atomic details of the interaction. This would inspire the search for small molecules to target this interface as it could be another potential target for a variety of cancers (see below). Ultimately, to follow up the cryo-EM characterization of human telomerase, future studies should attempt to use TPP1, the POT1-TPP1 complex, or the complete shelterin complex, to uncover the full atomic details of the telomerase-telomere interface.

4.3.3 Targeting telomerase recruitment for anti-cancer purposes

It can be argued that an anti-telomerase recruitment drug would also shorten telomeres in stem cells. However, it is known that most stem cell populations have much longer telomeres than cancer cells, which are typically operating barely above the critical threshold of telomere length required for continued proliferation. Therefore a drug that causes telomere shortening will likely push cancer cell telomeres below the critical threshold well before they affect stem cells.

Appendix

TPP1-POT1-DNA[4]

A.1 Introduction

The POT1-TPP1 heterodimer aids in maintaining chromosome ends by both protecting them and recruiting telomerase to synthesize telomeric repeats. POT1 protects chromosome ends from being misrecognized as a DNA lesion by excluding DNA damage response machinery from the chromosome end [1]. It carries out this function using two N-terminal OB domains that bind single stranded telomeric DNA (specifically the TTAGGGTTAG sequence) with high affinity and specificity [13]. This same sequence is the substrate for telomerase catalysis. Given this, it is not surprising that POT1 binding to a telomeric primer inhibits telomerase activity *in vitro*. POT1 binds with 10-fold higher affinity (reducing the kD from 10 nM to 1 nM) when associated with its binding partner, TPP1 [64]. Thus one would predict the POT1-TPP1 to be an inhibitor of telomerase, but in sharp contrast POT1-TPP1 increases the activity and processivity of telomerase. How binding of TPP1 to POT1 switches POT1 from being an inhibitor of

[4] The work in this chapter was performed in collaboration with Dr. Valerie Tesmer. Valerie performed the EMSAs in Figure A.2.Both Valerie and I independently expressed and purified the TPP1-POT1-DNA protein complexes and attempted crystallography. I expressed and purified all TPP1-N mutants and performed all experiments with those mutants. The OB-DBD crystals were initially obtained by Valerie Tesmer. Attempts at phasing were performed in collaboration. Valerie designed and performed experiments with the BrdU containing oligomers. Jayakrishnan Nandakumar, Valerie Tesmer, and I attempted data collection. We independently processed data of a variety of OB-DBD crystals that were obtained.

telomerase to a stimulator of this enzyme is still poorly understood. Given these dichotomous roles it is unclear how POT1 and TPP1 work together to both protect chromosome ends and allow telomerase access to that same end to facilitate end replication. To address this question, I describe in this Section my ongoing work to elucidate the structure of the POT1-TPP1 heterodimer in complex with DNA.

A.2 Results

A.2.1 TPP1-POT1-DNA complex formation

Prior to TPP1-POT1-DNA complex formation several experiments were carried out to determine the optimal DNA substrate and TPP1 constructs to use in our crystallography trials. C-terminal truncations of TPP1 were engineered based on the results of limited proteolysis experiments. TPP1 is made up of an N-terminal OB domain that is responsible for recruiting telomerase, a central POT1 binding domain, and a C-terminal TIN2 binding domain (Figure A.1A). Here we utilize a truncated version of TPP1, which eliminates the TIN2 binding domain, but contains the N-terminal OB domain and POT1 binding domain. We expressed and purified TPP1 (87-337) from high five insect cells. After five minutes of digestion with chymotrypsin, TPP1 (87-337) degrades into a band that migrates near 22 kD (Figure A.1B). After ten minutes this further degrades into what we suspect is the OB domain of TPP1 which is approximately 18 kD. Upon inspection of the TPP1 sequence, constructs ending at amino acids 300 and 287 were engineered with (87-287) being the most stable TPP1 construct (Figure A.1B). We also performed crystallization trials with POT1 constructs that lacked the DNA binding domain (POT1 299-634 and POT1 334-634) (Table A.1).

We were also able to express, purify, and attempt crystallization of mouse TPP1-POT1a-DNA (Table A.1).

To determine the optimal DNA for crystallization trials we performed a series of electrophoretic mobility shift assays (EMSA). In these experiments we tested the ability of TPP1-POT1 to bind a variety of telomeric oligomers (Figure A.2A). The oligomers were designed based on the solved crystal structure of the POT1 DBD. We found that the POT1-TPP1 heterodimer bound oligomers with two (SS3 and SS8) or three (SS4) 5' guanosines with higher affinity than constructs with one 5' guanosine or a 5' thymidine (Figure A.2B). The DNA oligomers SS3, SS4, and SS8 were used in crystallization trials described below.

A.2.2 TPP1-POT1-DNA crystallography

After determining which DNAs, POT1, and TPP1 constructs to use for crystallography, we began forming TPP1-POT1-DNA complexes using size exclusion chromatography (Figure A.3A and B). The ratio of absorbance at 260 nm and at 280 nm was used to confirm that the complex contained DNA. Once these complexes were concentrated to suitable amounts for crystallography (~10 mg/ml), trays were set using either an Oryx 8 crystallography robot (sitting drop) or by hand in a 24 well format (hanging drop) at 20 °C, 16 ° C, and 4° C. The combinations of proteins and DNAs screened can be found in table A.2. We screened for conditions that yielded crystals with a homemade PEG screen and ammonium sulfate screen along with the Qiagen PEG suite, Qiagen Classics suite, and Qiagen JCSG+ suite. Crystals of TPP1(87-334)-POT1-SS3 were obtained with 28% PEG 4000, 0.2 M Li_2SO4, 0.1 M Tris (pH 8.5)

(Figure A.4). These crystals were cryoprotected and data was collected at the APS beamline. The diffraction pattern yielded very few spots at low resolution.

A.2.3 Mapping the TPP1-POT1 binding interface

Concurrent with our attempts to elucidate the structure of the TPP1-POT1-DNA complex, we biochemically characterized the interface between these two proteins. To do this we employed a scanning alanine mutagenesis screen, where we mutated residues in the previously identified POT1 binding domain of TPP1 (PDB). We engineered 14 mutants in total, two single mutants and twelve double mutants, which spanned the PBD of TPP1. Using sequence conservation and the TEBP-α-β structure as guides, we mutated conserved residues predicted to be on the surface of the human PBD. All mutants were expressed as C-terminal truncated TPP1 constructs, called TPP1-N (87-334) that lacked the C-terminal TIN2 binding domain. Initially we expressed and purified these constructs in *E. coli* (Table A.1). Several constructs expressed and concentrated as well as wild type (1-3 mg from 3 L of culture), but T286A and T291A/W293A both showed sizeable protein loss during concentration (1-2 mg). After expressing and purifying all constructs, I was able to perform a chymotrypsin digest to determine which constructs were correctly folded (Figure A.5). We found that both TPP1 T286A and TPP1 T291A/W293A both had digest patterns that did not match that of wild type. This data along with the difficulty in concentrating both proteins during purification suggests that the proteins are not well folded. After determining that a majority of the mutations did not grossly affect TPP1 protein folding we set out to test the ability of these proteins to interact with POT1. To this end we performed a fluorescence-based quantitative binding assay. This assay involves the immobilization of POT1 on beads

using biotin-streptavidin chemistry and the labeling of TPP1 with fluorophores using thiol-reactive reagents. We incubated the POT1 with fluorescently labeled wild type TPP1 and titrated in unlabeled WT and mutant proteins to displace the previously bound fluorescently labeled WT TPP1 protein. We found that TPP1 S255A/L257A, L271A/L274A, T291A/W293A, Y306A/V308A, L313A/I315A, and L323A were all defective relative to (unlabeled) WT in displacing Alexa Fluor labeled WT TPP1 from POT1 (Figure A.6). While mutants S255A/L257A and L271A/L274A were tested in triplicate, the other mutants were tested in only a single experiment. During the course of these experiments two separate labs solved structures of the PBD of TPP1 in complex with the third OB domain of POT1 that also contained a Holliday junction resolvase like domain insertion, providing high resolution atomic details of this interface (Figure A.7) [56,57]. Both structures were in agreement with the interface mutants we identified in our screen.

A.2.4 OB-DBD crystallographic studies

Due to our inability to obtain TPP1-POT1-DNA crystals with full length POT1 and TPP1-N constructs, we employed an alternative approach to try to understand how POT1 orients the TPP1 OB domain for telomerase recruitment and putative DNA binding. In this approach we utilized a 20 amino acid serine/glycine linker to connect TPP1's OB domain with POT1's DBD. Although previous biochemical data has not detected an interaction between these two domains, we hypothesized that the POT1 DBD influences how TPP1's OB domain is oriented with respect to the 3' end of the telomeric DNA. Additionally both of these domains have been previously crystalized individually, but not in the presence of the other. Published work from the lab has

demonstrated that this tethered OB-DBD construct is able to stimulate telomerase activity and processivity to the same extent as the POT1-TPP1-N heterodimer [69]. This suggests that POT1 simply acts as an anchor for the OB domain of TPP1, aiding it in recruiting telomerase by ensuring its placement at the end of telomeric DNA. To gain a better understanding of how POT1-DBD is able to help orient the OB domain of TPP1 and to identify putative residues that interact between the two domains we set out to crystallize an OB-DBD-DNA complex. After expressing and purifying the fusion protein from *E. coli* we obtained crystals from two different conditions. Both conditions contained 20% PEG 6000, 0.1 M Sodium Citrate (pH 5.0), but differed in having either 0.1 M LiCl or 0.2 M Li_2SO_4 (Figure A.8). The crystals were cryoprotected by introducing 20% ethylene glycol into the crystallization conditions. Crystals from the LiCl conditions diffracted to a resolution of 3.1 Å, while the crystals from the Li_2SO_4 conditions diffracted to 2.7 Å. Upon data processing the LiCl crystals indexed to I121 (a= 81.75 b= 48.20 c= 114.44 α= 90 β= 94.90 γ= 90) (Table A.3). Molecular replacement was attempted using several truncated versions of TPP1 OB and POT1 DBD, but Phaser [143,144] often found greater than 20 solutions with low z-scores and the highest scored solutions were unable to be refined. Upon data processing the Li_2SO_4 crystals indexed to $P12_11$ (a= 48.23 b= 140.5 c= 72.62 α= 90 β= 99.27 γ= 90). Molecular replacement was attempted with Phaser using various combinations and truncated versions of the TPP1 OB domain and DBD as the search models (100% sequence similarity), but no reasonable solutions were obtained. Data were collected from additional crystals grown in Li_2SO_4 and processed. Initially these data processed to C121 (a= 116.39 b=116.39 c= 162.27 α= 90 β= 90 γ= 90), but Xtriage indicated that there was a significant twin fraction, even

though the intensity statistics did not suggest twinning. The symmetry operators predicted a higher order space group $P4_122/P4_322$ (a= 82.42 b= 82.40 c= 162.56 α= 90 β=90 γ=90) (Table A.4). After the data was reprocessed to $P4_122$ the phasing of the data was attempted by molecular replacement using Phaser with various combinations of the TPP1 OB domain and POT1 DBD as the search models (100% sequence similarity). The enantiomeric space group $P4_322$ was also tested in molecular replacement. Matthews coefficient determination suggested that the asymmetric unit contained one copy each of the TPP1 OB domain and the POT1 DBD (made up of two OB domains). Attempts at molecular replacement with TPP1 or POT1 OB domains yielded MR solutions with unimpressive z-scores that did not improve substantially upon placement of additional OB domains. These solutions did not improve upon refinement as indicated by the fact the R_{Free} was consistently above 0.5 regardless of how many (of the three) OB domains were present in the solution.

After multiple iterations of molecular replacement with varying combinations of truncated search models we attempted to phase the crystals *de novo*. We took three separate approaches to do this: heavy metal soaks, selenomethionine incorporation, and brominated DNA. Crystals grown in LiCl and Li_2SO_4 conditions were soaked in 50 mM thimerosal for either 1 h or overnight (~16 h). Crystals grown in both conditions were also soaked for 5 min or 10 min in one of the following: mercury (II) acetate (10 mM or 1 mM), platinum (IV) chloride (10 mM or 50 mM), potassium tetrachloroplatinate (II) (50 mM), gold chloride (10 mM or 50 mM), and sodium tetrachloroaurate (10 mM or 50 mM). A crystal grown in Li_2SO_4 and soaked overnight in 50 mM thimerosal did diffract to 3.5 Å, but only had weak anomalous signal to 6.9 Å. LiCl crystals soaked in

mercury (II) acetate diffracted to 3.1 Å, but only had weak anomalous signal that extended to 5.8 Å and had low completeness (<50%). Due to the fact that heavy metal soaks didn't yield any useful datasets that could be used to phase our crystals we next attempted selenomethionine incorporation into the protein. Although the OB domain of TPP1 (90-250) doesn't contain any methionines, the DBD of POT1 contains five. The fusion protein was expressed in an auxotrophic strain of *E. coli* with selenomethionine supplemented media. Crystals formed in 23-25% PEG 6000, 0.2 M Li_2SO_4, and either 0.1 M Bis-Tris (pH 5.5) or 0.1 M MES (pH 6.0). The crystals were harvested and cryoprotected by introducing 20% ethylene glycol in the crystallization conditions. Many crystals grown under these conditions failed to diffract or diffracted very poorly. Crystals that diffracted well also failed to yield any significant anomalous signal although the fluorescence scan indicated the presence of selenium. Finally, we complexed the OB-DBD construct with two different BrdU incorporated DNA oligomers [5'-(BrdU)GGTTAGGGTTAG-3' and 5'-(BrdU)GGTTAGGG(BrdU)TAG-3']. We obtained crystals in 23-28% PEG 6000, 0.2 M Li_2SO_4, 0.1 M sodium citrate (pH 5.5). Upon harvesting, the crystals were cryoprotected with 20% ethylene glycol. Although many crystals diffracted well (~3 Å) we failed to detect any significant anomalous signal. In the future we plan to continue to try to phase the crystals by trying alternative heavy metals and attempting to collect data on more crystals with BrdU incorporated DNA.

A.3 Materials and methods

A.3.1 Plasmid constructs

The pET-Smt3-TPP1-N plasmid for expression and purification of human TPP1-N was described previously. Full length POT1 was cloned into the pFASTBAC HTB vector

using restriction cloning. Site directed mutagenesis was carried out to introduce mutations in TPP1 and POT1-expression plasmids. These mutations were introduced with mutagenic primers (Integrated DNA Technologies) using the QuikChange® Site-Directed Mutagenesis Kit (Agilent Technologies). The TPP1 and POT1 sequences in the mutant plasmids were sequenced using Sanger sequencing to confirm both the presence of the intended mutation and the absence of unwanted errors introduced during PCR amplification/cloning

A.3.2 Protein expression and purification

WT and mutant constructs of Smt3-TPP1-N and TPP1 OB-POT1 DBD proteins were obtained upon purification from lysates of BL21(DE3) cells induced with isopropyl β-d-thiogalactopyranoside as described previously [127,69]. Lysate obtained from these cells was first passed over a Nickel-agarose column, and once the protein was eluted it was treated with Ulp1 protease (MTA with Cornell University for pUlp1 vector) to cleave the Smt3 tag. Size-exclusion chromatography (Superdex 75; GE Life Sciences) was performed as the final step of protein purification. The His-Sumostar-hPOT1 baculoviral expression plasmid described previously was used to express full-length POT1 in baculovirus-infected High Five cells (Life Technologies) using vendor recommendations [127]. Sumostar-POT1 fusion protein was purified from insect cell lysates by passing the lysate over a nickel-agarose column. After elution the tag was cleaved with SUMOstar protease (Life Sensors) and the POT1 protein was further purified by anion exchange (HiTrap Q HP; GE Life Sciences), and size-exclusion chromatography (Superdex 200; GE Life Sciences). All protein-DNA complexes, including ones with

BrdU incorporation were formed by mixing proteins/DNA prior (2:1 molar ratio of DNA to protein) prior to injection onto a size-exclusion column (S200).

A.3.3 Chymotrypsin proteolysis experiments

Initially all concentrations of proteins were determined by protein assay reagent (Bio-Rad). Chymotrypsin (Promega; V160) was dissolved at 1 mg/ml in 50 mM Tris (pH 8.0), 50 mM NaCl, 2 mM $CaCl_2$. 16 µl digestion reactions were carried out a ratio of 1:62.5 of chymotrypsin to protein. 4 µl of reaction was removed at the indicated time and mixed with 4 µl of 2X SDS-loading dye and heated at 90 °C for 10 min before being loaded on an 10% SDS-PAGE gel.

A.3.4 Electrophoretic Mobility Shift Assays

Each telomeric DNA oligomer was 5' labeled with ^{32}P using T4 PNK (New England Biolabs). The reaction was performed with [γ-32P] ATP, 10 units PNK, and 2 µM primer in 1X PNK buffer, 8 mM Tris (pH 8.0), 5 mM DTT for 30 min at 37 °C. After the reaction 28 µl of Tris (pH 8.0) was added and to quench the reaction EDTA was added to a final concentration of 10 mM and the reaction was heated to 65°C for five min. To get rid of unincorporated radiolabel the reaction was passed through a Quick Spin Protein Column (Rouche, G25 Sephadex). The EMSA was performed in a 10 µl binding reaction which contained 1 µM of each cold DNA oligomer and trace amounts of the ^{32}P labeled DNA oligomer (described above). The DNA oligomers were diluted in 50 mM Tris (pH 8.0), 6% glycerol, and 80 mM NaCl. A 4 µM POT1-TPP1(87-337) stock was made in the same buffer the DNA oligomers were diluted in. Then the proteins were serial diluted to 400 nM, 200 nM, 100 nM, and 50 nM. The binding reactions were then electrophoresed on a 6% acrylamide-bisacrylamide-0.5X TBE gel. The gel was pre-run

for 30 min at 100 V before the samples were loaded and the gel was run for 45 min at 100 V. After being run the gel was vacuum dried for 1 h at 80 °C. The radioactive signal was detected by exposure to a phosphorimager screen and by imaging on a storm phosphorimager.

A.3.5 Flow cytometry based protein-protein binding assays

Labeling reactions: Initially, proteins were labeled with either biotin or a fluorophore as described previously [145,146]. Briefly, proteins were passed through a Micro Bio-spin 6 spin column (Bio-Rad) to remove DTT. The concentrations of the proteins were calculated using the Protein Assay Reagent (Bio-Rad). To label TPP1 with a fluorophore and POT1 with biotin we used a 2:1 mole ratio of Alexafluor488-C5-maleimide (Life technologies) to TPP1 or a 2:1 mole ratio of biotin maleimide (Sigma; B1267) to POT1. Each reaction was allowed to proceed for 20 min at room temperature and then passed through a second spin column to remove any unreacted label.

Competition experiments: 24 µl of uniformly-sized streptavidin beads (Spherotech; SCP-20-5) were washed three times with 200 µl of flow buffer (20 mM Tris (pH 8.0), 100 mM NaCl, 2 mM DTT, 1% bovine serum albumin, and 0.1% lubrol). The beads were then resuspended in 320 µl of flow buffer. Biotin labeled POT1 was added to the beads at a final concentration of 150 nM and was incubated with the beads on ice for 1 h. After 1 h the beads were washed three times with flow buffer to remove unbound POT1. Then 100 nM of Alexa Fluor labeled WT TPP1 was incubated with the beads. The unlabeled mutant TPP1 constructs were serial diluted in flow buffer in a 96 well plate (400 nM – 2.125 nM final concentration). The beads containing biotin POT1 and Alexa Fluor labeled TPP1 were added to each well and left to incubate on ice for 4 h. After

incubation on ice samples were loaded on an Accuri C6 flow cytometer (BD biosciences) using a Hypercyt autosampler (IntelliCyt). The median fluorescence intensity on the beads for technical duplicates which were performed on the same plate was calculated using the Hypercyt software. Median fluorescence values were fit to a one-site competition curve in Prism 7.0 (GraphPad).

A.3.6 Crystallography experiments

After purification all proteins crystal trays were set either using an Oryx 8 crystallography robot or by hand. When crystal trials were set with the robot, 50 µl of each screen solution was pipetted by hand into the wells of an MRC 2 Lens Crystallization Microplate (MRC96T-UVP). Screens used include: Qiagen PEG suite (Qiagen; 130704), Qiagen Classics Suite (Qiagen; 130701), Qiagen MPD Suite (Qiagen; 130706), and NeXtal JCSG+ Suite (Qiagen; 130720). The robot then pipetted 0.5 µl of the well solution and 0.5 µl of the protein as a sitting drop. To optimize conditions with potential crystal hits additional screens were set by hand using 24 well plates (hanging drop). All crystal trays were kept in incubators (16°C or 20°C) or in a cold room (4°C). Crystals were cryoprotected as reported in the results section and X-ray diffraction data were obtained at the Life Sciences Collaborative Access Team (LS-CAT) beam line 21-ID-D of the Advanced Photon Source. The data for BrdU containing crystals was collected at 13.5 keV and the data for SeMet containing crystals was collected at 12.7 keV. Data sets were processed by iMosflm (CCP4) or Dials (CCP4). Scaling and merging were performed using Aimless (CCP4) and Pointless (CCP4). In addition to manual inspection of the data, Xtriage (Phenix) was used to aid in

determining the quality of the data. Molecular replacement was performed in Phaser (Phenix). All attempts at refinement were performed with phenix.refine (Phenix).

A.4 Figures and Tables

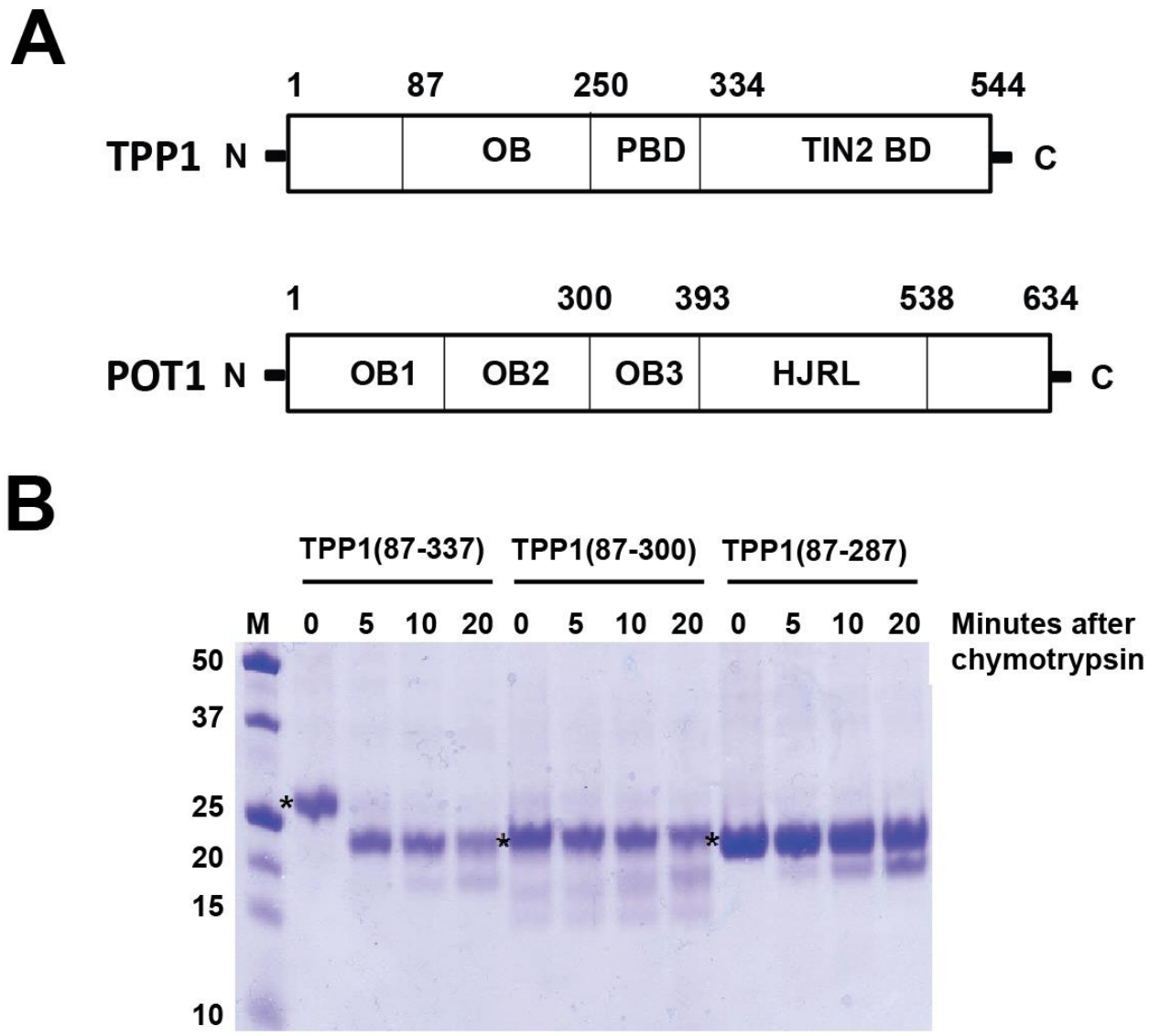

Figure A.1 Determining stable constructs of TPP1.
(A) Domain diagrams of TPP1 and POT1. PBD stands for POT1 binding domain. HJRL stands for Holliday junction resolvase like domain. (B) Coomassie-blue stained SDS-PAGE gel of various TPP1 constructs incubated with chymotrypsin for the indicated amount of time. Stars indicate size of proteins at time zero.

A

Name	Sequence
SS1	TTAGGGTTAG
SS2	GTTAGGGTTAG
SS3	GGTTAGGGTTAG
SS4	GGGTTAGGGTTAG
SS5	TTAGGGTTAGG
SS6	TTAGGGTTAGGG
SS7	GTTAGGGTTAGG
SS8	GGTTAGGGTTAGG

B

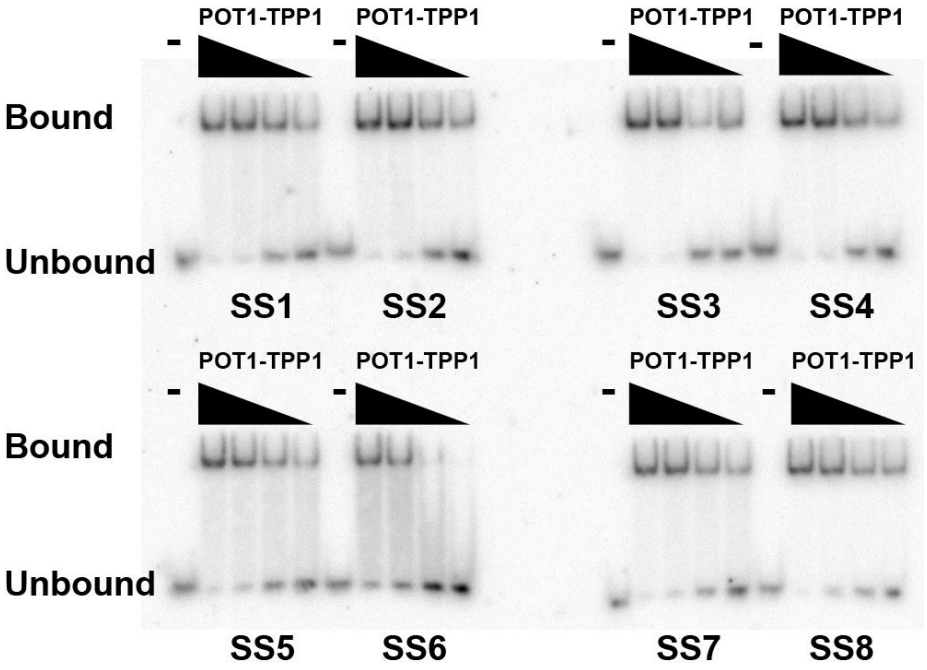

Figure A.2 Affinity of TPP1-POT1 for telomeric DNA oligomers.
(A) The composition of the single stranded DNA oligomers used in EMSA assays and crystallization studies. Purple shows the telomeric DNA sequence that the POT1 DBD was crystallized with. (B) Electrophoretic mobility shift assays (EMSA) measuring the affinity of POT1-TPP1 for telomeric DNA oligomers. Binding reactions were performed either without TPP1-POT1 (- lane) or with increasing amounts of TPP1-POT1 complex (50 nM, 100 nM, 200 nM, and 400 nM) and a constant amount (1 μM) of the indicated oligomer.

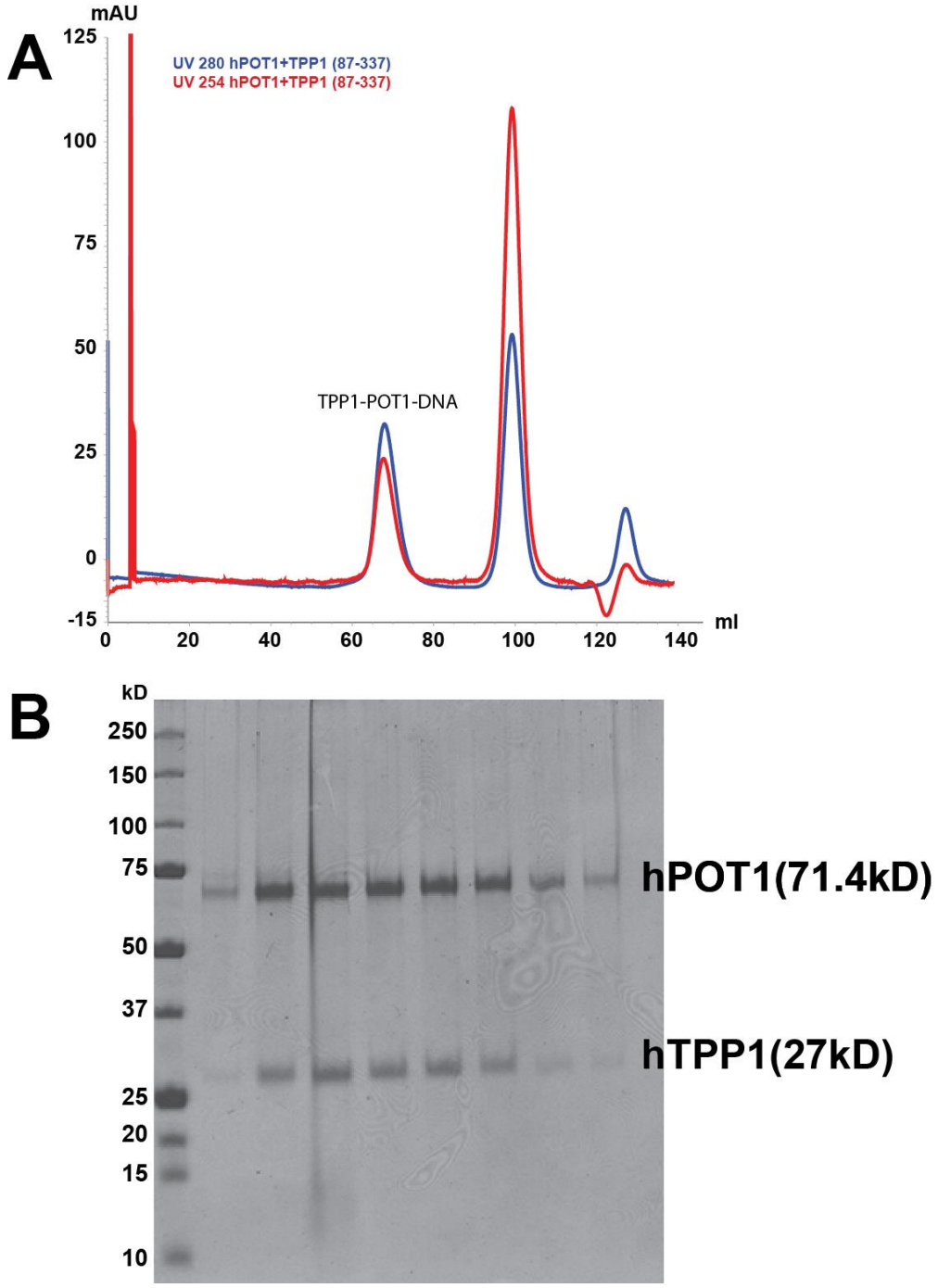

Figure A.3 Purification of a TPP1-POT1-DNA complex.
(A) Representative chromatogram from the isolation of the TPP1-POT1-DNA complex after purification by size exclusion chromatography (S75 column). The absorbance at 280 nm is shown in blue and the absorbance at 254 nm is shown in red. (B) Coomassie blue stained SDS-PAGE gel of fractions obtained from the gel filtration run in A.

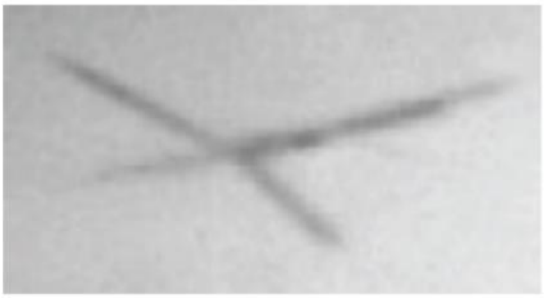

28% PEG 4000, 0.2 M LiSO4, 0.1 M Tris pH (8.5)

Figure A.4 TPP1-POT1-DNA crystallography.
Crystals of TPP1-POT1-DNA (TPP1-N and SS3 DNA) grown in the specified solution at 20 °C.

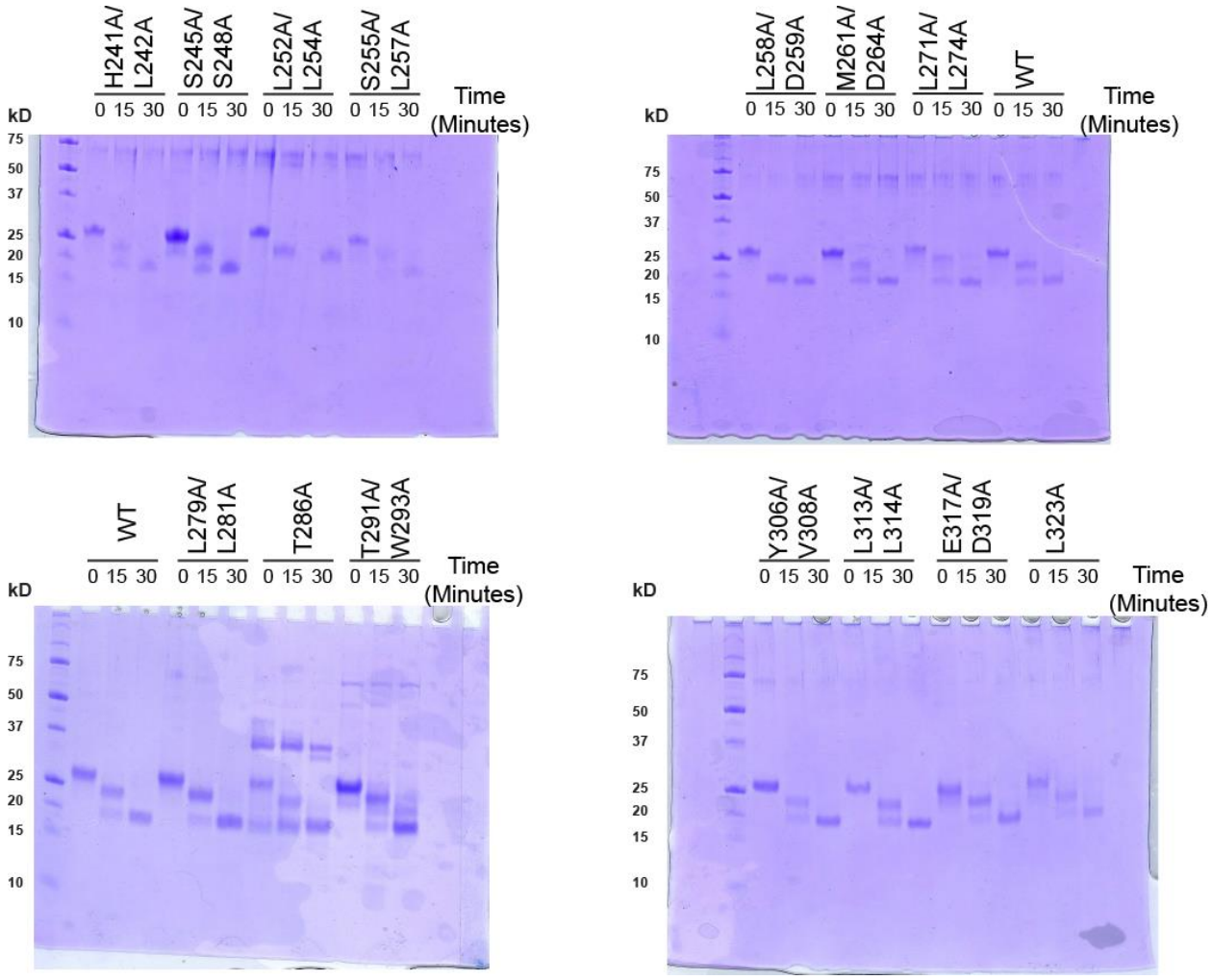

Figure A.5 Analysis of protein stability by limited proteolysis.
Time course analysis by SDS-PAGE of the chymotrypsin digest of the indicated TPP1-N constructs. Samples were taken from the reaction at the specified times. TPP1-N runs at 27 kD; the OB domain of TPP1 is known to migrate as an 18 kD species.

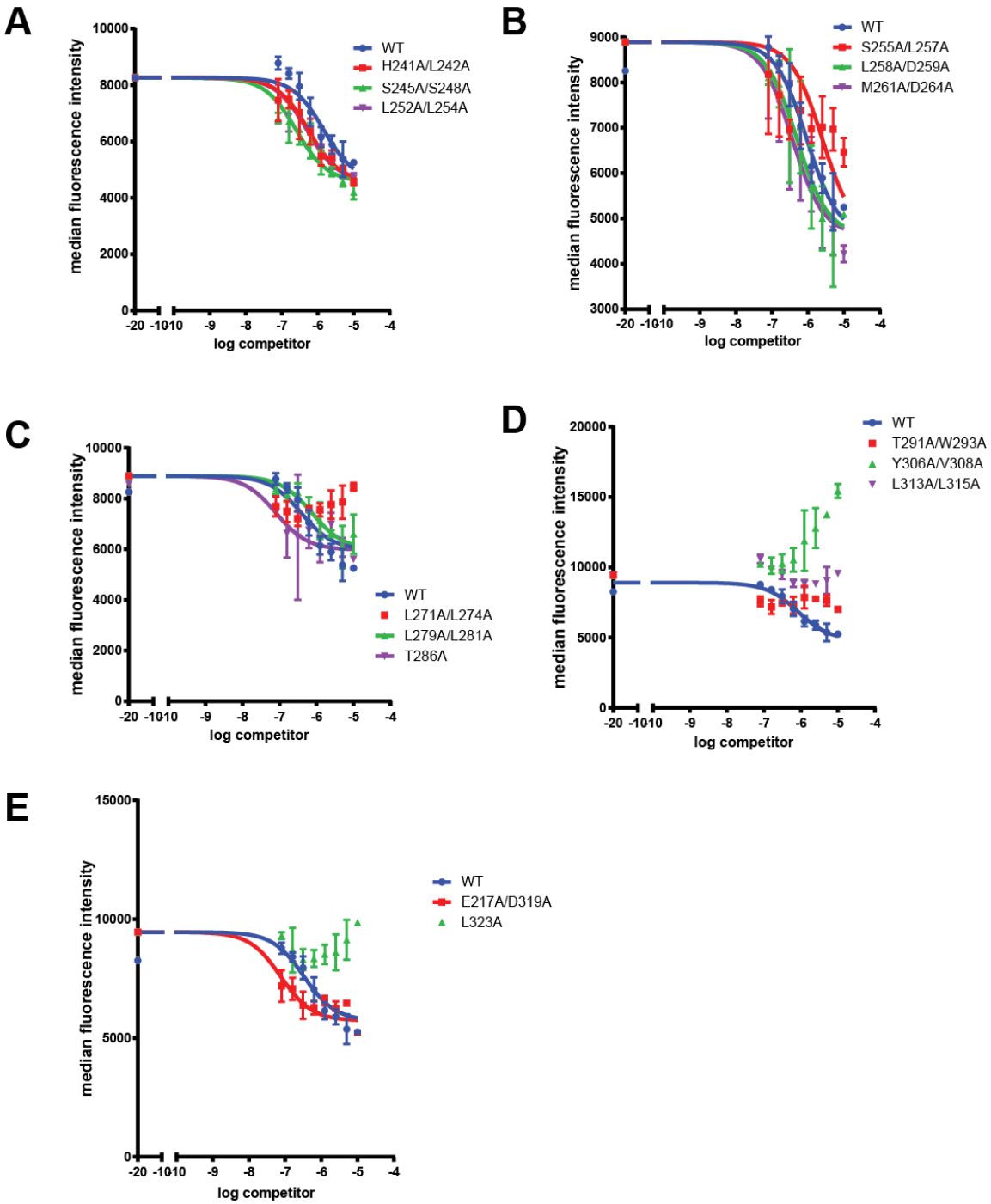

Figure A.6 Biochemical analysis of the POT1-TPP1 binding interface. Fluorescence-based competition experiments using Alexa Fluor labeled WT TPP1-N bound to biotin labeled POT1 on streptavidin beads titrated with varying amounts of the unlabeled mutant or WT TPP1-N constructs. The mean of a technical duplicate performed on the same plate is plotted for each experiment. Mutants H214A/L242A, S245A/S248A, L252A/L254A, and S255A/L257A were assayed in triplicate. All others were tested as technical duplicates in a single experiment. Error bars represent standard deviation of technical duplicates.

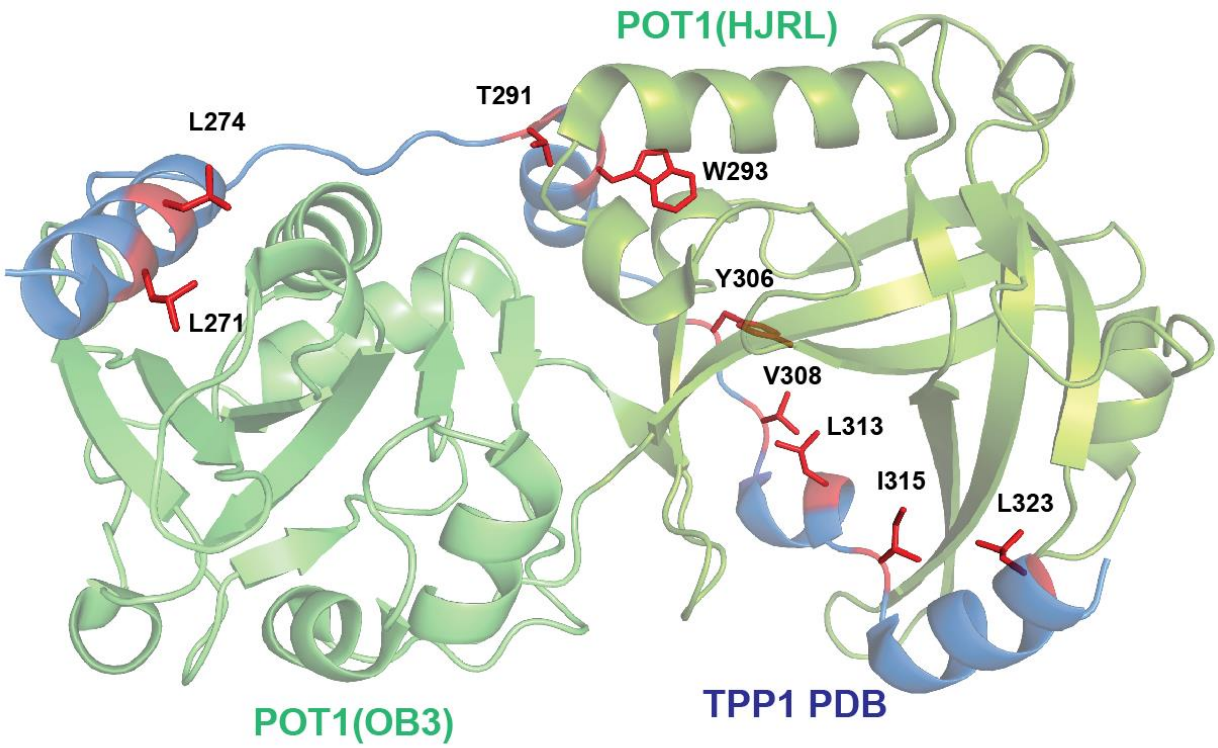

Figure A.7 Mapping biochemically identified residues onto the structure of POT1-TPP1.
Solved crystal structure of the third OB domain of POT1 (forest green) and the Holliday junction resolvase like domain (HJRL) of POT1 (lime green) in complex with the TPP1 POT1 binding domain (PBD) (Blue) (PDB ID: 5H65 and 5UN7). Residues that were found to be important in our alanine mutagenesis screen are shown as sticks in red.

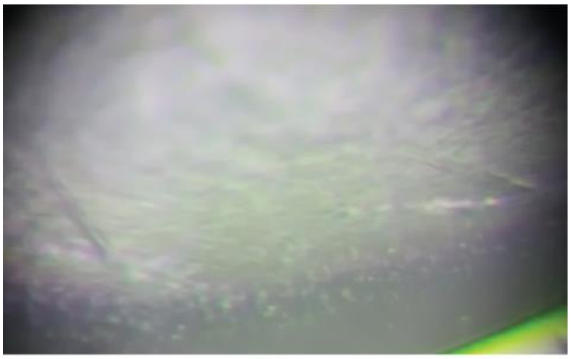

20% PEG 6000,
0.1M Sodium Citrate pH (5.0), 0.1 M LiCl

20% PEG 6000,
0.1 M Sodium Citrate pH (5.0), 0.2 M Li_2S0_4

Figure A.8 Crystals of TPP1 OB-POT1 DBD fusion in complex with telomeric DNA. Photographs of crystals of TPP1 OB linked to the DBD of POT1 with a 20 amino acid long serine/glycine linker grown in hanging drops at 20°C.

A.5 Tables

Table A.1 Constructs used in crystallization trials.

TPP1 Construct (complex with full length POT1)	DNA
TPP1 87-544	SS3, SS4, SS8
TPP1 87-354	SS3, SS4, SS8
TPP1 87-337	SS3, SS4, SS8
TPP1 87-334	SS3, SS4, SS8
TPP1 87-300	SS3, SS4, SS8
TPP1 87-337+ POT1 (334-649)	N/A
TPP1 87-337+ POT1(299-649)	N/A
mPOT1a-TPP1	SS3, SS4, SS8

Table A.2 Residues mutated in alanine scanning mutagenesis screen.

Construct (All mutants are to ala)	
Wild Type	L279/L281
H241/L242	T286
S245/S248	T291/W293
L252/L254	Y306/V308
S255/L257	L313/L315
L258/D259	E317/D319
M261/D264	L323
L271/L274	

Table A.3 Representative summary table from data processing of crystals obtained in conditions with LiCl.

Pointless log			
Best solution	space group I 1 2 1		
Reindex operator	[-l,k,h+l]		
Laue group probability	0.64		
Systematic absence probability	1		
Total probability	0.64		
Space group confidence	0.423		
Laue group confidence	0.423		
Aimless log	Overall	Inner	Outer
Low resolution limit	69.13	69.13	3.31
High resolution limit	3.1	8.77	3.1
Rmerge(within I+/I-)	0.153	0.05	0.432
Rmerge(all I+ and I-)	0.176	0.059	0.514
Rmeas (within I+/I-)	0.207	0.067	0.592
Rmeas (all I+ & I-)	0.208	0.07	0.607
Rpim (within I+/I-)	0.139	0.044	0.402
Rpim (all I+ & I-)	0.107	0.035	0.318
Rmerge in top intensity bin	0.074		
Number of observations	30234	1474	5457
Number unique	8025	396	1451
Mean((I)/sd(I))	6.4	10.8	3.3
Half-set correlation CC(1/2)	0.963	0.992	0.625
Completeness %	97.2	99.9	98.3
Multiplicity	3.8	3.7	3.8
Anomalous completeness %	94	96.5	94.7
Anomalous multiplicity	2	2.1	2
DelAnom CC(1/2)	-0.056	0.147	0.054

Table A.4 Representative summary table from data processing of crystals obtained in conditions with Li_2SO_4.

Pointless log			
Best solution	space group P 41 2 2		
Reindex operator	[h,k,l]		
Laue group probability	0.993		
Systematic absence probability	0.782		
Total probability	0.776		
Space group confidence	0.72		
Laue group confidence	0.99		
Aimless log	Overall	Inner	Outer
Low resolution limit	47.36	47.36	2.71
High resolution limit	2.6	9	2.6
Rmerge(within I+/I-)	0.103	0.033	0.553
Rmerge(all I+ and I-)	0.111	0.036	0.594
Rmeas (within I+/I-)	0.121	0.039	0.648
Rmeas (all I+ & I-)	0.121	0.04	0.643
Rpim (within I+/I-)	0.063	0.02	0.334
Rpim (all I+ & I-)	0.047	0.016	0.242
Rmerge in top intensity bin	0.048		
Number of observations	117693	2941	14683
Number unique	17950	511	2123
Mean((I)/sd(I))	10.7	26	3
Half-set correlation CC(1/2)	0.997	0.999	0.939
Completeness %	99.8	99.3	99.2
Multiplicity	6.6	5.8	6.9
Anomalous completeness %	99.7	100	99.2
Anomalous multiplicity	3.6	3.7	3.6
DelAnom CC(1/2)	-0.006	-0.007	-0.027

Bibliography

1. Palm W, de Lange T (2008) How shelterin protects mammalian telomeres. Annu Rev Genet 42:301-334. doi:10.1146/annurev.genet.41.110306.130350

2. Bianchi A, Smith S, Chong L, Elias P, de Lange T (1997) TRF1 is a dimer and bends telomeric DNA. EMBO J 16 (7):1785-1794. doi:10.1093/emboj/16.7.1785

3. Broccoli D, Chong L, Oelmann S, Fernald AA, Marziliano N, van Steensel B, Kipling D, Le Beau MM, de Lange T (1997) Comparison of the human and mouse genes encoding the telomeric protein, TRF1: chromosomal localization, expression and conserved protein domains. Hum Mol Genet 6 (1):69-76

4. Bilaud T, Brun C, Ancelin K, Koering CE, Laroche T, Gilson E (1997) Telomeric localization of TRF2, a novel human telobox protein. Nat Genet 17 (2):236-239. doi:10.1038/ng1097-236

5. Broccoli D, Smogorzewska A, Chong L, de Lange T (1997) Human telomeres contain two distinct Myb-related proteins, TRF1 and TRF2. Nat Genet 17 (2):231-235. doi:10.1038/ng1097-231

6. Hardy CF, Sussel L, Shore D (1992) A RAP1-interacting protein involved in transcriptional silencing and telomere length regulation. Genes Dev 6 (5):801-814

7. Baumann P, Cech TR (2001) Pot1, the putative telomere end-binding protein in fission yeast and humans. Science 292 (5519):1171-1175. doi:10.1126/science.1060036

8. Liu D, Safari A, O'Connor MS, Chan DW, Laegeler A, Qin J, Songyang Z (2004) PTOP interacts with POT1 and regulates its localization to telomeres. Nat Cell Biol 6 (7):673-680. doi:10.1038/ncb1142

9. Ye JZ, Hockemeyer D, Krutchinsky AN, Loayza D, Hooper SM, Chait BT, de Lange T (2004) POT1-interacting protein PIP1: a telomere length regulator that recruits POT1 to the TIN2/TRF1 complex. Genes Dev 18 (14):1649-1654. doi:10.1101/gad.1215404

10. Houghtaling BR, Cuttonaro L, Chang W, Smith S (2004) A dynamic molecular link between the telomere length regulator TRF1 and the chromosome end protector TRF2. Curr Biol 14 (18):1621-1631. doi:10.1016/j.cub.2004.08.052

11. Li B, Oestreich S, de Lange T (2000) Identification of human Rap1: implications for telomere evolution. Cell 101 (5):471-483

12. Kim SH, Kaminker P, Campisi J (1999) TIN2, a new regulator of telomere length in human cells. Nat Genet 23 (4):405-412. doi:10.1038/70508

13. Lei M, Podell ER, Cech TR (2004) Structure of human POT1 bound to telomeric single-stranded DNA provides a model for chromosome end-protection. Nat Struct Mol Biol 11 (12):1223-1229. doi:10.1038/nsmb867

14. Jones M, Bisht K, Savage SA, Nandakumar J, Keegan CE, Maillard I (2016) The shelterin complex and hematopoiesis. J Clin Invest 126 (5):1621-1629. doi:10.1172/JCI84547

15. Lingner J, Hughes TR, Shevchenko A, Mann M, Lundblad V, Cech TR (1997) Reverse transcriptase motifs in the catalytic subunit of telomerase. Science 276 (5312):561-567

16. Counter CM, Meyerson M, Eaton EN, Weinberg RA (1997) The catalytic subunit of yeast telomerase. Proc Natl Acad Sci U S A 94 (17):9202-9207

17. Meyerson M, Counter CM, Eaton EN, Ellisen LW, Steiner P, Caddle SD, Ziaugra L, Beijersbergen RL, Davidoff MJ, Liu Q, Bacchetti S, Haber DA, Weinberg RA (1997) hEST2, the putative human telomerase catalytic subunit gene, is up-regulated in tumor cells and during immortalization. Cell 90 (4):785-795

18. Greider CW, Blackburn EH (1987) The telomere terminal transferase of Tetrahymena is a ribonucleoprotein enzyme with two kinds of primer specificity. Cell 51 (6):887-898

19. Greider CW, Blackburn EH (1989) A telomeric sequence in the RNA of Tetrahymena telomerase required for telomere repeat synthesis. Nature 337 (6205):331-337. doi:10.1038/337331a0

20. Greider CW, Blackburn EH (1985) Identification of a specific telomere terminal transferase activity in Tetrahymena extracts. Cell 43 (2 Pt 1):405-413

21. Shay JW, Wright WE (2010) Telomeres and telomerase in normal and cancer stem cells. FEBS Lett 584 (17):3819-3825. doi:10.1016/j.febslet.2010.05.026

22. Dokal I (2011) Dyskeratosis congenita. Hematology Am Soc Hematol Educ Program 2011:480-486. doi:10.1182/asheducation-2011.1.480

23. Savage SA (2014) Human telomeres and telomere biology disorders. Prog Mol Biol Transl Sci 125:41-66. doi:10.1016/B978-0-12-397898-1.00002-5

24. Bodnar AG, Ouellette M, Frolkis M, Holt SE, Chiu CP, Morin GB, Harley CB, Shay JW, Lichtsteiner S, Wright WE (1998) Extension of life-span by introduction of telomerase into normal human cells. Science 279 (5349):349-352

25. Kim NW, Piatyszek MA, Prowse KR, Harley CB, West MD, Ho PL, Coviello GM, Wright WE, Weinrich SL, Shay JW (1994) Specific association of human telomerase activity with immortal cells and cancer. Science 266 (5193):2011-2015

26. Wright WE, Pereira-Smith OM, Shay JW (1989) Reversible cellular senescence: implications for immortalization of normal human diploid fibroblasts. Mol Cell Biol 9 (7):3088-3092

27. Stewart SA, Weinberg RA (2006) Telomeres: cancer to human aging. Annu Rev Cell Dev Biol 22:531-557. doi:10.1146/annurev.cellbio.22.010305.104518

28. Shay JW, Wright WE (2011) Role of telomeres and telomerase in cancer. Semin Cancer Biol 21 (6):349-353. doi:10.1016/j.semcancer.2011.10.001

29. Chong L, van Steensel B, Broccoli D, Erdjument-Bromage H, Hanish J, Tempst P, de Lange T (1995) A human telomeric protein. Science 270 (5242):1663-1667

30. Court R, Chapman L, Fairall L, Rhodes D (2005) How the human telomeric proteins TRF1 and TRF2 recognize telomeric DNA: a view from high-resolution crystal structures. EMBO Rep 6 (1):39-45. doi:10.1038/sj.embor.7400314

31. Hanaoka S, Nagadoi A, Nishimura Y (2005) Comparison between TRF2 and TRF1 of their telomeric DNA-bound structures and DNA-binding activities. Protein Sci 14 (1):119-130. doi:10.1110/ps.04983705

32. Nishikawa T, Okamura H, Nagadoi A, Koig P, Rhodes D, Nishimura Y (2001) Structure of the DNA-binding domain of human telomeric protein, TRF1 and its interaction with telomeric DNA. Nucleic Acids Res Suppl (1):273-274

33. Nishikawa T, Okamura H, Nagadoi A, Konig P, Rhodes D, Nishimura Y (2001) Solution structure of a telomeric DNA complex of human TRF1. Structure 9 (12):1237-1251

34. Karlseder J, Broccoli D, Dai Y, Hardy S, de Lange T (1999) p53- and ATM-dependent apoptosis induced by telomeres lacking TRF2. Science 283 (5406):1321-1325

35. Karlseder J, Hoke K, Mirzoeva OK, Bakkenist C, Kastan MB, Petrini JH, de Lange T (2004) The telomeric protein TRF2 binds the ATM kinase and can inhibit the ATM-dependent DNA damage response. PLoS Biol 2 (8):E240. doi:10.1371/journal.pbio.0020240

36. Takai H, Smogorzewska A, de Lange T (2003) DNA damage foci at dysfunctional telomeres. Curr Biol 13 (17):1549-1556

37. Benarroch-Popivker D, Pisano S, Mendez-Bermudez A, Lototska L, Kaur P, Bauwens S, Djerbi N, Latrick CM, Fraisier V, Pei B, Gay A, Jaune E, Foucher K, Cherfils-Vicini J, Aeby E, Miron S, Londono-Vallejo A, Ye J, Le Du MH, Wang H, Gilson E, Giraud-Panis MJ (2016) TRF2-Mediated Control of Telomere DNA Topology as a Mechanism for Chromosome-End Protection. Mol Cell 61 (2):274-286. doi:10.1016/j.molcel.2015.12.009

38. Doksani Y, Wu JY, de Lange T, Zhuang X (2013) Super-resolution fluorescence imaging of telomeres reveals TRF2-dependent T-loop formation. Cell 155 (2):345-356. doi:10.1016/j.cell.2013.09.048

39. Griffith JD, Comeau L, Rosenfield S, Stansel RM, Bianchi A, Moss H, de Lange T (1999) Mammalian telomeres end in a large duplex loop. Cell 97 (4):503-514

40. Fairall L, Chapman L, Moss H, de Lange T, Rhodes D (2001) Structure of the TRFH dimerization domain of the human telomeric proteins TRF1 and TRF2. Mol Cell 8 (2):351-361

41. Chen Y, Yang Y, van Overbeek M, Donigian JR, Baciu P, de Lange T, Lei M (2008) A shared docking motif in TRF1 and TRF2 used for differential recruitment of telomeric proteins. Science 319 (5866):1092-1096. doi:10.1126/science.1151804

42. Rai R, Chen Y, Lei M, Chang S (2016) TRF2-RAP1 is required to protect telomeres from engaging in homologous recombination-mediated deletions and fusions. Nat Commun 7:10881. doi:10.1038/ncomms10881

43. Sfeir A, Kabir S, van Overbeek M, Celli GB, de Lange T (2010) Loss of Rap1 induces telomere recombination in the absence of NHEJ or a DNA damage signal. Science 327 (5973):1657-1661. doi:10.1126/science.1185100

44. Celli GB, de Lange T (2005) DNA processing is not required for ATM-mediated telomere damage response after TRF2 deletion. Nat Cell Biol 7 (7):712-718. doi:10.1038/ncb1275

45. Karlseder J, Kachatrian L, Takai H, Mercer K, Hingorani S, Jacks T, de Lange T (2003) Targeted deletion reveals an essential function for the telomere length regulator Trf1. Mol Cell Biol 23 (18):6533-6541

46. Gray JT, Celander DW, Price CM, Cech TR (1991) Cloning and expression of genes for the Oxytricha telomere-binding protein: specific subunit interactions in the telomeric complex. Cell 67 (4):807-814

47. Horvath MP, Schweiker VL, Bevilacqua JM, Ruggles JA, Schultz SC (1998) Crystal structure of the Oxytricha nova telomere end binding protein complexed with single strand DNA. Cell 95 (7):963-974

48. Buczek P, Horvath MP (2006) Structural reorganization and the cooperative binding of single-stranded telomere DNA in Sterkiella nova. J Biol Chem 281 (52):40124-40134. doi:10.1074/jbc.M607749200

49. Lei M, Podell ER, Baumann P, Cech TR (2003) DNA self-recognition in the structure of Pot1 bound to telomeric single-stranded DNA. Nature 426 (6963):198-203. doi:10.1038/nature02092

50. Dickey TH, McKercher MA, Wuttke DS (2013) Nonspecific recognition is achieved in Pot1pC through the use of multiple binding modes. Structure 21 (1):121-132. doi:10.1016/j.str.2012.10.015

51. Denchi EL, de Lange T (2007) Protection of telomeres through independent control of ATM and ATR by TRF2 and POT1. Nature 448 (7157):1068-1071. doi:10.1038/nature06065

52. Fan J, Pavletich NP (2012) Structure and conformational change of a replication protein A heterotrimer bound to ssDNA. Genes Dev 26 (20):2337-2347. doi:10.1101/gad.194787.112

53. Takai KK, Kibe T, Donigian JR, Frescas D, de Lange T (2011) Telomere protection by TPP1/POT1 requires tethering to TIN2. Mol Cell 44 (4):647-659. doi:10.1016/j.molcel.2011.08.043

54. Gu P, Wang Y, Bisht KK, Wu L, Kukova L, Smith EM, Xiao Y, Bailey SM, Lei M, Nandakumar J, Chang S (2017) Pot1 OB-fold mutations unleash telomere instability to initiate tumorigenesis. Oncogene 36 (14):1939-1951. doi:10.1038/onc.2016.405

55. Pinzaru AM, Hom RA, Beal A, Phillips AF, Ni E, Cardozo T, Nair N, Choi J, Wuttke DS, Sfeir A, Denchi EL (2016) Telomere Replication Stress Induced by POT1 Inactivation Accelerates Tumorigenesis. Cell Rep 15 (10):2170-2184. doi:10.1016/j.celrep.2016.05.008

56. Chen C, Gu P, Wu J, Chen X, Niu S, Sun H, Wu L, Li N, Peng J, Shi S, Fan C, Huang M, Wong CC, Gong Q, Kumar-Sinha C, Zhang R, Pusztai L, Rai R, Chang S, Lei M (2017) Structural insights into POT1-TPP1 interaction and POT1 C-terminal mutations in human cancer. Nat Commun 8:14929. doi:10.1038/ncomms14929

57. Rice C, Shastrula PK, Kossenkov AV, Hills R, Baird DM, Showe LC, Doukov T, Janicki S, Skordalakes E (2017) Structural and functional analysis of the human POT1-TPP1 telomeric complex. Nat Commun 8:14928. doi:10.1038/ncomms14928

58. Hockemeyer D, Palm W, Else T, Daniels JP, Takai KK, Ye JZ, Keegan CE, de Lange T, Hammer GD (2007) Telomere protection by mammalian Pot1 requires interaction with Tpp1. Nat Struct Mol Biol 14 (8):754-761. doi:10.1038/nsmb1270

59. Gong Y, de Lange T (2010) A Shld1-controlled POT1a provides support for repression of ATR signaling at telomeres through RPA exclusion. Mol Cell 40 (3):377-387. doi:10.1016/j.molcel.2010.10.016

60. Abreu E, Aritonovska E, Reichenbach P, Cristofari G, Culp B, Terns RM, Lingner J, Terns MP (2010) TIN2-tethered TPP1 recruits human telomerase to telomeres in vivo. Mol Cell Biol 30 (12):2971-2982. doi:10.1128/MCB.00240-10

61. O'Connor MS, Safari A, Xin H, Liu D, Songyang Z (2006) A critical role for TPP1 and TIN2 interaction in high-order telomeric complex assembly. Proc Natl Acad Sci U S A 103 (32):11874-11879. doi:10.1073/pnas.0605303103

62. Frescas D, de Lange T (2014) TRF2-tethered TIN2 can mediate telomere protection by TPP1/POT1. Mol Cell Biol 34 (7):1349-1362. doi:10.1128/MCB.01052-13

63. Kim SH, Beausejour C, Davalos AR, Kaminker P, Heo SJ, Campisi J (2004) TIN2 mediates functions of TRF2 at human telomeres. J Biol Chem 279 (42):43799-43804. doi:10.1074/jbc.M408650200

64. Wang F, Podell ER, Zaug AJ, Yang Y, Baciu P, Cech TR, Lei M (2007) The POT1-TPP1 telomere complex is a telomerase processivity factor. Nature 445 (7127):506-510. doi:10.1038/nature05454

65. Xin H, Liu D, Wan M, Safari A, Kim H, Sun W, O'Connor MS, Songyang Z (2007) TPP1 is a homologue of ciliate TEBP-beta and interacts with POT1 to recruit telomerase. Nature 445 (7127):559-562. doi:10.1038/nature05469

66. Nandakumar J, Bell CF, Weidenfeld I, Zaug AJ, Leinwand LA, Cech TR (2012) The TEL patch of telomere protein TPP1 mediates telomerase recruitment and processivity. Nature 492 (7428):285-289. doi:10.1038/nature11648

67. Sexton AN, Youmans DT, Collins K (2012) Specificity requirements for human telomere protein interaction with telomerase holoenzyme. J Biol Chem 287 (41):34455-34464. doi:10.1074/jbc.M112.394767

68. Zhong FL, Batista LF, Freund A, Pech MF, Venteicher AS, Artandi SE (2012) TPP1 OB-fold domain controls telomere maintenance by recruiting telomerase to chromosome ends. Cell 150 (3):481-494. doi:10.1016/j.cell.2012.07.012

69. Grill S, Tesmer VM, Nandakumar J (2018) The N Terminus of the OB Domain of Telomere Protein TPP1 Is Critical for Telomerase Action. Cell Rep 22 (5):1132-1140. doi:10.1016/j.celrep.2018.01.012

70. Schmidt JC, Dalby AB, Cech TR (2014) Identification of human TERT elements necessary for telomerase recruitment to telomeres. Elife 3. doi:10.7554/eLife.03563

71. Zhang Q, Kim NK, Feigon J (2011) Architecture of human telomerase RNA. Proc Natl Acad Sci U S A 108 (51):20325-20332. doi:10.1073/pnas.1100279108

72. Chen JL, Blasco MA, Greider CW (2000) Secondary structure of vertebrate telomerase RNA. Cell 100 (5):503-514

73. Chen JL, Greider CW (2003) Template boundary definition in mammalian telomerase. Genes Dev 17 (22):2747-2752. doi:10.1101/gad.1140303

74. Tzfati Y, Fulton TB, Roy J, Blackburn EH (2000) Template boundary in a yeast telomerase specified by RNA structure. Science 288 (5467):863-867

75. Box JA, Bunch JT, Zappulla DC, Glynn EF, Baumann P (2008) A flexible template boundary element in the RNA subunit of fission yeast telomerase. J Biol Chem 283 (35):24224-24233. doi:10.1074/jbc.M802043200

76. Miller MC, Collins K (2002) Telomerase recognizes its template by using an adjacent RNA motif. Proc Natl Acad Sci U S A 99 (10):6585-6590. doi:10.1073/pnas.102024699

77. Lai CK, Miller MC, Collins K (2003) Roles for RNA in telomerase nucleotide and repeat addition processivity. Mol Cell 11 (6):1673-1683

78. Berman AJ, Akiyama BM, Stone MD, Cech TR (2011) The RNA accordion model for template positioning by telomerase RNA during telomeric DNA synthesis. Nat Struct Mol Biol 18 (12):1371-1375. doi:10.1038/nsmb.2174

79. Yang W, Lee YS (2015) A DNA-hairpin model for repeat-addition processivity in telomere synthesis. Nat Struct Mol Biol 22 (11):844-847. doi:10.1038/nsmb.3098

80. Wang Y, Yesselman JD, Zhang Q, Kang M, Feigon J (2016) Structural conservation in the template/pseudoknot domain of vertebrate telomerase RNA from teleost fish to human. Proc Natl Acad Sci U S A 113 (35):E5125-5134. doi:10.1073/pnas.1607411113

81. Chan H, Wang Y, Feigon J (2017) Progress in Human and Tetrahymena Telomerase Structure Determination. Annu Rev Biophys 46:199-225. doi:10.1146/annurev-biophys-062215-011140

82. Bley CJ, Qi X, Rand DP, Borges CR, Nelson RW, Chen JJ (2011) RNA-protein binding interface in the telomerase ribonucleoprotein. Proc Natl Acad Sci U S A 108 (51):20333-20338. doi:10.1073/pnas.1100270108

83. Huang J, Brown AF, Wu J, Xue J, Bley CJ, Rand DP, Wu L, Zhang R, Chen JJ, Lei M (2014) Structural basis for protein-RNA recognition in telomerase. Nat Struct Mol Biol 21 (6):507-512. doi:10.1038/nsmb.2819

84. Leeper T, Leulliot N, Varani G (2003) The solution structure of an essential stem-loop of human telomerase RNA. Nucleic Acids Res 31 (10):2614-2621

85. Harkisheimer M, Mason M, Shuvaeva E, Skordalakes E (2013) A motif in the vertebrate telomerase N-terminal linker of TERT contributes to RNA binding and telomerase activity and processivity. Structure 21 (10):1870-1878. doi:10.1016/j.str.2013.08.013

86. Rouda S, Skordalakes E (2007) Structure of the RNA-binding domain of telomerase: implications for RNA recognition and binding. Structure 15 (11):1403-1412. doi:10.1016/j.str.2007.09.007

87. Gillis AJ, Schuller AP, Skordalakes E (2008) Structure of the Tribolium castaneum telomerase catalytic subunit TERT. Nature 455 (7213):633-637. doi:10.1038/nature07283

88. Mitchell M, Gillis A, Futahashi M, Fujiwara H, Skordalakes E (2010) Structural basis for telomerase catalytic subunit TERT binding to RNA template and telomeric DNA. Nat Struct Mol Biol 17 (4):513-518. doi:10.1038/nsmb.1777

89. Jansson LI, Akiyama BM, Ooms A, Lu C, Rubin SM, Stone MD (2015) Structural basis of template-boundary definition in Tetrahymena telomerase. Nat Struct Mol Biol 22 (11):883-888. doi:10.1038/nsmb.3101

90. Egan ED, Collins K (2012) Biogenesis of telomerase ribonucleoproteins. RNA 18 (10):1747-1759. doi:10.1261/rna.034629.112

91. Mitchell JR, Wood E, Collins K (1999) A telomerase component is defective in the human disease dyskeratosis congenita. Nature 402 (6761):551-555. doi:10.1038/990141

92. Kiss T, Fayet-Lebaron E, Jady BE (2010) Box H/ACA small ribonucleoproteins. Mol Cell 37 (5):597-606. doi:10.1016/j.molcel.2010.01.032

93. Venteicher AS, Abreu EB, Meng Z, McCann KE, Terns RM, Veenstra TD, Terns MP, Artandi SE (2009) A human telomerase holoenzyme protein required for Cajal body localization and telomere synthesis. Science 323 (5914):644-648. doi:10.1126/science.1165357

94. Tycowski KT, Shu MD, Kukoyi A, Steitz JA (2009) A conserved WD40 protein binds the Cajal body localization signal of scaRNP particles. Mol Cell 34 (1):47-57. doi:10.1016/j.molcel.2009.02.020

95. Venteicher AS, Artandi SE (2009) TCAB1: driving telomerase to Cajal bodies. Cell Cycle 8 (9):1329-1331. doi:10.4161/cc.8.9.8288

96. Chen L, Roake CM, Freund A, Batista PJ, Tian S, Yin YA, Gajera CR, Lin S, Lee B, Pech MF, Venteicher AS, Das R, Chang HY, Artandi SE (2018) An Activity Switch in Human Telomerase Based on RNA Conformation and Shaped by TCAB1. Cell. doi:10.1016/j.cell.2018.04.039

97. Nguyen THD, Tam J, Wu RA, Greber BJ, Toso D, Nogales E, Collins K (2018) Cryo-EM structure of substrate-bound human telomerase holoenzyme. Nature 557 (7704):190-195. doi:10.1038/s41586-018-0062-x

98. Podlevsky JD, Chen JJ (2012) It all comes together at the ends: telomerase structure, function, and biogenesis. Mutat Res 730 (1-2):3-11. doi:10.1016/j.mrfmmm.2011.11.002

99. Jacobs SA, Podell ER, Cech TR (2006) Crystal structure of the essential N-terminal domain of telomerase reverse transcriptase. Nat Struct Mol Biol 13 (3):218-225. doi:10.1038/nsmb1054

100. Petrova OA, Mantsyzov AB, Rodina EV, Efimov SV, Hackenberg C, Hakanpaa J, Klochkov VV, Lebedev AA, Chugunova AA, Malyavko AN, Zatsepin TS, Mishin AV, Zvereva MI, Lamzin VS, Dontsova OA, Polshakov VI (2017) Structure and function of the N-terminal domain of the yeast telomerase reverse transcriptase. Nucleic Acids Res. doi:10.1093/nar/gkx1275

101. Armbruster BN, Banik SS, Guo C, Smith AC, Counter CM (2001) N-terminal domains of the human telomerase catalytic subunit required for enzyme activity in vivo. Mol Cell Biol 21 (22):7775-7786. doi:10.1128/MCB.21.22.7775-7786.2001

102. Armbruster BN, Linardic CM, Veldman T, Bansal NP, Downie DL, Counter CM (2004) Rescue of an hTERT mutant defective in telomere elongation by fusion with hPot1. Mol Cell Biol 24 (8):3552-3561

103. Zaug AJ, Podell ER, Nandakumar J, Cech TR (2010) Functional interaction between telomere protein TPP1 and telomerase. Genes Dev 24 (6):613-622. doi:10.1101/gad.1881810

104. Sexton AN, Regalado SG, Lai CS, Cost GJ, O'Neil CM, Urnov FD, Gregory PD, Jaenisch R, Collins K, Hockemeyer D (2014) Genetic and molecular identification of three human TPP1 functions in telomerase action: recruitment, activation, and homeostasis set point regulation. Genes Dev 28 (17):1885-1899. doi:10.1101/gad.246819.114

105. Wu RA, Collins K (2014) Human telomerase specialization for repeat synthesis by unique handling of primer-template duplex. EMBO J 33 (8):921-935. doi:10.1002/embj.201387205

106. Lue NF (2005) A physical and functional constituent of telomerase anchor site. J Biol Chem 280 (28):26586-26591. doi:10.1074/jbc.M503028200

107. Zaug AJ, Podell ER, Cech TR (2008) Mutation in TERT separates processivity from anchor-site function. Nat Struct Mol Biol 15 (8):870-872. doi:10.1038/nsmb.1462

108. Hoffman H, Rice C, Skordalakes E (2017) Structural Analysis Reveals the Deleterious Effects of Telomerase Mutations in Bone Marrow Failure Syndromes. J Biol Chem 292 (11):4593-4601. doi:10.1074/jbc.M116.771204

109. Bryan C, Rice C, Hoffman H, Harkisheimer M, Sweeney M, Skordalakes E (2015) Structural Basis of Telomerase Inhibition by the Highly Specific BIBR1532. Structure 23 (10):1934-1942. doi:10.1016/j.str.2015.08.006

110. Banik SS, Guo C, Smith AC, Margolis SS, Richardson DA, Tirado CA, Counter CM (2002) C-terminal regions of the human telomerase catalytic subunit essential for in vivo enzyme activity. Mol Cell Biol 22 (17):6234-6246

111. Lue NF, Lin YC, Mian IS (2003) A conserved telomerase motif within the catalytic domain of telomerase reverse transcriptase is specifically required for repeat addition processivity. Mol Cell Biol 23 (23):8440-8449

112. Chu TW, D'Souza Y, Autexier C (2016) The Insertion in Fingers Domain in Human Telomerase Can Mediate Enzyme Processivity and Telomerase Recruitment to Telomeres in a TPP1-Dependent Manner. Mol Cell Biol 36 (1):210-222. doi:10.1128/MCB.00746-15

113. Chu TW, MacNeil DE, Autexier C (2016) Multiple Mechanisms Contribute to the Cell Growth Defects Imparted by Human Telomerase Insertion in Fingers Domain Mutations Associated with Premature Aging Diseases. J Biol Chem 291 (16):8374-8386. doi:10.1074/jbc.M116.714782

114. Sauerwald A, Sandin S, Cristofari G, Scheres SH, Lingner J, Rhodes D (2013) Structure of active dimeric human telomerase. Nat Struct Mol Biol 20 (4):454-460. doi:10.1038/nsmb.2530

115. Jiang J, Chan H, Cash DD, Miracco EJ, Ogorzalek Loo RR, Upton HE, Cascio D, O'Brien Johnson R, Collins K, Loo JA, Zhou ZH, Feigon J (2015) Structure of Tetrahymena telomerase reveals previously unknown subunits, functions, and interactions. Science 350 (6260):aab4070. doi:10.1126/science.aab4070

116. Jiang J, Miracco EJ, Hong K, Eckert B, Chan H, Cash DD, Min B, Zhou ZH, Collins K, Feigon J (2013) The architecture of Tetrahymena telomerase holoenzyme. Nature 496 (7444):187-192. doi:10.1038/nature12062

117. Ren X, Gavory G, Li H, Ying L, Klenerman D, Balasubramanian S (2003) Identification of a new RNA.RNA interaction site for human telomerase RNA (hTR): structural implications for hTR accumulation and a dyskeratosis congenita point mutation. Nucleic Acids Res 31 (22):6509-6515

118. Alves D, Li H, Codrington R, Orte A, Ren X, Klenerman D, Balasubramanian S (2008) Single-molecule analysis of human telomerase monomer. Nat Chem Biol 4 (5):287-289. doi:10.1038/nchembio.82

119. Egan ED, Collins K (2010) Specificity and stoichiometry of subunit interactions in the human telomerase holoenzyme assembled in vivo. Mol Cell Biol 30 (11):2775-2786. doi:10.1128/MCB.00151-10

120. Wenz C, Enenkel B, Amacker M, Kelleher C, Damm K, Lingner J (2001) Human telomerase contains two cooperating telomerase RNA molecules. EMBO J 20 (13):3526-3534. doi:10.1093/emboj/20.13.3526

121. Jiang J, Wang Y, Susac L, Chan H, Basu R, Zhou ZH, Feigon J (2018) Structure of Telomerase with Telomeric DNA. Cell 173 (5):1179-1190 e1113. doi:10.1016/j.cell.2018.04.038

122. Ballew BJ, Savage SA (2013) Updates on the biology and management of dyskeratosis congenita and related telomere biology disorders. Expert Rev Hematol 6 (3):327-337. doi:10.1586/ehm.13.23

123. Savage SA, Bertuch AA (2010) The genetics and clinical manifestations of telomere biology disorders. Genet Med 12 (12):753-764. doi:10.1097/GIM.0b013e3181f415b5

124. Kocak H, Ballew BJ, Bisht K, Eggebeen R, Hicks BD, Suman S, O'Neil A, Giri N, Laboratory NDCGR, Group NDCSW, Maillard I, Alter BP, Keegan CE, Nandakumar J, Savage SA (2014) Hoyeraal-Hreidarsson syndrome caused by a germline mutation in the TEL patch of the telomere protein TPP1. Genes Dev 28 (19):2090-2102. doi:10.1101/gad.248567.114

125. Guo Y, Kartawinata M, Li J, Pickett HA, Teo J, Kilo T, Barbaro PM, Keating B, Chen Y, Tian L, Al-Odaib A, Reddel RR, Christodoulou J, Xu X, Hakonarson H, Bryan TM (2014) Inherited bone marrow failure associated with germline mutation of ACD, the gene encoding telomere protein TPP1. Blood 124 (18):2767-2774. doi:10.1182/blood-2014-08-596445

126. Alter BP, Rosenberg PS, Giri N, Baerlocher GM, Lansdorp PM, Savage SA (2012) Telomere length is associated with disease severity and declines with age in dyskeratosis congenita. Haematologica 97 (3):353-359. doi:10.3324/haematol.2011.055269

127. Bisht K, Smith EM, Tesmer VM, Nandakumar J (2016) Structural and functional consequences of a disease mutation in the telomere protein TPP1. Proc Natl Acad Sci U S A 113 (46):13021-13026. doi:10.1073/pnas.1605685113

128. Sarek G, Marzec P, Margalef P, Boulton SJ (2015) Molecular basis of telomere dysfunction in human genetic diseases. Nat Struct Mol Biol 22 (11):867-874. doi:10.1038/nsmb.3093

129. Nakashima M, Nandakumar J, Sullivan KD, Espinosa JM, Cech TR (2013) Inhibition of telomerase recruitment and cancer cell death. J Biol Chem 288 (46):33171-33180. doi:10.1074/jbc.M113.518175

130. Nandakumar J, Bell CF, Weidenfeld I, Zaug AJ, Leinwand LA, Cech TR (2012) The TEL patch of telomere protein TPP1 mediates telomerase recruitment and processivity. Nature 492:285-289

131. Hsu PD, Lander ES, Zhang F (2014) Development and applications of CRISPR-Cas9 for genome engineering. Cell 157 (6):1262-1278. doi:10.1016/j.cell.2014.05.010

132. Wright AV, Nunez JK, Doudna JA (2016) Biology and Applications of CRISPR Systems: Harnessing Nature's Toolbox for Genome Engineering. Cell 164 (1-2):29-44. doi:10.1016/j.cell.2015.12.035

133. Cong L, Ran FA, Cox D, Lin S, Barretto R, Habib N, Hsu PD, Wu X, Jiang W, Marraffini LA, Zhang F (2013) Multiplex genome engineering using CRISPR/Cas systems. Science 339 (6121):819-823. doi:10.1126/science.1231143

134. Wu RA, Dagdas YS, Yilmaz ST, Yildiz A, Collins K (2015) Single-molecule imaging of telomerase reverse transcriptase in human telomerase holoenzyme and minimal RNP complexes. Elife 4. doi:10.7554/eLife.08363

135. Weidenfeld I (2012) Inducible microRNA-mediated knockdown of the endogenous human lamin A/C gene. Methods Mol Biol 815:289-305. doi:10.1007/978-1-61779-424-7_22

136. Otwinowski Z, Minor W (1997) Processing of x-ray diffraction data collected in oscillation mode. . Methods in enzymology 276:307–326

137. Read RJ, Sussman JL (2007) NATO Science Series. NATO Science Series 245:41-51

138. CCP4 (Collaborative Computational Project N (1994) The CCP4 suite: programs for protein crystallography. Acta Crystallogr D Biol Crystallogr 50 (Pt 5):760-763. doi:10.1107/S0907444994003112

S0907444994003112 [pii]

139. Emsley P, Cowtan K (2004) Coot: model-building tools for molecular graphics. Acta Crystallogr D Biol Crystallogr 60 (Pt 12 Pt 1):2126-2132. doi:10.1107/S0907444904019158

140. Abreu E, Terns RM, Terns MP (2011) Visualization of human telomerase localization by fluorescence microscopy techniques. Methods Mol Biol 735:125-137. doi:10.1007/978-1-61779-092-8_12

141. Hwang H, Opresko P, Myong S (2014) Single-molecule real-time detection of telomerase extension activity. Sci Rep 4:6391. doi:10.1038/srep06391

142. Hug N, Lingner J (2006) Telomere length homeostasis. Chromosoma 115 (6):413-425. doi:10.1007/s00412-006-0067-3

143. Terwilliger TC, Adams PD, Read RJ, McCoy AJ, Moriarty NW, Grosse-Kunstleve RW, Afonine PV, Zwart PH, Hung LW (2009) Decision-making in structure solution using Bayesian estimates of map quality: the PHENIX AutoSol wizard. Acta Crystallogr D Biol Crystallogr 65 (Pt 6):582-601. doi:10.1107/S0907444909012098

144. Terwilliger TC, Grosse-Kunstleve RW, Afonine PV, Moriarty NW, Zwart PH, Hung LW, Read RJ, Adams PD (2008) Iterative model building, structure refinement and density modification with the PHENIX AutoBuild wizard. Acta Crystallogr D Biol Crystallogr 64 (Pt 1):61-69. doi:10.1107/S090744490705024X

145. Pendlebury DF, Fujiwara Y, Tesmer VM, Smith EM, Shibuya H, Watanabe Y, Nandakumar J (2017) Dissecting the telomere-inner nuclear membrane interface formed in meiosis. Nat Struct Mol Biol 24 (12):1064-1072. doi:10.1038/nsmb.3493

146. Blazer LL, Roman DL, Muxlow MR, Neubig RR (2010) Use of flow cytometric methods to quantify protein-protein interactions. Curr Protoc Cytom Chapter 13:Unit 13 11 11-15. doi:10.1002/0471142956.cy1311s51